Feasible and Reliable Ab initio Atomistic Modeling for Nuclear Waste Management

George Beridze

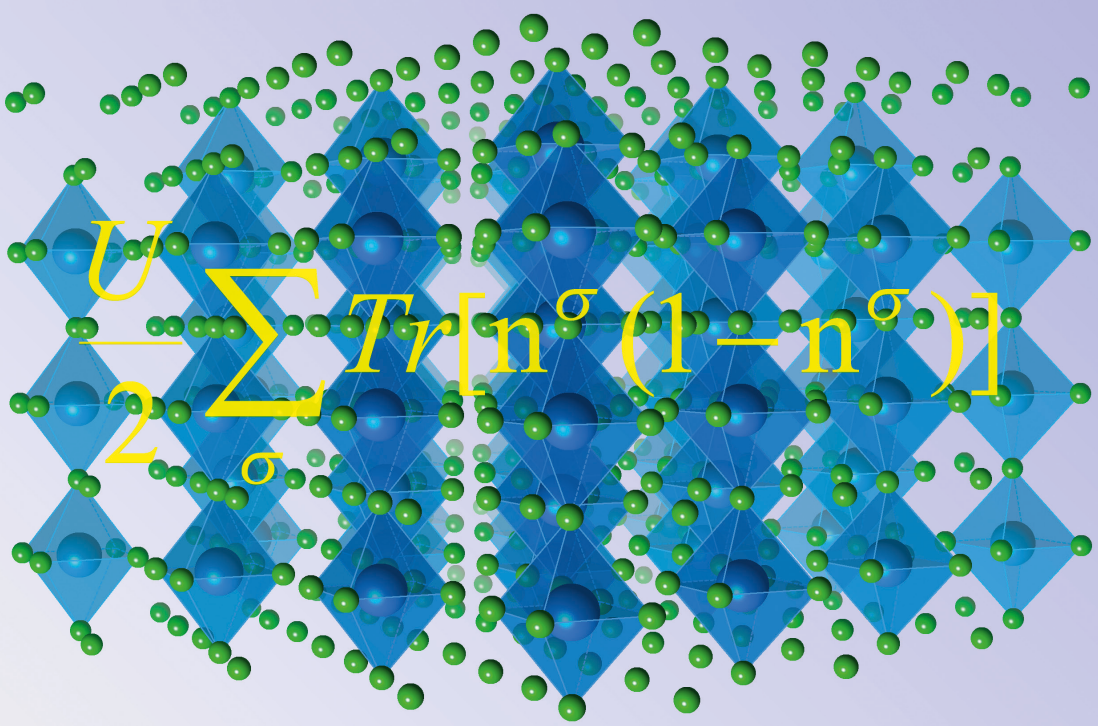

Energie & Umwelt / Energy & Environment
Band / Volume 325
ISBN 978-3-95806-151-4

JÜLICH FORSCHUNGSZENTRUM

Schriften des Forschungszentrums Jülich
Reihe Energie & Umwelt / Energy & Environment Band / Volume 325

Forschungszentrum Jülich GmbH
Institute of Energy and Climate Research
Nukleare Entsorgung und Reaktorsicherheit (IEK-6)

Feasible and Reliable Ab initio Atomistic Modeling for Nuclear Waste Management

George Beridze

Schriften des Forschungszentrums Jülich
Reihe Energie & Umwelt / Energy & Environment Band / Volume 325

ISSN 1866-1793 ISBN 978-3-95806-151-4

Bibliographic information published by the Deutsche Nationalbibliothek.
The Deutsche Nationalbibliothek lists this publication in the Deutsche
Nationalbibliografie; detailed bibliographic data are available in the
Internet at http://dnb.d-nb.de.

Publisher and Distributor: Forschungszentrum Jülich GmbH
Zentralbibliothek
52425 Jülich
Tel: +49 2461 61-5368
Fax: +49 2461 61-6103
Email: zb-publikation@fz-juelich.de
www.fz-juelich.de/zb

Cover Design: Grafische Medien, Forschungszentrum Jülich GmbH

Printer: Grafische Medien, Forschungszentrum Jülich GmbH

Schriften des Forschungszentrums Jülich
Reihe Energie & Umwelt / Energy & Environment, Band / Volume 325

D 82 (Diss. RWTH Aachen University, 2016)

ISSN 1866-1793
ISBN 978-3-95806-151-4

The complete volume is freely available on the Internet on the Jülicher Open Access Server (JuSER)
at www.fz-juelich.de/zb/openaccess.

Zusammenfassung

Die vorliegende Dissertation befasst sich mit der Untersuchung und Weiterentwicklung praktikabler und mit vertretbarem Rechenaufwand machbaren *Ab-initio*-Methoden zur zuverlässigen atomistischen Modellierung nuklearer Materialien. Hierzu wurde die Leistungsfähigkeit von verschiedenen DFT-Funktionalen und DFT-basierten Methoden (beispielsweise vom DFT+U-Verfahren) untersucht, die explizit die Elektronenkorrelation beschreiben, um damit die strukturellen und thermochemischen Eigenschaften von lanthaniden- und aktinidenhaltigen Materialien korrekt beschreiben und vorhersagen zu können.

In früheren Untersuchungen wurde der Wert des Hubbard-U-Parameters, der beim DFT+U-Verfahren erforderlich ist, oft nur erraten oder empirisch abgeleitet. Im Gegensatz dazu wurden hier in jüngerer Zeit entwickelte *Ab-initio*-Methodenwie die 'constrained Local Density Approximation' (cLDA) und die 'constrained Random Phase Approximation' (cRPA) angewendet und intensiv getestet, um die Hubbard-U-Parameterwerte aus den Grundprinzipien zu berechnen. Hierdurch wird die DFT+U Methode zu einem echten parameterfreien *Ab-initio*-Verfahren. Unsere erfolgreichen Benchmarking-Studien des parameterfreien DFT+U-Verfahrens zur Vorhersage von Strukturen und Reaktionsenthalpien An- und Ln-haltiger Moleküle und Festkörper zeigen, dass die linear-response-Methode (cLDA) eine sehr gute Schätzung der Hubbard-U-Parameter ermöglicht und konsistent mit den cRPA-Berechnungen ist. Insbesondere konnte gezeigt werden, dass der Hubbard-U-Parameterwert, der die Stärke der Coulomb-Abstoßung zwischen den f-Elektronen beschreibt, wesentlich von der Oxidationsstufe des f-Elements, sowie auch von der Kristallstruktur der Materialien abhängt, was bisher noch nicht im Detail betrachtet wurde. Es konnte gezeigt werden, dass der verwendete Berechnungsansatz die Fehler der prognostizierten Reaktionsenthalpien signifikant reduziert, wodurch die Genauigkeit dieser Vorhersage vergleichbar mit den Unsicherheiten rechnenintensiverer quantenchemischer Berechnungsmethoden höherer Ordnung oder auch von Experimenten ist. Mit der entwickelten Methode wurden er-

folgreich verschiedene, bezüglich der Langzeitstabilitätwichtige, thermochemische und thermodynamische Eigenschaften potenzieller keramischer Abfallformen für, wie Monazit und Pyrochlor simuliert. Hierbei wurden insbesondere die Wärmekapazitäten, die Exzessenthalpien der Mischkristalle so wie thermochemische Parameter der Phasenübergänge betrachtet. Die hier durchgeführte Benchmarking- und Anwendungsstudien zeigen Wege für die Suche und Weiterentwicklung rechnerisch handhabbarer *Ab-initio*-Berechnungsmethoden, für eine zuverlässige und aussagekräftige Simulation von Materialien mit Relevanz für die Entsorgung radioaktiver Abfälle. german

Abstract

The studies in this PhD dissertation focus on finding a computationally feasible *ab initio* methodology which would make the reliable first principle atomistic modeling of nuclear materials possible. Here we tested the performance of the different DFT functionals and the DFT-based methods that explicitly account for the electronic correlations, such as the DFT+U approach, for prediction of structural and thermochemical properties of lanthanide- and actinide-bearing materials. In the previous studies, the value of the Hubbard U parameter, required by the DFT+U method, was often guessed or empirically derived. We applied and extensively tested the recently developed *ab initio* methods such as the constrained local density approximation (cLDA) and the constrained random phase approximation (cRPA), to compute the Hubbard U parameter values from first principles, thus making the DFT+U method a real *ab inito* parameter free approach.

Our successful benchmarking studies of the parameter-free DFT+U method, for prediction of the structures and the reaction enthalpies of actinide- and lanthanide-bearing molecular compounds and solids indicate, that the linear response method (cLDA) provides a very good, and consistent with the cRPA prediction, estimate of the Hubbard U parameter. In particular, we found that the Hubbard U parameter value, which describes the strength of the on-site Coulomb repulsion between f-electrons, depends strongly on the oxidation state of the f-element, its local bonding environment and crystalline structure of the materials, which has never been considered in such detail before. We have shown, that the applied computational approach substantially, if not dramatically, reduces the error of the predicted reaction enthalpies making the accuracy of the prediction comparable with the uncertainty of the computational unfeasible, higher order methods of quantum chemistry, and experiments. The derived methodology resulted in various, already published, successful modeling of the important, from the long-term stability point of view, thermochemical and thermodynamical properties of the prospective nuclear waste forms, such as monazite- and pyrochlore-

type ceramics. These include the heat capacities, the excess enthalpies of mixing or thermochemical parameters of phase transitions, to name but a few. The performed here benchmarking and application studies give a solid basis and paths for the quest to find and design computationally feasible *ab initio* computational methods, which would allow for reliable and meaningful simulations of materials relevant for nuclear waste management.

Acknowledgments

I would like to express my gratitude to Prof. Dirk Bosbach, director of IEK-6 and my official *Doktorvater* and Dr. Piotr Kowalski, head of the Atomistic Modeling group at IEK-6 and direct supervisor of this dissertation research, for giving me the opportunity to do the PhD studies at Forschungszentrum Jülich (IEK-6) and for their support and expertise that helped in successful finalization of my PhD studies. I also want to thank Prof. Georg Roth for being the second reviewer of my PhD thesis and Prof. Evgeny Alekseev for chairing the oral defense session.

I am especially thankful to my direct supervisor at IEK-6, Dr. Piotr Kowalski for his extensive mentoring on a daily basis, for sharing many ideas, for effective guidance and broad scientific expertise, that were crucial for execution of this research. I am thankful for having the excellent opportunities to attend many research-oriented international schools and tutorials, and for having a chance to promote my research at various international scientific workshops and conferences and for essential help in efficient networking with the scientific community.

I want to thank all other colleagues and co-workers from the Atomistic Modeling group, in particular Dr. Ariadna Blanca-Romero, Dr. Yan Li, Yaqi Ji, Sarah Koniski, April Birnie, Rebecca Forward and Jose Jorge Rios Ramirez for the fruitful joint research and enjoyable time. I would also like to acknowledge all the colleagues from IEK-6 with who I have had pleasure to interact with, in particular Dr. Victor Vinograd, Dr. Guido Deissmann, Dr. Bin Xiao, Dr. Sarah Finkeldei and Dr. Felix Brandt, for shearing their expertise, excellent joint research and fun time together. Special thanks to colleagues from PGI-1 institute, Dr. Ersoy Şaşıoğlu, Dr. Christoph Friedrich and Prof. Stefan Blügel for essential tutoring on the Jülich FLEUR and SPEX codes, and help in utilization of the cRPA method for calculations of the Hubbard U parameter.

I would also like to thank my previous universities and advisors, in particular Prof. Notker Rösch and Dr. Sven Krüger at the Technical University of Munich and Prof. Shota Samsonia at the Tbilisi State University for giving me a solid academic

background that allowed for successful execution of this dissertation. Many thanks to all my friends and colleagues from Georgia, Germany and elsewhere who supported me during the last there years.

I would like to acknowledge the JARA-HPC for providing the access to the excellent supercomputing facilities and DAAD-RISE program for financing two of my proposals, which allowed me to host and mentor two undergraduate students: Ms. Sarah Koniski (U. of Rochester, USA) and Ms. April Birnie (Smith College, USA).

Last but not least, I am especially thankful to my parents, Marina and Tengiz for their continuous love, support and care, which was crucial for the development of my scientific carrier. Special thanks to my father, who as a professor of biochemistry and a member of the Georgian National Academy of Sciences provided me with valuable advices and professional mentoring during the past years that lead to my, up to date, successful and enjoyable scientific adventure.

Contents

List of Figures

List of Tables

Chapter 1

Introduction

1.1 Nuclear waste management: current state and prospects of atomistic modeling

Nuclear waste is a material that contains radionuclides with concentration larger than certain clearance levels determined by national laws [1]. Being radioactive, it represents a threat to the health of people and environment. Safe management of nuclear waste is thus an important problem related to the safety of our and future generations. The main source of the radioactive waste is the nuclear fuel cycle. Because in the year 2016, there are 437 operational nuclear reactors in 31 countries and 64 new reactors are currently under construction [1], the amount of the accumulated nuclear waste will increase in the future. Most of the nuclear countries utilize the open-nuclear fuel cycle in which the spent nuclear fuel is not reprocessed and reused (the closed nuclear fuel cycle is sometimes utilized [2, 3]) and the back-end of nuclear fuel cycle (called "high-level waste") contains the long-lived actinide isotopes such as ^{238}U, ^{235}U, ^{239}Pu, minor actinides ^{237}Np, ^{243}Am, ^{244}Cm, and the wide range of fission products [1]. The total inventory of the high-level waste in storage around the world amounts to $2,7 \times 10^6$ m^3 [1], and by 2022 Germany alone will have $2,8 \times 10^4$ m^3 of waste which has to be disposed [4]. In long-term safety analysis for deep geological disposal of spent nuclear

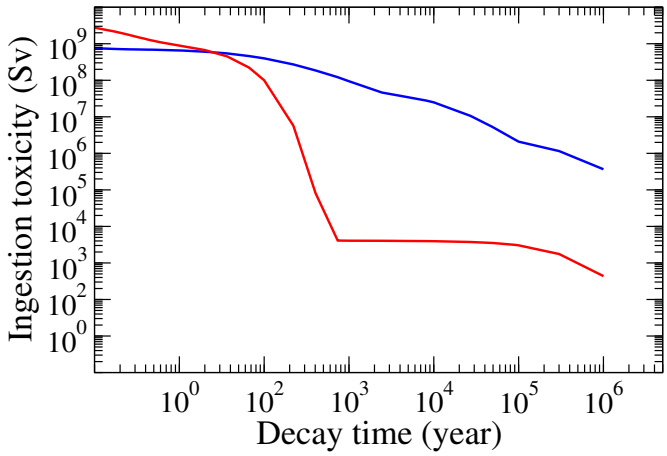

Figure 1.1: Relative radiotoxicity over 10^6 years of spent nuclear fuel with burn-up of 55 megawatt days/kg U of pressure water reactor with 4.5% UOX fuel. Actinides are depicted in blue and fission products in red [6].

fuel or high-level radioactive wastes, some long-lived fission products (e.g. Se-79, I-129, Cs-135) are the radionuclides dominating the biosphere dose, whereas Pu and the minor actinides listed above require attention due to their high radiotoxicity (see Fig. 1.1) [5].

Although significant amounts of electric power in Germany has been produced by nuclear power plants (17% in 2015 [1]), as a consequence of the Fukushima accident, in May 2011 Germany decided to phase-out of nuclear power and to stop the operation of all its nuclear power plants (except the research reactors) by the year 2022 [7]. The accumulated spent nuclear fuel is scheduled for the direct geological disposal [8]. It is the last step of the management of radioactive waste, during which the waste is permanently disposed in deep geological formation.

In July 2013 Germany passed the Repository Site Selection Act and plans to start the evaluation of the best final disposal candidate sites [9]. Some countries have already decided on their nuclear waste disposal strategy and some also on the disposal location. For example, Sweden and Finland plan to dispose their spent nuclear fuel in the crystalline rock formations at Forsmark and Olkiluoto Island, respectively [10,

11]. In November 2015 the government of Finland granted the license to the expert organization in nuclear waste management to build the disposal facility [12].

There is a consensus that before disposal, the radionuclides have to be safely stored with various barriers preventing their potential migration and any possibility of their dispersion into environment [1]. One such barrier is the waste form itself. It is considered to seclude the radionuclides into a stable, radiation-resistant material [1, 13]. There are several materials which are being considered for the immobilization of all types of nuclear waste: glass, crystalline ceramics such as monazite and pyrochlore, glass composite materials, cements, geopolymers, bitumen and metals [1].

However, the number of types of available materials with well characterized properties is very limited due to the lack of in-depth understanding of their behavior after incorporation of radionuclides into their structures. The important materials properties, such as durability, radiations damage resistance or thermodynamical stability, are mainly determined by the atomic-scale processes. Significant experimental [5, 14–22] and theoretical [23–31] efforts and initiatives have been ongoing to characterize properties of potential nuclear waste forms and investigate the mechanisms of their interaction with the disposal environment. Atomistic modeling has been starting to play an important role in these efforts, not only as an effect of increasing availability of computing power, but especially because of no limitation as for the radiotoxicity or form of the investigated materials, which, on the other hand, cause a significant limitations of the experimental techniques [22].

The Nuclear Waste Management Institute (IEK-6) at Forschungszentrum Jülich, Germany, performs fundamental and applied research focused on safe management of nuclear waste. One of the main research scopes is the long-term safety of nuclear waste disposal. Therefore, various aspects of this problem are investigated. These include the corrosion of spent nuclear fuel [32], formation of secondary phases [33, 34], novel nuclear waste forms such as ceramic materials [21, 19, 35] or solid state chemistry of actinides [36, 37], to name but a few. Important new addition to these studies is the utilization of the supercomputers and the state-of-the-art software that have been

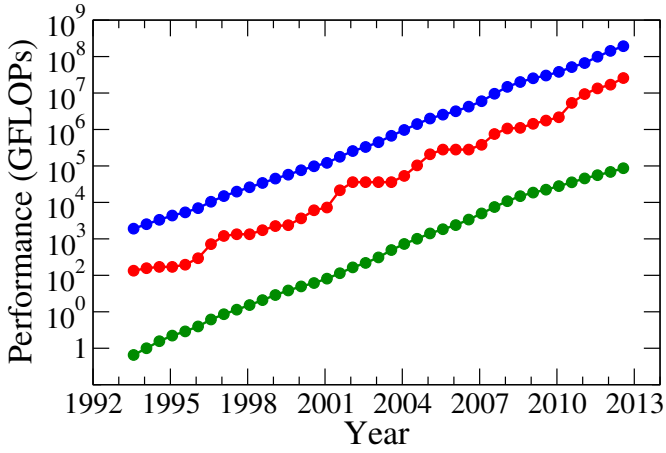

Figure 1.2: Growth of supercomputers performance (red - fastest supercomputer, green - supercomputer on 500th place, blue - combined performance of the 500 largest supercomputers). Data taken from www.top500.org.

becoming extensively used for modeling of various atomic scale and reactive transport processes.

Steady and exponential in time increase in the availability of computing power (Fig. 1.2) has made atomistic simulation methods a popular research tool in various research fields [38–43]. Because of internal complexity of the quantum mechanical equations, first *ab initio* simulations of complex materials, utilizing first principle methods of quantum mechanics, were performed in the last decade of 20th century [44, 38]. The steady increase in the popularity of these methods, which is related to the possibility of simulation of more structurally and chemically complex systems with more powerful supercomputing resources, is reflected by the steady increasing number of relevant scientific publications, as illustrated in Figure 1.3. There is no doubt that this trend will continue in the future and that because of reasoning outlined in the previous paragraph these methods will gain more popularity in actinide-science, including nuclear waste management.

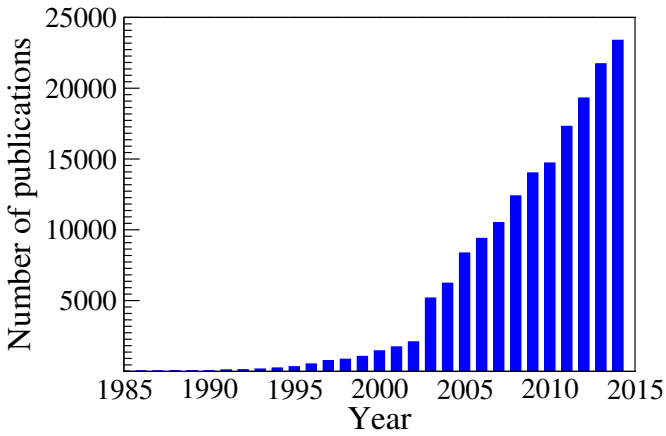

Figure 1.3: Number of scientific publications published every year since 1985 to 2014 which mention DFT. Data taken from ISI Web of Knowledge.

1.2 Current state of the atomistic modeling of f-materials

In the last two decades the *ab initio* methods of computational quantum chemistry have been successfully applied in many research fields [38]. Most of these studies where performed using density functional theory (DFT) which is the most computationally feasible method allowing for simulations of chemically complex systems (currently up to a few hundred atoms). However, containing strongly correlated f electrons, lanthanides and actinides are the most challenging elements for computational quantum chemistry methods. This is especially true for DFT, where its crucial approximations, namely the exchange-correlation functionals, originate from the free electron gas limits and the electronic properties of light elements. Because f electrons are usually packed in large numbers on localized f-orbitals, the correlations between them resulting from strong Coulomb repulsion are often not adequately captured by this method. In addition, different problems arise such as potentially strong relativistic and spin-orbit effects or menagerie of different electronic and magnetic states [45, 46]. Although DFT has been applied for computation of f-elements, including actinides [28–31, 47–

49], various studies have shown that it can fail, even dramatically, for lanthanide and actinide systems [29–31]. For example, it easily fails even on the qualitative level, wrongly predicting metallic state for actinide oxides such as UO_2 (which is a wide gap Mott insulator) [29] (Fig. 1.4). On the quantitative level, the difference between the enthalpies of reactions predicted by DFT and the measured ones, between various uranium-bearing molecular compounds, are highly overestimated by $\sim 100\,\mathrm{kJ/mol}$, a value which is unacceptably large from the experimental and practical point of view [24, 30, 50, 51]. This is especially unfortunate because *ab initio* methods could be precious in estimation of the thermodynamic parameters of actinide-bearing materials, including potential nuclear waste forms.

Because of the failure of DFT, it is often proposed in the literature, that more accurate, higher order, but much more computationally demanding methods of quantum chemistry (eg. hybrid functionals [52], MP2 or CCSD(T) [53]) should be used [30] in *ab initio* modeling of f-electron-bearing materials. Unfortunately, because of bad scaling with the number of modelled electrons (N, scaling N^4-N^7) these methods are in general unfeasible, and will remain so in the next decades, for computation of large and chemically complex systems, which would prevent *ab initio* based simulations of materials that are important for nuclear waste management. As an example, computation of the electronic structure of a ~ 100 atoms containing solid would take half a year for hybrid functionals, 12 years for MP2 and 3 million years for CCSD(T) methods using average size nowadays supercomputing resources (~ 100 CPUs). This shows that DFT or its simple modification to better account for the strong correlations between f electrons and the only reasonable choice as an *ab initio* method for computation of complex, f-elements bearing materials [54–56].

The DFT+U method is a modification of DFT to account for strong electronic correlation using the Hubbard model [58] and is usually applied to d and f orbitals and electrons. In this method an additional term is added to the Hamiltonian [56]. It contains a so called Hubbard U parameter which describes the strength of the on-site Coulomb repulsion between electrons occupying the same d or f orbital. This

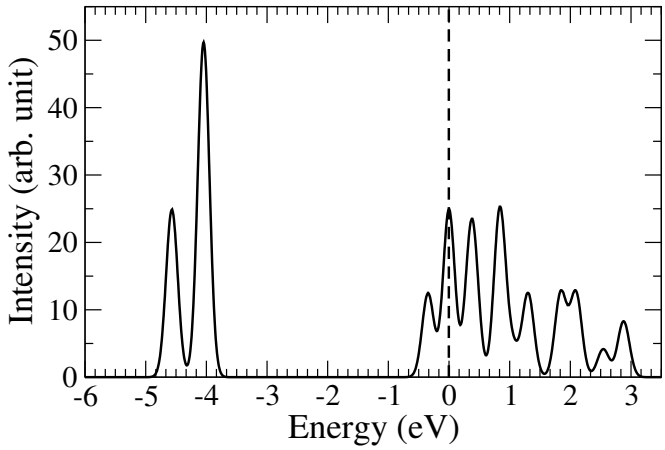

Figure 1.4: Total density of states of UO_2 oxide calculated using regular PBE [57] functional. Fermi level (E_f) is set to zero.

parameter makes the DFT+U method a parameter dependent approach. Usually, the value of this parameter is selected empirically so that the method reproduces certain experimentally measured properties, such as the lattice constants or band gaps, but is usually "guessed" and only rarely estimated basing on the sparsely available experimental data, for instance X-ray photoelectron spectroscopy (XPS) [59–64]. In spite of these potential shortcomings, the DFT+U has been already successfully applied in calculation of actinide-bearing materials. Wen et al. [45] have shown that using the DFT+U method one can correctly model the band gaps of actinide oxides and predict insulating state for these solids. Among others, this method has been successfully used in the description of UO_2 and its metastable states [65, 66], in the calculation of U(VI) aqua complexes on titania particles [50] and in the investigation of incorporation of uranium in the ferric garnet matrices [67]. It was also shown that DFT+U can correctly predict the magnetic state of actinide compounds [68] and full phonon dispersion of strongly correlated materials [69]. Recently, a few methods have been developed and applied to compute the Hubbard U parameters from first principles. The two leading approaches are the constrained local density approximation (cLDA) [70–72], also known as the linear response approach [72], and the constrained random

phase approximation (cRPA) [73–78]. However, at the time of starting these studies, these methods had never been applied to actinide-bearing systems. Application and validation of these methods for prediction of properties of nuclear materials were one of the main tasks of this dissertation studies.

The importance of feasible and reliable modeling nuclear materials was highlighted in a report of the US Department of Energy in 2010 [79]. It postulates the need for a feasible *ab initio* methodology, capable to produce reliable results for systems containing strongly correlated f electrons, which could make reliable simulations of nuclear materials possible. This is also the motivation which initiated this dissertation studies and the results reported here represent an important step towards achieving the postulated goal.

1.3 Aims and outlook of the thesis

The leading goal of this PhD study was to find, validate and apply reliable and feasible *ab initio* methodologies which could be used for modeling of f-element-bearing materials relevant for nuclear waste management. Because the feasibility of a computational method is of the utmost importance, the focus is on the DFT+U method and especially on testing and application of the recently developed *ab initio*-based methods for derivation of the Hubbard U parameters. The derived methodologies were then extensively tested and applied to predict different structural and thermodynamic properties of various nuclear materials, including actinide-bearing complexes and monazite- and pyrochlore-type ceramic waste forms.

The starting point was the systematic benchmarking studies of performance of different DFT functionals and the DFT+U method for uranium-baring complexes for which large sets of relevant experimental data exists [17, 30, 31] and which were also computed using computationally intensive methods such as CCSD(T) [30, 31]. Up to now there have been no systematic test calculations of the structural parameters and the reaction enthalpies of actinide-baring molecules or solids using the DFT+U

method, where the Hubbard U parameter values have been derived *ab initio*, and the extensive studies of the performance of the linear response method [72] presented here are first of such kind [24]. The follow-up studies were performed on molecular complexes of transuranic elements Np, Pu and Am [80]. These calculations showed the dependence of Hubbard U parameter value on oxidation state of the actinide, which has never been found or considered before [24].

For the derivation of the Hubbard U parameters, we mostly used the linear response approach (cLDA) [70–72], which was applied by using the Quantum-ESPRESSO package [81]. However, we also used the cRPA approach [73–78] for the selected systems in order to check the consistence of the two methods, which is sometimes disputed in the literature [77]. For the cRPA calculations we used FLEUR and FLEUR-SPEX codes [82] developed at the Peter-Grünberg-Institute at Forschungszentrum Jülich. These calculations has been performed in close collaboration with the code developers and aimed into comparison of the performance of cLDA and cRPA methods for f-elements, which to our knowledge has not been done before.

Having obtained successful results for actinides with the parameter free DFT+U method, we tested its performance on the structural and thermochemical properties of monazite-type ceramics, considered as potential nuclear waste disposal form. The Hubbard U parameter values were calculated for series of lanthanide orthophosphates (LnPO$_4$, where Ln = La to Dy) [21, 23] and for lanthanide-oxides (Ln_2O$_3$) using both cLDA and cRPA methods. We compared the obtained structural and thermochemical parameters to DFT calculations [28] and available experimental data [83]. Besides the further testing of the DFT+U method, the goal of these studies was also to complement the ongoing experimental research on monazite-type ceramics ongoing at IEK-6 institute and at partner institutions. Excellent results obtained in the scope of our studies allowed for selecting a correct computational methodology which was subsequently used for prediction of various properties of monazite-type ceramics. These studies are now being extended to xenotime-type compounds (LnPO$_4$, where Ln = Tb to Lu).

Testing different computational methodologies helped us in understanding the electronic structure of f-materials and the performance of different computational approaches, which is essential for correct prediction of the thermodynamic parameters of f-element-bearing materials. These parameters such as the excess enthalpies of mixing, the heat capacity or the entropy are useful in the assessment of the stability of different nuclear waste forms under repository conditions. Excellent results have been obtained for the heat capacity of monazite-type ceramics. Although the heat capacities have been measured for many lanthanide monazites, there exist only limited data on the actinide analogues ($An\mathrm{PO}_4$)[84, 85]. Dependence of heat capacity and entropy on the physical and chemical properties of Ln and An cations is also poorly understood [84]. Using density functional perturbation theory [25] we thus computed the heat capacities and the standard entropies of the actinide- and lanthanide-bearing monazite-type ceramics. The results for $Ln\mathrm{PO}_4$ were found to be in an excellent agreement with the existing experimental data and provided complete information on the variation of the heat capacities and entropies along the lanthanide and actinide series [25]. We demonstrated the importance of Schottky contribution arising from the thermal excitations of f electrons for the correct description of heat capacities of these materials [25]. This contribution required the knowledge of the excited states of Ln^{+3} and An^{+3} cations in the considered materials, which were derived as apart of the dissertation studies using the Crystal Field Theory.

The derived methodology was also applied to model properties of the pyrochlore-type ceramics ($\mathrm{A_2B_2O_7}$, where A and B are metallic cations) [27], which are also considered as a potential host matrix for high level waste [1, 15, 86, 87] and are actively investigated at IEK-6 institute. We tried to understand better the order-disorder transition from ordered pyrochlore to disordered fluorite phase, which is responsible for enhanced radiation damage tolerance of some pyrochlore compositions (e.g. $\mathrm{Gd_2Zr_2O_7}$, [15]). Our investigation of the transition temperatures from ordered to disordered phase, resulting in good match of the modeled and computed temperatures, show excellent performance of the parameter free DFT+U method for pyrochlore phases.

Subsequent atomistic modeling studies allowed for derivation of the significantly improved maps of defect (cation antisite and anion Frenkel pair) formation energies in pyrochlore systems and finding interesting correlations of these parameters with the stability field of pyrochlores.

The computational methodologies developed and applied in the scope of this PhD thesis proved to be successful in modeling the properties of lanthanide- and actinide-bearing compounds, including the novel nuclear waste forms. We have shown that by explicit accounting for the electronic correlations, the parameter free DFT+U method gives superior predictions to DFT, being on many occasions well consistent with the experiment. The found that the Hubbard U parameter value can depend strongly on the local coordination and oxidation state of the f-element cation, which indicates the necessity of deriving this parameter from first principles for each considered cation and structure. We hope that the work performed in this project sets path for future progress towards the feasible and reliable modeling of complex materials relevant for nuclear waste management.

Studies reported in this thesis were performed in the recently established (in 2012) at IEK-6 institute Atomistic Modeling research group under direct supervision of the group's leader Dr. Piotr Kowalski. The research of the group focuses on the application of the atomistic modeling techniques and supercomputers for investigation of nuclear materials relevant for nuclear waste management. This dissertation is the first PhD thesis coming out of this group. It resulted in 4 published papers [23–25, 27], including one awarded a front page cover [23], and the obtained results have been acknowledged by the poster prize awarded at Goldschmidt2015 conference by the European Mineralogical Union to the author. The research has been performed mainly using the supercomputing resources provided within Jülich-Aachen Research Alliance-High Performance Computing (JARA-HPC) [88]. In particular, Forschungszentrum Jülich JUQUEEN, JUROPA, JURECA, RWTH Aachen Bullx and Dortmund LIDO supercomputers were used for the calculations.

Chapter 2

Computational Methods

In this chapter we discuss the different methods that have been tested and applied in this thesis. In particular we discuss the status of the *ab initio* methods of computational quantum chemistry and materials science, focusing on the density functional theory (DFT) and the DFT+U method, which is an extension of DFT that improves the description of the strongly correlated (f-) electrons and which we extensive testing was a leading goal of this thesis. In addition we discuss all the modeling methods that have been used in the execution of the applied part of this dissertation research.

2.1 An overview of the wave function-based *ab initio* methods

The ultimate goal of most of the quantum chemical calculations is to compute the total energy, E, of an atomic system, which can be done by solving the time-independent Schrödinger equation:

$$\hat{H}\Psi = E\Psi \tag{2.1}$$

where $\hat{H}$ is the Hamilton operator of the system, which contains all the interactions between the N electrons and the M nuclei that constitute the considered system, and Ψ is the N electrons wave function which depends on 3N spatial and N spin coordi-

nates of the electrons and 3M coordinates of the nuclei. Although the Schrödinger equation gives an exact description of the system, because it requires integrations in the multi-dimensional space, solving it for atoms heavier than lithium is a very complicated and computationally demanding task. In order to make a feasible calculations one has to use approximate Hamiltonians, try to simplify the wave functions or use alternative approaches (such as the Density Functional Theory (Section 2.2)) [89, 90]. One of the widely known approaches to find an approximate wave function is the Hartree-Fock method (HF) [91], in which the many-electron wave function is approximated by a Slater determinant constructed from a set of one electron wave functions. This method describes electrons as being independent and interacting with other electrons through an average mean field produced by the other electrons. The calculations are performed using the variational principle [92] to find the best Slater determinant which minimizes the energy [53]. The energy obtained from the Hartree-Fock method is always larger than the exact ground state energy of a considered system because applying a single electron approximation it does not account for the electronic correlations, which lower the energy. The difference between the Hartree-Fock and the real energies is thus called as *the correlation energy* [53]. There are various wave functions based *ab initio* approaches which try to account for correlations. One of these methods is Configuration Interaction (CI) approach [90], in which the trial wave function is written as a linear combination of determinants with the expansion coefficients chosen by the requirement that the total energy is a minimum. If we include all possible determinants, we will have a so called 'full CI' wave function, which will give a correct correlation energy and will be exact. Unfortunately, the factorial growth of the number of determinants makes it usable only for only small systems. Even calculating a single water molecule with 10 electrons will require diagonalizing very large matrices of size 30046752×30046752 [53], which is barely manageable on current computing resources. If one reduces the number of excited determinants in the wavefunction and includes only single, double and/or triple excitations (CIS, CISD, CISDT), one can make this approach more feasible, with the CISDT method still scaling with the eighth power of

the system size (as N^8), while the regular Hartree-Fock calculations, that are already computationally demanding, scale with only the fourth power (as N^4) [53].

Another post Hartree-Fock approach uses the Møller-Plesset perturbation theory [93]. In this method, the Hamilton operator is modified and divided into the reference and the perturbation parts. The reference Hamiltonian consists of one-electron Fock operators, and the electron correlations are computed as a perturbation of the zero-order reference Hamiltonian (Hartree-Fock solution). Subsequent applications of the second order perturbations results in the MP2, MP3 and MP4 approaches. Convergence of these methods is usually extremely slow due to the scaling from fifth to seventh power (as $N^4 - N^7$) [53].

The coupled cluster (CC) method [94] is an alternative post-HF approach which tries to fully account for the electron correlation effects. In this approach, the wave function of a system is re-written as an exponent of Slater determinants in the power of a cluster operator [53]. However, the cluster operator must be truncated to make this method feasible at least for small systems. Similar to the CI methods, single, double and/or triple excitations (S, D, T, Q) are usually included and the CCSD(T) is the most accurate method used in this theory, although the scaling with the size of the system (seventh power) remains the limiting factor preventing using this method on larger scale.

There are several commercial and academic codes which can perform HF and post-HF calculations: NWchem [95], Gaussian [96], CP2K [97], MOLPRO [98], FLEUR [82], GAMESS [99] and TURBOMOLE [100], to name but few. The majority of these programs are written in the FORTRAN programming language [101], which we also used for scripting purposes. Even though the listed post-HF methods could provide very accurate results for geometries and energetics of various materials [53], due to the unfavorable scaling of these methods with the system size, these approach can be applied to molecular complexes containing no more than 100 electrons, which is way to small for calculations of actinide-bearing solid systems. Application of these methods the modeling of nuclear waste related materials is thus extremely limited.

An alternative and more computationally feasible *ab initio* method that is equivalent to solving the Schrödinger equation is the Density Functional Theory (DFT). It is based on using the electron charge density - a function of only three spatial variables - instead of the more complex wave function [92]. This method will be explained in the next section.

2.2 Density Functional Theory

The Density functional theory (DFT) dates itself back to 1920's, i.e. the founding years of quantum mechanics, when Thomas and Fermi formulated the kinetic energy of the electronic system as a function of the electron density [92, 102, 103]. However, the Thomas-Fermi model was not successful in chemical applications, failing to reproduce the shell structure of atomic electronic configurations. This failure is mainly due to insufficient description of kinetic energy and the electron correlation effects [92]. Nevertheless, in 1951 Slater [104] described the exchange contribution to the Hartree-Fock representation using only the electron density.

In 1964 Hohenberg and Kohn [105] published a notable paper connecting the charge density of the electronic system to its wave function by postulating and proving two simple, but of extreme importance, theorems. First Hohenberg-Kohn theorem shows that the external potential V_{ext} of the system is a unique functional of the electronic charge density ($\rho(\mathbf{r})$). Thus it shows that the ground state charge density also uniquely determines the Hamiltonian of the system and its ground state. Hohenberg and Kohn defined the functional $F_{HK}[\rho]$ as:

$$F_{HK}[\rho] = T[\rho] + E_{ee}[\rho] = \langle \Psi | T + V_{ee} | \Psi \rangle, \tag{2.2}$$

where $T[\rho]$ is the kinetic energy functional, $E_{ee}[\rho]$ is the functional that describes the electron-electron repulsion, V_{ee} is the electron-electron repulsion operator and Ψ is the ground state wave function of the system. DFT is, in principle, an exact and equivalent

to the Schrödinger equation theory and the knowledge of $F_{HK}[\rho]$ would be equivalent to the solution of the Schrödinger equation (Eq. 2.1) [92]. But the exact expression for the constituting functional, including $T[\rho]$, is unknown. From the electron-electron repulsion functional only the classical part, $J[\rho]$, can be described explicitly:

$$E_{ee}[\rho] = J[\rho] + E_{ncl}[\rho]. \tag{2.3}$$

The non-classical part E_{ncl} in the Eq. 2.3 is an unknown and contains the self-interaction correction, exchange and Coulomb correlation effects.

The second Hohenberg-Kohn theorem uses the variational principle to prove that the functional $F_{HK}[\rho]$, which delivers the ground state energy of the system, does so only if the input ρ is the true ground state density [105], showing uniqueness of the ground state density. Even though these two theorems prove the existence of the connection between the ground state density and the wave function of the system, they do not give us a pathway to construct the functional F_{HK}.

The issue of the unknown functional describing the ground state properties of the system was addressed by Kohn and Sham [106]. In their 1965 publication, the authors introduced the idea of a non-interacting reference system (similar to the Hartree-Fock approach). Kohn and Sham [106] approached the problem of unknown form of the kinetic energy by proposing $T[\rho]$ to be the same as the one for the non-interacting system, $T_s[\rho]$. They defined the exchange-correlation functional as

$$E_{XC}[\rho] = (T[\rho] - T_S[\rho]) + (E_{ee}[\rho] - J[\rho]) = T_C[\rho] + E_{ncl}[\rho]. \tag{2.4}$$

This functional contains all the unknown parts in DFT: the residual part of the kinetic energy T_C and the already mentioned E_{ncl}. In the Kohn-Sham formalism, the energy functional of the real system is expressed as:

$$E[\rho(\mathbf{r})] = T_S[\rho] + J[\rho] + E_{XC}[\rho] + E_{Ne}[\rho] \tag{2.5}$$

Only term which has no explicit form is E_{XC} Numerous approximations of this exchange-correlation energy exist [57, 107–117], but current state of the research indicates that there is no straightforward way to improve the functional or to find its exact form.

2.2.1 Exchange-Correlation functionals

Kohn and Sham [106] themselves proposed the form of the exchange-correlation functional called Local Density Approximation (LDA). This approximation is based on uniform electron gas, which is a system of electrons moving in a positively charged background and which is the one of the few cases for which the exact quantum mechanical solution is known. The E_{XC} is expressed as

$$E_{XC}^{LDA} = \int \rho(\mathbf{r})\varepsilon_{XC}(\rho(\mathbf{r}))d\mathbf{r}, \tag{2.6}$$

where ε_{XC} is the exchange-correlation energy per unit volume of the uniform electron gas. In LDA, the exchange part of the energy functional is similar to the Slater's description, only the pre-factor is different. The correlation part of the functional was analytically derived based on quantum Monte-Carlo simulations of the uniform electron gas [92]. Widely used LDA functional, VWN was developed by Vosko et al. [107] in 1980. It is a good starting approximation and performs well for atoms and molecules and gives good results for the systems with the slowly varying density. Despite many successes the LDA has some notable drawbacks such as strong overbinding and thus had a wider use in solid state physics, where electrons are more delocalized, than in computational chemistry [92]. In general LDA is not enough for accurate description of the real chemical systems and an extension has been proposed. First step was to implement the gradient of the charge density in construction of the relevant functionals, i.e. to explicitly account for the spacial variation of the electronic charge density. Such a Generalized Gradient Approximation (GGA) could be realized

in the following way:

$$E_X^{GGA} = E_X^{LDA} - \beta \sum_\sigma \int \frac{(\nabla \rho_\sigma)^2}{\rho_\sigma^{4/3}}, \tag{2.7}$$

where different β parameters values were suggested over the years by Becke [108] and others [109–114]. Other form of the GGA exchange functional was suggested by Perdew [115] and simplified by Perdew and Wang [116, 117]:

$$E_X^{GGA} = -\frac{3}{4}(\frac{3}{\pi})^{1/3} \int \rho^{4/3} F_X(s) d\mathbf{r}, \tag{2.8}$$

where the reduced electron density, s, is equal to:

$$s = \frac{|\nabla \rho(r)|}{2\kappa\rho}, \tag{2.9}$$

and the exchange energy functional enhancement function is described as

$$F_X(s) = (1 + 1.296s^2 + 14s^4 + 0.2s^6)^{1/15} \tag{2.10}$$

and

$$\kappa = (3\pi^2\rho)^{1/3}. \tag{2.11}$$

In 1996 Perdew et al. [57] proposed a simplified and more computationally stable form of the enchancement function, $F_X(s)$, as

$$F_X(s) = 1 + \kappa - \frac{\kappa}{1 - \mu s^2/\kappa}, \tag{2.12}$$

with κ=0.0804 and μ=0.21951. This approach, known as PBE, is currently the most widely used DFT exchange-correlation functional.

Usually, the different forms of the exchange-correlation functionals are dictated by their ability to reproduce certain results [92]. The fact that by switching to a different GGA functional one can improve the prediction of the reaction enthalpies at a cost of worsening the structural parameters and vice versa, is a known shortcoming

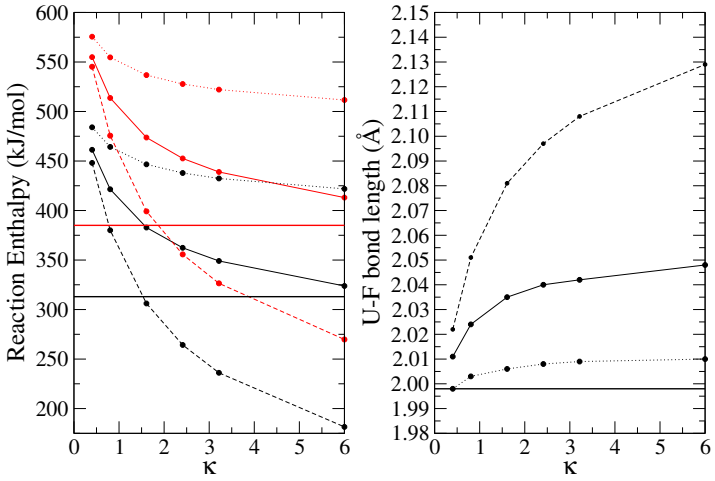

Figure 2.1: Left panel: The enthalpies of dissociation reactions of UF_6 molecule (red, upper set of curves) and UF_5 molecule (black, lower set of curves) computed with the PBE-like functionals and different values of κ (horizontal axis) and μ =0.109755 (dashed lines), 0.21951 (solid lines, PBE) and 0.43209 (dotted lines). μ and κ determine the enhancement function of the exchange functional (see Eq. 2.12). Right panel: the $U - F$ bond length of UF_6. The different results are marked using the convention applied in right panel. On both panels, the horizontal lines indicate the experimental values.

of today's exchange-correlation functionals. Such behavior was investigated in this work by computing the U-F bond length in UF_6 (uranium hexafluoride) molecule and the dissociation enthalpies of UF_6 and UF_5 (uranium pentafluoride) molecules with a modification of PBE functional [24] (See Section 3.2.1).

PBEsol functional used in this theses is a PBE-like functional with $\mu = 10/81 = 0.123456789$, which was derived from the exact solution for the slowly varying electron density limit [118]. Another functional used in this work is BPBE [119, 57], which differs from PBE functional only by the exchange part (they have the same PBE correlation energy functional [57]). Especially instructive is the mixture of the BPBE and PBE results, labeled as PBE-BPBE corr., which will also be discussed in Section 3.2.1.

In this dissertation we also attempted a modification of the PBE functional, hereafter we call such a new function the "*modified* PBE", to make better prediction for

the U-F bond length in UF_6 and the dissociation enthalpies of UF_6 and UF_5 molecules. The modification was made by treating κ (PBE value of 0.804) and μ (PBE value of 0.21951) parameters of the exchange energy functional enhancement function $F_{\mathrm{x}}(s)$ (Eq. 2.12, [57]) as free parameters., The result is given in Figure 2.1. It is clearly seen that the smaller μ results in a better bond length. In fact, this result with μ being half the value of that of the PBE functional, which closely resembles the case of PBEsol functional [118], gives better U-F bond length than PBE. On the other hand, the computed reaction enthalpy become worse and it can not be easily improved by just modifying κ. For a fixed value of μ, increase of κ always leads to better description of the reaction enthalpies, but at a cost of worsening the bond length. The larger the μ, the worse the U-F bond length that results in good enthalpy, is. In the subsequent sections we will show the performance of the *modified* PBE functional, where keeping the PBE value of $\mu = 0.21951$ we set κ to 6. Such set of parameters was chosen because it results in relatively good prediction of the dissociation enthalpies of UF_6 and UF_5 molecules, which is indicated in Figure 2.1.

2.2.2 Hybrid functionals

The other types of DFT functionals used in the literature are the so called hybrid functionals in which the Hartree-Fock theory and the DFT are combined. They incorporate the part of the exact exchange from the first theory and the number of exchange and correlation density functionals. The most popular hybrid functional is the B3LYP functional [120], which has the following form:

$$E_{XC}^{B3LYP} = (1-a)E_X^{LSDA} + aE_X^{HF} + bE_X^{B88} + cE_C^{LYP} + (1-c)E_C^{VWN,} \tag{2.13}$$

where a=0.20, b=0.72 and c=0.81 are the mixing weights of different functionals that were fitted empirically to to reproduce the selected properties of molecular systems. In Equation 2.13, LSDA (the local spin density approximation), the standard exchange functional [92], the VWN [107] correlation functional, the Becke exchange functional

(B88) [119] and the LYP correlation functional Lee et al. [121] are used. The other widely used hybrid functional is the PBE0 functional [57, 122] which is a non-empirical, parameter-free functional designed basing on the theoretical consideration. This hybrid functional mixes the PBE [57] correlation energy with the PBE and HF exchange energies:

$$E_{XC}^{PBE0} = E_{XC}^{PBE} + 0.25(E_X^{HF} - E_X^{PBE}). \tag{2.14}$$

In fact, the most of the meaningful DFT studies of actinide-bearing materials were performed using the hybrid functionals such as B3LYP, PBE0 or HSE [46, 123–126]. However, the usage of these types of functionals or any post-Hartree-Fock method requires substantial computational resources. This limits the applicability of these methods to the simplest molecular compounds and solids, although it can improve in the in coming decades with increasing in the available computational power. Materials that are interesting for nuclear engineering have usually complex chemical compositions and structures with supercells containing often more than hundred atoms. This is especially true when solid solutions with diluted concentration of elements are of interest [21, 26]. Therefore, we found the hybrid functionals unfeasible for our purposes.

2.3 Plane-waves and pseudopotentials

All *ab initio* methods use known functions called "basis sets" that are used in the construction of the approximations to the unknown wavefunctions functions such as molecular orbitals. Most of the post-Hartree-Fock-based codes listed in previous section use two types of atomic orbitals: Gaussian Type Orbitals (GTO) or Slater Type Orbitals (STO). In general, functional form of STO makes them superior to GTOs. This is because three times more GTOs are needed to achieve the same accuracy as with STOs. However, calculation of the required integrals in case of the former orbital functions are easier and more computationally efficient. Therefore, GTOs are more often used in quantum chemical codes [53].

For the extended systems such as solids, plane waves are usually used as basis sets, since the outer valence electrons in metals behave similarly to free electrons and plane waves are the solutions of the Schrödinger equation for a free moving electrons. The plane waves can also be applied for modeling molecular systems using a supercell approach, in which the molecule is placed in a large-enough unit cell so that it does not interact with its image in the neighboring cells [92]. For condensed systems such as solids it is favorable to use plane waves rather than GTOs or STOs, since the number of plane waves depends only on the size of the periodic cell and not on the number of atoms in the cell.

When representing the wave functions of valence electrons with a plane wave basis set, large oscillations occur near the core region, giving rise to the significant kinetic energy. Very large number of plane-waves will thus be needed to correctly model this behavior. This problem is even more pronounced in case of the heavier elements such as lanthanides and actinides. Fortunately, only the electrons in the outer shells determine the nature of chemical bonding in molecules and crystals. Thus, one can divide the electrons into core valence ones and replace the effects of their presence by a modified interaction potential (Fig. 2.2). Such a potential is called an effective core potential (ECP) or a pseudopotential. The idea of pseudopotentials was introduced independently by Hellmann [127], Fermi [128] and Gombas [129] in 1930s. The method was later extended to systems with many-valence electrons by Weeks and Rice [130].

By using pseudopotentials, one reduces the computational time needed for the calculations of solids by reducing the number of electrons that required explicit computation and terms which are required for the plane wave description of the wave function [131]. Furthermore, the relativistic effects can be included in the pseudopotential and be even better addressed than by all-electron calculations [132].

In the plane wave codes, most frequently used pseudopotential types are the norm-conserving [133] and the ultrasoft [134, 135] pseudopotentials. In the norm-conserving pseudopotentials the total valence electron density within the core radius equals to the density in the all-electron case. For ultrasoft pseudopotentials this constrain is

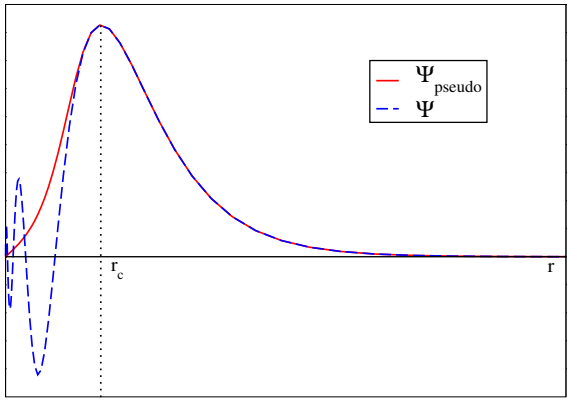

Figure 2.2: Schematic plot of pseudopotential. The blue line represents the all-electron function and the red line - pseudopotential approximation.

removed which results in smaller number of plane-wave basis that have to be used, which substantially saves the computational time [131].

The pseudopotentials are generated using the *ab initio* atomistic calculations and usually number of test calculations are necessary to check their quality. Several software packages exist for building different types of pseudopotentials. The one used by us to generate the ultrasoft pseudopotentials has been developed by Vanderbilt [134].

Studies of Shamov et al. [30], Schreckenbach and Shamov [31] and Odoh and Schreckenbach [136] indicate that the results of calculations of different actinide-bearing systems can also depend on the number of core-electrons modeled by pseudopotentials and that at least 32 electrons of uranium atom ($5s^2 5p^6 5d^{10} 6s^2 6p^6 5f^3 6d^1 7s^2$) should be treated explicitly, which increases the computational cost. However, it has to be noted, that this result is still in dispute. For instance, Iche-Tarrat and Marsden [51] have shown that the explicit treatment of 32 electrons of uranium atom only marginally improves the performance of either DFT or hybrid-DFT functionals over the case when only 14 valence electrons of uranium ($6s^2 6p^6 5f^3 6d^1 7s^2$) are treated explicitly. Results reported in this dissertation studies implicitly support the later conclusion. In our studies the core electrons of the computed atoms were replaced by the ultrasoft pseudopotentials [134]. In case of actinides, $6s^2 6p^6 5f^3 6d^1 7s^2$ electrons

of uranium atom, $6s^2 6p^6 5f^4 6d^1 7s^2$ electrons of neptunium atom, $6s^2 6p^6 5f^6 7s^2$ of plutonium atom and $6s^2 6p^6 5f^7 7s^2$ electrons of americium atom were treated explicitly. Such pseudopotentials are referred to as *"large core pseudopotential"*.

Considering other type of pseudopotentials-based approaches, one of the simplest approaches to calculate the electronic structure of a solid is to solve the Schrödinger equations for the one-atom unit cells inside the solid and at the boundary of these cells to match the atomic functions with each other. To achieve this, one can use the augmented plane waves, which contain atomic functions in the atomic spheres and a single plane wave outside of it. The FLAPW method is considered as one of the most accurate approaches for band-structure calculations [137]. Several quantum chemistry codes (FLEUR [82], WIEN2k [138], ELK [139]) use a so called full potential linearized augmented plane wave (FLAPW) method [140], which is considered to be one of the most accurate methods for performing electronic-structure calculations.

2.4 DFT+U formalism

Characteristic properties of f-electrons bearing materials are determined by the partially filled f-shell of these elements. The standard model based on the properties of free electron gas is thus not suitable to describe the correlation effects in these strongly correlated electronic systems exibiting narrowly laying energy bands. A so called DFT+U method, an extension of DFT, has been proposed to cure the inadequate description of strongly correlated materials by the standard DFT approximations [141–144].

The DFT+U approach is based on a model proposed by Hubbard [58], in which the on-site repulsion between electrons is described by the Hubbard U parameter. The method was initially designed for the s-bands [58] and was later extended to more challenging cases of d- and f-electrons [145–149]. The model was implemented in DFT after Anisimov et al. [141, 142] and Solovyev et al. [143] suggested adding an energy correction term to the energy functional and applied them successfully to transition

metal oxides. The total energy functional in DFT+U is given as

$$E_{DFT+U}[\rho, n^\sigma] = E_{DFT} + E_U[n^\sigma] = E_{DFT}[\rho] + E_{Hub}[n^\sigma] - E_{dc}[n^\sigma], \tag{2.15}$$

where n^σ is the given (f-) orbital occupation matrix, σ is the spin of electrons and E_{DFT} is the approximate DFT energy functional. The correction term, E_U, is divided into two terms, where E_{Hub} contains the Hubbard Hamiltonian, which describes the correlated states [150]. The *double-counting* term, E_{dc}, is a mean-field approximation to E_{Hub} and describes the part of the electron correlations that is already accounted for by DFT [144, 151]. The more general, rotationally invariant form of E_{Hub} and E_{dc} term is given by Liechtenstein et al. [152]:

$$\begin{aligned} E_{Hub}[n] = \frac{1}{2}\sum_{m,\sigma}(&< m, m''|V_{ee}|m', m''' > n^\sigma_{mm'} n^{-\sigma}_{m''m'''} \\ &+ (< m, m''|V_{ee}|m', m''' > - < m, m''|V_{ee}|m''', m' >) n^\sigma_{mm'} n^{-\sigma}_{m''m'''}), \end{aligned} \tag{2.16}$$

$$E_{dc}[n^\sigma] = \frac{1}{2}Un(n-1) - \frac{1}{2}J[n^\uparrow(n^\uparrow - 1) + n^\downarrow(n^\downarrow - 1)], \tag{2.17}$$

where m is a state index and V_{ee} integrals represent the screened Coulomb interaction between two electrons on the localized orbital. n^σ=Tr($n^\sigma_{mm'}$), $n = n^\uparrow + n^\downarrow$ and U and J parameters represent the strength of the screened Coulomb and exchange interactions [152, 71]. In terms of the spherical harmonics, the V_{ee} integrals can be written as:

$$< m, m''|V_{ee}|m', m''' >= \sum_k a_k(m, m', m'', m''')F^k, \tag{2.18}$$

where F^k are the radial Slater integrals describing the electron-electron interaction and a_k are the so called Clebsch-Gordan coefficients [150]. The parameters that describe the on-site Coulomb and exchange interactions can be expressed by the Slater integrals:

$$U = \frac{1}{(2l+1)^2}\sum_{m,m''} < m, m''|V_{ee}|m, m'' >= F^0 \tag{2.19}$$

and

$$J = U - \frac{1}{2l(2l+1)} \sum_{m,m''} [< m, m''|V_{ee}|m, m'' > - < m, m''|V_{ee}|m'', m >)] \\ = F^0 - \frac{286F^2 + 195F^4 + 250F^6}{6435} \quad (2.20)$$

where l=3 for f-electron-bearing systems [144]. For the simplified case, to estimate the F^0 one can, for instance, use the value of the band gap in the case of Mott system (eg. UO_2) and the higher order Slater integrals can be estimated from fitting the atomistic calculation to the experimental spectroscopic data [153].

More simplistic form of the DFT+U correction term was proposed by Dudarev et al. [154] and implemented first by Shick et al. [155] and later adjusted by Cococcioni and de Gironcoli [72]. In this approach, the higher order Slater integrals, F^2, F^4 and F^6 are set to 0 and the energy correction term E_U is described simply as

$$E_U = E_{Hub} - E_{dc} = \sum_{l,\sigma} \frac{U_{eff}}{2} Tr[\mathbf{n}^{l,\sigma}(1 - \mathbf{n}^{l,\sigma})] \quad (2.21)$$

where $U_{eff} = U - J$ is the *effective* screened Coulomb parameter that is assumed to account for the exchange term [151, 154]. This approach we have used in our calculations by the linear response method [72].

2.4.1 *Ab initio* calculation of the Hubbard U parameter values

The successful application of the DFT+U method depends on the good choice or the accurate derivation of the Hubbard U parameter. There are several ways that could be used to obtain the desired value of this parameter. One way is to reproduce certain experimental observable of a system, such as the band gap, the lattice constants, or the formation energies. But such cases, the predictive power of the method could be limited due to specific choice of the Hubbard U parameter. The best and most reliable

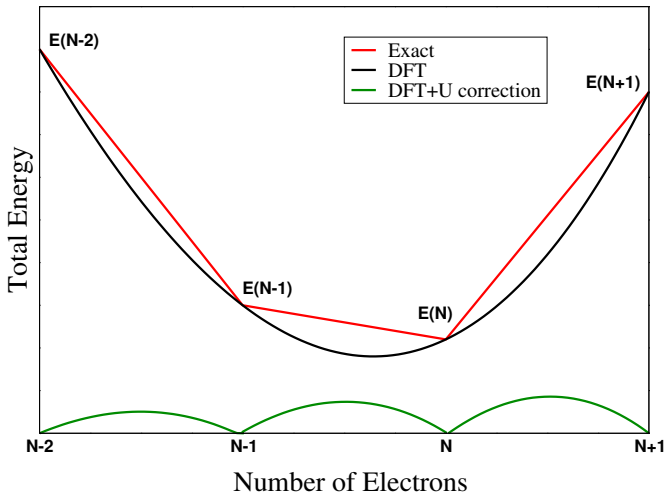

Figure 2.3: Total energy profile of the system as a function of the number of electrons. The red lines represent the exact energy of the system, the black lines - the DFT energy and the green line - the difference between the two.

way to obtain the Hubbard U parameter values is to calculate them *ab initio*. There are two main methods to calculate the Hubbard U parameters from the first principles. First one is the constrained local density approximation (cLDA) [70–72], which has been frequently used throughout this work. The second method, the constrained random phase approximation (cRPA) [73–78] was also utilized in order to validate the calculated Hubbard U parameter values obtained by the cLDA approach and to have a better understanding of the differences between and the reliability of the two methods in case of f electrons, which is still to great extend an unexplored research topic. In theory, both methods should give the same Hubbard U parameter values, but because of the differences in the ways they are implemented, significant divergences between the values derived using these two methods have been previously reported [77].

One of the recently introduced ways to calculate the Hubbard U parameter value is cLDA, also called the *linear response* method (hereafter, we will call the so derived U parameter values as U_{LR} and the method a DFT+U_{LR}) following Cococcioni and de Gironcoli [72]. This approach is implemented in the Quantum-ESPRESSO package

[81] - a plane waves and pseudopotentials-based DFT code utilized in our research. The *linear response* method offers an intuitive and straightforward approach to calculate the U parameter values. It is based on the idea of improving the regular DFT description of the total energy profile of the open system (system where an atom A can exchange the electrons with an atom B). The correct total energy depiction of this open system, or energy in case of the fractional charges, can be visualized by the straight lines connecting the energies of states with different number of electrons and discontinuities for the integral charges, whereas the DFT calculation results a continuous change of energy as a function of charges and introduction of an artificial curvature (Fig. 2.3) [156, 157]. DFT thus underestimates the derivatives of the total energy as a function of charge density which results in incorrect description (underestimation) of the fundamental gap of the computed system [72]. The difference between the two lines on the Fig. 2.3 can be seen as the correction of the DFT energy represented by the Eq. (2.21), where the U parameter value is equal to the artificial curvature of the DFT energy. In order to calculate the Hubbard U parameter value one needs thus to obtain the second derivative of the energy of the system with respect to the occupations of the localized states and subtract the second derivative of the energy of the perturbed, non-interacting system computed with the same ground state charge density

$$U = \frac{d^2 E^{DFT}[n_f]}{d(n_f)^2} - \frac{d^2 E_0^{DFT}[n_f]}{d(n_f)^2}, \tag{2.22}$$

where E^{DFT} and E_0^{DFT} are the total energies of the real system and non-interacting systems, respectively [72].

In the actual calculations performed in these dissertation studies, a perturbation with an amplitude α is applied to the external potential of an atom acting on a f orbital at site I

$$V_{ext}^P = V_{ext} + \alpha \sum_{m=-3,3} |\varphi_m^I\rangle\langle\varphi_m^I|. \tag{2.23}$$

After solving the Kohn-Sham equations for various values of α one can obtains the

amplitude dependent ground state energy

$$E(\alpha) = min_{\rho}\{E^{DFT}[\rho] + \alpha n_f^I\}. \tag{2.24}$$

Then, from Eq. (2.24) by using the Legendre transformation [158], one obtains the occupations dependent energy

$$E(n_f^I) = min_{\alpha}\{E[\alpha] + \alpha n_f^I\}, \tag{2.25}$$

from which the second derivatives of the energy with respect to the occupations can be derived

$$\frac{d^2E}{dn_f^2} = -\frac{d\alpha}{dn_f}. \tag{2.26}$$

In the *linear response* calculations using the Quantum-ESPRESSO code [81], the Kohn-Sham equation is solved for various different α shifted systematically from 0 and the changes of n_f^I are monitored. These values are stored in the response matrix

$$\chi_{IJ} = \frac{dn^I}{d\alpha^J}, \tag{2.27}$$

where I and J are the site indices that label the atom to which the perturbation α is applied. To obtain the Hubbard U value one needs to subtract the obtained response matrix with the one computed for the non-interacting system (Eq. (2.22))

$$U = \frac{d\alpha^I}{dn_{f0}^I} - \frac{d\alpha^I}{dn_f^I} = (\chi_0^{-1} - \chi^{-1})_{IJ}. \tag{2.28}$$

To obtain the exchange parameter J by the same method, the *linear response* method was further improved by Himmetoglu et al. [159]. The response of the on-site magnetization $m = n \uparrow - n \downarrow$ with respect to a magnetic perturbation βm is considered. Similar to the U calculation, the exchange parameter J is obtained as

$$J = -2[(\chi^0)_{II}^{-1} - (\chi)_{II}^{-1}], \tag{2.29}$$

where the response matrix χ can be expressed as

$$\chi_{IJ} = \frac{\partial m^I}{\partial \beta^J} \tag{2.30}$$

and χ^0 is the bare response matrix of the non-interacting Kohn-Sham system and could be obtained in a similar way as χ.

The direct calculation of the Hubbard U parameter can be also performed using the constrained Random Phase Approximation (cRPA) approach [73–78]. This method allows the determination of individual elements of the Coulomb matrix, but is more computationally intensive than the linear response method [160]. In this method, the fully screened Coulomb interaction W is given as

$$W = \frac{v}{1 - vP}, \tag{2.31}$$

where v is the bare Coulomb interaction and P is the polarization function [144, 75, 161]. After dividing the Hilbert space in two, f (where the narrow f band is located) and r (the rest of the bands) subspaces, the polarization function P is divides in two parts

$$P = P_f + P_r. \tag{2.32}$$

where P_f contains the transitions between the f orbitals only and P_r is the rest of the polarization [144, 75]. The effective interaction between the electrons in the narrow energy band can be expressed as

$$W_r = \frac{v}{1 - vP_r}. \tag{2.33}$$

Multiplying W_r with the localized basis functions and integrating over space yields the following effective screened Coulomb interaction [162]:

$$U_{mm'';m'm'''} = \int\int \omega^*_m(\mathbf{r})\omega_{m''}(\mathbf{r})W_r(\mathbf{r},\mathbf{r}')\omega^*_{m'''}(\mathbf{r}')\omega_{m'}(\mathbf{r}')drdr', \tag{2.34}$$

from which the on site Hubbard U and J parameter values can be derived using the following formulas [160]:

$$U = \frac{1}{L^2} \sum_{m,m'=1} U_{mm',mm'} = F^0 \tag{2.35}$$

and

$$J = \frac{1}{L(L-1)} \sum_{m \neq m'=1} U_{mm',m'm}, \tag{2.36}$$

where L=7 in case of the f-orbitals and F^0 is the previously mentioned Slater integral (Eq. 2.19). We note that the derivation of the Hubbard U parameter value using cRPA depends strongly on the choice of the energy window in which the localized orbital basis (Wannier orbitals [163] in this case) is formed [164].

The cRPA calculations reported here were performed using SPEX [165] code. In this code the maximally localized Wannier functions (MLWFs) [162, 166–168] are internally constructed. The FLEUR [82] code, which uses full-potential linearized augmented-plane-wave (FLAPW) method [169] was used for the initial ground state calculations.

Several studies report calculation of the Hubbard U parameter values using cRPA method, mostly for d- but a few for f-electrons-bearing materials [77, 160, 162, 164, 170, 171]. However, up to now, only few of these studies directly compare the results of cLDA and cRPA approaches. We note that discrepancies between the Hubbard U parameter values calculated using cLDA and cRPA methods were observed towards the end of the $3d$ element series by Aryasetiawan et al. [77].

2.5 Computing heat capacities of f-materials

Vibrational contribution to the heat capacity can be estimated after calculating full phonon dispersions. In this work the density functional perturbation theory (DFPT) [172] was used for estimation of the phonon frequencies and the density of states using

the Quantum-ESPRESSO package [81]. The heat capacity can be expressed as:

$$C_V = \sum_q k_B (\frac{\hbar\omega_q(V)}{2k_BT})^2 cosh^2(\frac{\hbar\omega_q(V)}{k_BT})^2, \tag{2.37}$$

where k_B is the Boltzmann constant $\hbar$ is the reduced Planck constant and $\omega_q(V)$ is the frequency of the phonon with the wave vector q at constant volume V [173]. Accurate description of the heat capacities and entropies of the f-element-bearing systems requires consideration of the thermal excitation of f-electrons by computing the so called Schottky contributions [84, 174, 175]. The Schottky term is given by

$$C_{exs} = Q^{-1}R^{-1}T^{-2}\sum_i g_i\epsilon_i^2 \exp(-\epsilon_i/RT) \\ - Q^{-2}R^{-1}T^{-2}(\sum_i g_i\epsilon_i \exp(-\epsilon_i/RT))^2, \tag{2.38}$$

where

$$Q = \sum_i g_i \exp(\epsilon_i/RT) \tag{2.39}$$

is the partition function, ϵ_i is the energy of i-th excited state of degeneracy g_i, R is the gas constant and T is the temperature. The excess contribution to the entropy is given by:

$$S_{exc} = RQ^{-1}T^{-1}\sum_i g_i\epsilon_i \exp(-\epsilon_i/RT) + R\ln(Q). \tag{2.40}$$

Here, the code LANTHANIDE [176] was used for calculating the energy levels of Ln^{3+} and An^{3+} ions by constructing the relevant Hamiltonian and diagonalizing the matrix containing all allowed electronic states for a certain configuration. In general, the commonly used Hamiltonian of the rare-earth cations [177] consists of spherical, non-spherical and crystal field parts:

$$H = H_s + H_{ns} + H_{cf} \tag{2.41}$$

The non-spherical part of the Hamiltonian (H_{ns}) contains the electrostatic parameter, the spin-orbit interaction constant and the two and three body interaction terms [177, 176] (Judds and Trees parameters [178, 179]). All these parameters can be found in the literature for specific ions of interest [180, 181].

The crystal field effect [180] gives rise to the last term, H_{cf}, in the Eq. 2.41 which can be described as

$$H_{cf} = \sum_{k,q} B_q^k C_q^{(k)}. \tag{2.42}$$

This term contains the crystal field parameters B_q^k (where $k = 2, 4, 6$ and the value of q depends on the site-symmetry of the ion in the host crystal [177] and ranges from 0 to $\pm k$), which are usually empirical and are obtained from fitting the energy levels to the experimental ones. The number of the crystal field parameters can range from 2 to 27. $C_q^{(k)}$ terms are the many-electron spherical tensor operators for the $4-5f^n$ configurations.

While it is straightforward to compute the heat capacity at the constant volume, the heat capacity is usually measured at constant pressure. The difference between the two quantities is given by [182]:

$$C_p - C_V = N_A V \alpha^2 B T, \tag{2.43}$$

where N_A is the Avogadro constant, V is the molar volume, α is the thermal expansion coefficient, B is the bulk modulus and T is the temperature in K. The outlined here equations have been used in derivation of the heat capacities of monazite-type ceramics (Section 3.3.4).

2.5.1 Computation of the order-disorder transition temperature in pyrochlore

The temperatures of order-disorder transition from pyrochlore to defect fluorite phase, that will be discussed in Section 3.3.5, were computed following the procedure outlined

by Jiang et al. [183] and by modeling the disordered fluorite structure by a quasirandom structures derived in that studies. The transition temperature is derived from the thermodynamic consideration as:

$$T = \frac{\Delta H}{S_{\text{conf}}}, \tag{2.44}$$

where ΔH is the enthalpy difference between the two phases (it is computed *ab initio*) and $S_{\text{conf}} = -4k_B[x \ln x + (1-x)\ln(1-x) + 2y \ln(y) + 2(1-y)\ln(1-y)]$, k_B is the Boltzmann constant, x=1/2 and y=1/8, is the configurational entropy of the defect fluorite derived assuming full disordering of the cation and oxygen/oxygen-vacancy sublattices [183].

Chapter 3

Applications

This chapter summarizes the results and application part of the dissertation studies. We discuss here our extensive benchmarking studies of the DFT+U method, which includes the calculation of the Hubbard U parameter values using *ab initio* methods, and application of the derived computational methodologies to simulation of various properties of nuclear waste management related materials. Some parts of the reported studies were performed as joint projects with the members of the Atomistic Modeling group at IEK-6. The specific and independent contribution of the PhD candidate includes: derivation of the Hubbard U parameters values and benchmarking of the DFT+U method, calculation of the reaction enthalpies of *An*-bearing compounds and computation of the Schottky contribution to the heat capacities of monazite-type ceramics.

3.1 Derivation of the Hubbard U parameter values

In this section we present the results of systematic derivation of the Hubbard U parameter values (or the effective Hubbard U parameter $U_{\text{eff}} = U - J$) for the number of *Ln*- and *An*-bearing molecules and solids. For all compounds investigated in this thesis, these parameters were derived using the cLDA method [70–72] following the recent implementation of the linear response approach [72] in the DFT code Quantum-

ESPRESSO [81]. In addition, the Hubbard U parameter values were derived for the series of *Ln*-bearing oxides using the cRPA methodology [75–78] and the FLEUR-SPEX code [82]. The presented here systematic derivation of the Hubbard U parameter values for many molecular and solid compounds is the first such study conducted for the lanthanide- or actinide-bearing materials.

3.1.1 Uranium-bearing compounds

Molecular complexes

Using cLDA methodology [72] implemented in the Quantum-ESPRESSO code [81] we derived the Hubbard U parameter values for uranium-bearing molecules (fluorides, chlorides, halogenides, halcogenides and hydroxides) that contain uranium in various oxidation states from +3 to +6 (Table 3.1). These molecular complexes have been extensively studied experimentally [17, 18] and have also been investigated using various *ab initio* modeling methods [30, 31]. As indicated in Table 3.1 the resulted Hubbard U parameter values range from 1.9 eV to 3.1 eV and show a clear dependence on the oxidation state of the actinide cation, which is clearly seen in Figure 3.1. Increasing the oxidation state of uranium atom results in larger Hubbard U parameter values. In addition to consideration of the f-orbitals in the DFT+U calculations, we computed the on-site Coulomb repulsion on the d-orbitals in the uranium-bearing complexes. These results are also reported in Table 3.1. The values for d orbitals are similar for all species and ranging from 0.6 eV to 0.8 eV are substantially smaller than the Hubbard U parameter values derived for f orbitals. To check the performance of different exchange-correlation functionals we performed calculations with PBE [57] and PBEsol [118] functionals. We found that both functionals produce similar results in terms of the Hubbard U parameter. The values reported in Table 3.1 were subsequently used for the geometric optimizations (see Section 3.2.1) and the derivation of reaction enthalpies (see Section 3.3.1) of uranium-bearing molecular complexes.

Table 3.1: The Hubbard U parameter values for the uranium-bearing molecules calculated using the *linear response* method of Cococcioni and de Gironcoli [72]. The values are given in eV. The last column represents the values computed for the d-orbitals.

Molecule	Hubbard U_{LR}		
	PBE (f electrons)	PBEsol (f electrons)	PBE (d electrons)
UF_6	3.1	3.0	0.6
UF_5	2.3	2.3	0.6
UF_4	1.8	1.7	0.7
UF_3	1.9	1.9	0.8
UCl_6	2.2	2.2	0.5
UCl_5	2.2	2.2	0.5
UCl_4	1.7	1.7	0.5
UCl_3	1.4	1.5	0.6
UOF_4	2.8	2.7	0.6
UO_2F_2	3.1	3.1	0.7
$UO2(OH)_2$	2.8	2.8	0.6
UO_3	2.6	2.6	0.6
UO_2	2.0	1.9	0.6

Table 3.2: The Hubbard U parameter values for the uranium-bearing solids calculated using the *linear response* method of Cococcioni and de Gironcoli [72]. The values are given in eV.

Solids	Hubbard U_{LR}	
	PBE	PBEsol
UF_6	2.9	2.8
α-UF_5	2.3	2.3
β-UF_5	2.3	2.3
UF_4	1.4	1.3
UF_3	0.8	0.8
UCl_6	2.7	2.7
UCl_4	1.6	1.6
UCl_3	0.8	0.9
U_3O_8	2.4	2.3
α-UO_3	2.7	2.7
UO_2	1.8	1.7
α-U	1.9	1.9

Solids

We computed the Hubbard U parameter values also for various uranium-bearing solids. In this work we have considered twelve uranium-bearing crystals: α-U[184], UF_6[185], α-UF_5 [186], β-UF_5[187], UF_4[188], UF_3[189], UCl_6[190], UCl_4[191], UCl_3[191], UO_2[192], α-UO_3[193] and U_3O_8[194].

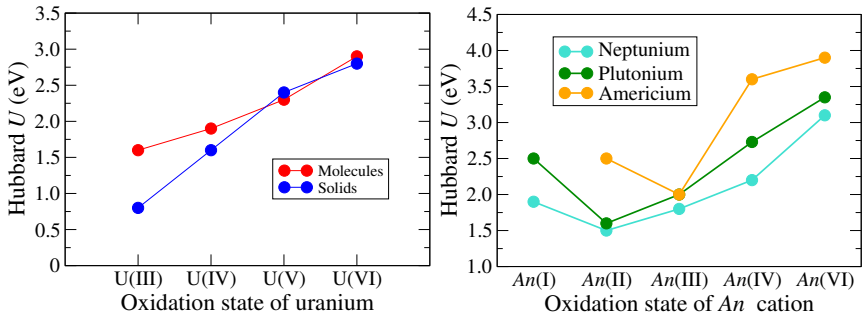

Figure 3.1: Dependence of Hubbard U parameter value on the oxidation state of uranium atom in molecular complexes and solids (left) and on various actinide atoms in actinide-baring complexes (right).

The results are presented in Table 3.2 and range from 0.8 eV to 2.9 eV. As indicated in Figure 3.1 (left) the dependence of the Hubbard U parameter values on the oxidation state of uranium atom is very similar to that obtained for molecular complexes. These results indicate that a common practice of choosing the same Hubbard U parameter value for calculations of different, but bearing the same actinide cation, solids is not justified. In the literature, usually the Hubbard U parameter value of 4.5 eV is used as the optimal parameter for the DFT+U calculations of uranium-bearing solids. This value is taken from the XPS and inverse photoemission spectroscopy (IPES) measurements of UO_2 by Baer and Schoenes [59] and Kotani and Yamazaki [61]. We note that in this work we get a smaller value of 1.8 eV for uranium dioxide and this discrepancy will be discussed in Section 3.3.1. Similar to the case of uranium-bearing molecules, the Hubbard U parameter values were calculated using both PBE and PBEsol functionals and, as shown in Table 3.2, no significant differences were found.

3.1.2 Other actinide-bearing compounds

Using the *linear response* approach [72] we derived the Hubbard U parameter values also for various neptunium-, plutonium- and americium-bearing molecules. The results of these calculations are presented in the Table 3.3. In this case we also considered

Table 3.3: The Hubbard U parameter values for uranium-, neptunium-, plutonium- and americium-bearing molecules calculated using the linear response method of Cococcioni and de Gironcoli [72]. Values are given in eV.

Molecule	U_{LR}	Molecule	U_{LR}
NpF_6	3.1	PuF_2	1.2
NpF_4	1.9	PuF	2.5
NpF_3	2.0	$PuCl_4$	2.8
NpF_2	1.0	$PuCl_3$	2.0
NpF	1.9	PuO_3	3.2
$NpCl_4$	2.2	PuO_2	2.9
$NpCl_3$	1.6	PuO	2.0
NpO_2	2.4	AmF_6	3.9
NpO	2.0	AmF_3	2.0
PuF_6	3.5	AmO_2	3.6
PuF_4	2.5	AmO	2.5
PuF_3	2.0		

actinides with oxidation states +1 (eg. NpF) and +2 (eg. NpF_2). Similarly to the case of uranium, the Hubbard U parameter values decrease with decreasing oxidation state of the An cations, however they increase slightly for An(I) (See Fig. 3.1 (right)). In general there is an increase in the strength of the on-site Coulomb repulsion from uranium to americium, considering the actinides having the same oxidation state. For instance, U(VI) has the average Hubbard U parameter value of 3.1 eV, while for Am(VI) we got 3.9 eV. The dependence of the Hubbard U parameter on the oxidation state of actinide-cation has never been considered before. In the next sections we will show that it influences the computed structural and thermochemical parameters.

3.1.3 Monazite- and xenotime-type ceramics

The values of the Hubbard U parameters derived here for A- (hexagonal), B- (monoclinic) and C-type (cubic) lanthanide-oxides and monazite- and xenotime-type ceramics using the *linear response* method [72] are reported in Tables 3.4 and 3.5. We found that the Hubbard U parameter value varies for different elements, rising with occupation of f orbitals and reaching the highest value for Eu. In most cases the values for oxides are consistent with those derived for monazite (Table 3.4). The largest difference is observed in the case of C-type oxides, especially for Tb and Dy. This is because among the considered oxides C-type structures exhibit most different Ln

Table 3.4: The Hubbard U parameter values in eV for $Ln\mathrm{PO_4}$ monazite and $Ln_2\mathrm{O_3}$ oxides using cLDA and cRPA methods. Although for some structures slightly different U values were obtained for distinctly different cation sites and applied in the calculations, here only the average values are reported.

Ln cation	$Ln_2\mathrm{O_3}$ (cLDA)	$Ln_2\mathrm{O_3}$ (cRPA)	$Ln\mathrm{PO_4}$
La (A)	2.8	5.2	3.2
Ce (A)	4.5	4.9	3.6
Pr (A)	4.8	5.8	4.1
Nd (A)	4.9	5.1	4.9
Pm (A)	5.2	6.0	5.5
Sm (A/B/C)	6.0/6.0/8.7	5.1	6.6
Eu (A/B/C)	9.6/7.1	6.5	8.1
Gd (A/B/C)	4.2/3.9	9.1	3.4
Tb (A/C)	4.5/10.0	4.9	4.9
Dy (A/C)	5.5/10.9	6.8	5.0

coordination (6 vs. 9 in monazite, and shorter *Ln*-O bond-lengths than in monazite). Our results are also consistent with a few published theoretical studies. We got the same value of the Hubbard U parameter for Ce in Ce_2O_3 (4.5 eV) as the one applied by Da Silva [195], Fabris et al. [196] and Fabris et al. [197] and only slightly larger than 7 eV applied for Eu by Concas et al. [198] and Kunes and Laskowski [199] in computation of Eu_2O_3. Hüfner and Wertheim [63] and Kotani and Yamazaki [61] derived the values of Hubbard U parameter for lanthanides from spectroscopic measurements. Hüfner and Wertheim [63] showed that the correlation energy can vary between different lanthanides and also between different structures having the same lanthanide cation. They also found that this energy is largest for cations exhibiting large magnetic moment. These results are consistent with our finding. On the other hand, in both mentioned studies the derived U values are usually larger than the values derived here. For instance, Kotani and Yamazaki [61] found U values for lanthanide-oxides ranging from 9.5 eV to 10.5 eV. We notice that such large values are inconsistent with the ones used in aforementioned theoretical studies. In the next sections we will show that our values result in excellent description of the structures and energetics for most of the investigated materials.

The derivation of the Hubbard U parameter values were extended to xenotime-type ceramics and lanthanide oxides beyond Dy (See Table 3.5). With the exception

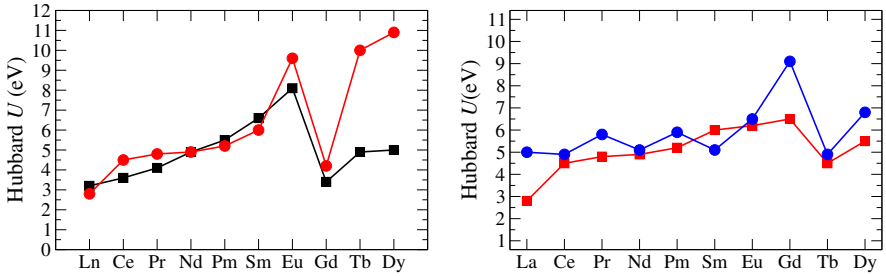

Figure 3.2: Left: The Hubbard U parameter values of $Ln\mathrm{PO}_4$ (black) and $Ln_2\mathrm{O}_3$ (red) as presented in Table 3.4. Right: The Hubbard U parameter values of a-type $Ln_2\mathrm{O}_3$ oxides calculated *ab initio* using cLDA (red) and cRPA (blue) methods.

of the Er case, the values for the oxides are larger than these obtained for xenotime. In case of xenotime, the largest Hubbard U parameter values were obtained for ErPO_4 (9.7 eV) and TmPO_4 (10.3 eV). The results of application of the derived Hubbard U parameter values in the calculations of the structural and thermodynamic parameters of lanthanide oxides and phosphates will be discussed in Sections 3.2.3 and 3.3.3. There is a discussion in the literature whenever the cLDA [72] and cRPA [75–78] *ab initio* methods used for calculation of the Hubbard U parameter value give consistent results. Significant discrepancies have been observed for the elements at the end of $3d$ series [77]. Therefore, after computing the Hubbard U parameter values using the linear response method (cLDA) we recomputed these values for the a-type Ln-oxides using the cRPA approach. The comparison of the results of the two methods is given in Figure 3.2 (right panel). The two calculations give very consistent results with the deviation not larger than 1 eV for most of the cases, except for La and Gd, where the deviation is larger than 2 eV. While this deviation is still acceptable, the larger differences can be attributed to the not fully adequate description of the cases where there is no f electrons ($\mathrm{La}_2\mathrm{O}_3$) and for the system with the half filled f-shell ($\mathrm{Gd}_2\mathrm{O}_3$).

Nevertheless, the obtained results show that the both methods give consistent values of the Hubbard U parameters and that they can be successfully utilized in computation of the Hubbard U parameter value for the lanthanide-bearing materials.

Table 3.5: The Hubbard U parameter values in eV for xenotime and the lanthanide oxides.

Cation	Hubbard U_{LR}	
	xenotime	oxide
Tb	4.8	10.0
Dy	7.9	10.9
Ho	5.6	10.8
Er	9.7	7.0
Tm	10.3	10.8
Yb	7.8	10.9

3.1.4 Pyrochlore-type ceramics

The Hubbard U parameter values were calculated for several pyrochlores using the *linear response* method of Cococcioni and de Gironcoli [72]. The results are presented in Table 3.6. Gd-bearing zirconate and hafnate resulted in the same value of the Hubbard U parameter, 3.4 eV. The values of Sm-zirconate and Tb-hafnate were higher by a factor of 2 and more. The derived values were used to calculate the transition temperatures from the ordered pyrochlore to the disordered fluorite phase and were applied in calculations of defect formation energies in pyrochlore compounds (Section 3.3.5).

Table 3.6: The Hubbard U parameter values (in eV) for different pyrochlores.

	Hubbard U_{LR}
$Gd_2Zr_2O_7$	3.4
$Sm_2Zr_2O_7$	6.5
$Tb_2Hf_2O_7$	7.3
$Gd_2Hf_2O_7$	3.4

3.1.5 The Hubbard U parameter values and the problem of band gaps

One of the shortcomings of standard DFT method is its inability to correctly predict the band gaps or even state (metal/insulator) of strongly correlated materials [38]. It usually underestimates the band gaps by as much as $\sim 40\%$ [156, 200, 38]. Therefore,

when investigating solids by the DFT+U method often the ability of this method to reproduce the band gaps of the considered materials is discussed (eg. [45]). In Table 3.7 the values of the band gap obtained in all our DFT+U calculations of uranium-bearing solids are provided. The experimental band gap of UO_2 is 2.1 ± 0.1 eV [201]. In the previous DFT+U studies that utilize the Hubbard U value of 4.5 eV and J = 0.51 eV Dorado et al. [65] got the band gap of 2.4 eV, which is only slightly larger than the experimental value. Our calculations with $U = 4.5$ eV give band gaps of 2.0 eV and 1.9 eV for PBE+U_{LR} and PBEsol+U_{LR} methods respectively,

Table 3.7: The values of band gaps (in eV) for the uranium-bearing solids calculated with PBE+U and PBEsol+U method for different U values.

	PBE+U				PBEsol+U			
Solids	3 eV	4.5 eV	6 eV	U_{LR}	3 eV	4.5 eV	6 eV	U_{LR}
UF_6	3.5	3.7	3.9	3.5	3.6	3.8	4.0	3.6
α-UF_5	3.3	4.4	4.4	2.8	3.1	4.3	4.7	2.6
β-UF_5	1.8	2.5	2.3	1.5	1.7	2.4	2.8	1.3
UF_4	2.0	2.9	3.6	1.0	1.9	2.8	3.6	1.0
UF_3	2.6	3.5	4.1	1.0	2.4	3.1	3.8	0.9
UCl_6	2.0	1.9	1.8	2.0	2.1	2.0	1.8	2.0
UCl_4	1.4	1.5	1.5	1.1	1.5	1.6	1.6	0.9
UCl_3	2.3	3.3	4.0	1.0	2.2	2.9	3.6	0.5
U_3O_8	2.1	2.4	2.4	1.8	1.8	2.5	2.5	1.2
α-UO_3	2.2	2.5	2.9	2.1	1.1	1.5	1.4	1.2
UO_2	1.2	2.0	2.6	0.7	1.1	1.9	2.5	0.4
α-U	1.4	2.0	2.1	0.4	1.2	2.0	2.2	0.3

which are very consistent with the experimental value. However, due to smaller values of the Hubbard U parameter derived by the *linear response* method (see Table 3.2), both the DFT+U_{LR} calculations resulted in much smaller band gap of 0.7 eV (PBE+U_{LR}) and 0.4 eV (PBEsol+U_{LR}), which is inconsistent with the aforementioned measurements. Similar performance of the DFT+U method is also observed for the considered lanthanide-oxides. It predicts metallic state for all the considered oxides, while all these systems have significant band gaps. With the DFT+U method these materials are correctly predicted to be insulators. In Table 3.8 we compare the band gaps derived by different methods, including PBEsol+U_{LR}. For most cases PBEsol+U_{LR} underestimates the band gaps by ~ 1.7 eV on average. The partial correction to the band gap by DFT+U is a well known feature of this method, because it

Table 3.8: Minimum band gaps (eV) of the some Rare Earth oxides obtained from different theoretical approaches and experiments.

Oxide (type)	PBEsol+U_{LR}	HSE06[202]	G_0W_0[203]	Exp.
La_2O_3 (A)	4.5	5.1	4.95	5.5^a , 5.34^b
Ce_2O_3 (A)	1.6	3.38	1.5	2.4^a
Pr_2O_3 (A)	2.8	3.77	2.86	3.9^a, 3.5^b
Nd_2O_3 (A)	2.3	4.63	4.5	4.7^a, 4.8^b
Sm_2O_3 (B/C)	1.5/3.1	3.4	4.38	5^a
Eu_2O_3 (B/C)	3/1.5	2.5	2.77	4.4^a
Gd_2O_3 (B/C)	2.7/3.6	5.26	4.89	5.4^a
Tb_2O_3 (C)	3.6	4	3.81	3.8^a
Dy_2O_3 (C)	3.6	4.9	4.41	4.9^a
M.A.E.	1.73	0.59	1.59	
A.E.	-1.73	-0.31	-0.05	

^{a}[204], ^{b} [205]

corrects only for energies of selected states (f orbitals in our case). On the other hand, we notice that the deviation from the experimental values is not significantly larger than for other methods such as GW or hybrid functionals. We notice however, that in principle the DFT is a ground state theory and the Kohn-Sham eigenvalues have no strict physical meaning [38, 156, 200]. This would imply that the interpretation of the Kohn-Sham band gap as the fundamental band gap, although performed on the regular basis, is also not well justified. In fact, Perdew and Levy [156] and Perdew [200] have shown that due to the discontinuity in the derivative of the exchange-correlation energy, even having the exact ground state density and the exact Kohn-Sham potential, the Kohn-Sham band gap is still expected to be underestimated. From this point of view the underestimation of the band gap by a DFT-based method can not be seen as a flaw. On the other hand, from the construction of the Hubbard energy functional it is expected that the DFT+U method with the correct Hubbard U parameter should result in the discontinuity in the derivative of the exchange-correlation energy and reproduce the fundamental band gap [56]. Thus, the possibility that the *linear response* method underestimates the U values and therefore the band gaps can not be excluded. On the other hand, as will be discussed in the next sections, the DFT+U_{LR} method results in good prediction of the reaction enthalpies, for the considered actinide- and lanthanide-bearing solids. The problem of potential underestimation of the Hubbard

U parameters by the *linear response* method of Cococcioni and de Gironcoli [72] could be further addressed by computation of the Hubbard U parameter values with other methods, such as cRPA [164]. We note however that an investigation reported here shows consistent prediction of the cLDA and cRPA methods (see Section 3.1.3). In general, the analysis of the band gap problem is also complicated due to lack of the experimental information on the band gaps of the most of the investigated materials. Therefore, being more interested in prediction of the thermochemical properties, we did not investigated further this problem. However, we notice that the performance of DFT+U for the prediction of the band gaps and the electronic densities of states was already a subject of many previous studies (eg. [45, 65]).

3.2 Structural properties of f-materials

In this chapter we benchmark the performance of different DFT functionals and DFT+U method with the fixed and derived the Hubbard U parameter values. As reference materials we used simple actinide-bearing molecules, lanthanide-containing oxides and monazite- and xenotime-type phosphates.

3.2.1 Uranium-bearing materials

The set of uranium-bearing molecular compounds, including U(VI), U(V), U(IV) and U(III) halogenide, oxide and oxyhalide molecules computed here contains all the species considered by Shamov et al. [30], Iche-Tarrat and Marsden [51] and Batista et al. [206]. In addition we computed the series of uranium-chlorides for which good experimental data exist.

Molecular compounds

The stable geometries of the uranium-bearing molecules found in our calculations are in agreement with previous studies of the same systems [30, 31, 51, 206]. Uranium hex-

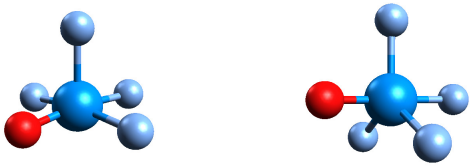

Figure 3.3: Two possible structures of UOF_4 molecule: the trigonal bipyramide (left) and the square pyramidal configuration (right).

ahalogenides (UX_6, where $X = F, Cl$) have O_h symmetry. The symmetry of uranium pentahalogenides (UX_5) is C_{4v} and that of UX_4 molecules is C_{2v}. UX_3 and UO_2F_2 molecules have C_{3v} and C_{2v} symmetries respectively. UO_3 molecule has T-shaped planar geometry and UO_2 has linear geometry. The two possible structures of UOF_4 are shown in Figure 3.3. The DFT-PBE calculation indicates that the square pyramidal structure is more stable than the trigonal bipyramide form by 2.4 kJ/mol, which is in agreement with the studies of Shamov et al. [30].

Three of the considered molecules, UF_6, UCl_6 and UCl_3, have measured structural parameters (the $U - F, Cl$ bond lengths and the $Cl - U - Cl$ angle in the case of UCl_3). Therefore, we started the analysis by an assessment of performance of different methods in prediction of the bond lengths in these compounds. First, we compared the U-F bond length computed for the gas-phase UF_6 molecule to the experimental value and to the previous theoretical estimates [207–209]. All the results are given in Table 3.9. The measured U-F bond length is 1.999 Å [207] and 1.997 Å [208]. The PBE functional overestimates the bond length by slightly more than 1%, which is a known feature of this functional [210]. The BLYP functional [209] gives even worse prediction, which is also expected [211]. The hybrid B3LYP functional used in the same studies improved the value of the bond distance and the Hartree-Fock calculation also shows surprisingly good agreement with the experiment. The all-electron PBE0 calculation [30] with 1.997 Å gives the best match to the experimental value.

Because the PBEsol functional recovers correctly the slowly varying density limit of the exact exchange energy functional, it usually improves description of the structural parameters over PBE [210, 118]. This is also visible in the calculations performed in

Table 3.9: The bond distances in UF_6, UCl_6 and UCl_3 molecules between uranium and halogen atoms and $U-Cl-U$ bond angle in UCl_3 molecule obtained using different computational methods. The bond lengths are given in Å and angles in degrees.

Functionals and methods	$U-F$	$U-Cl(UCl_6)$	$U-Cl(UCl_3)$	$Cl-U-Cl$	
PBE	2.024	2.469	2.509	106.4	
PBEsol	2.009	2.445	2.488	105.0	
BPBE	2.025	2.506	2.519	106.4	
modified PBE	2.048	2.471	2.559	111.8	
PBE+U (U=0.5 eV)	2.025	2.470	2.525	106.4	
PBE+U (U=1.5 eV)	2.027	2.472	2.550	106.7	
PBE+U (U=3.0 eV)	2.031	2.477	2.557	106.3	
PBE+U (U=4.5 eV)	2.034	2.486	2.570	106.7	
PBE+U (U=6.0 eV)	2.039	2.500	2.581	106.4	
PBE+U_{LR}	2.030	2.474	2.535	106.3	
PBEsol+U (U=0.5 eV)	2.010	2.446	2.495	105.4	[a]
PBEsol+U (U=1.5 eV)	2.012	2.449	2.504	105.1	
PBEsol+U (U=3.0 eV)	2.015	2.453	2.538	105.8	
PBEsol+U (U=4.5 eV)	2.024	2.462	2.548	106.3	
PBEsol+U (U=6.0 eV)	2.015	2.474	2.563	106.2	
PBEsol+U_{LR}	2.015	2.451	2.509	105.1	
BLYP[a]	2.043				
PBE0[a]	1.997		2.565	109.5	
HF[b,c]	1.984	2.48			
B3LYP[a]	2.014		2.592	114.5	
MP2[a]	2.005		2.521	106.9	
exp.[d,e,f,g]	1.999 (1.996)	2.42 (2.461)	2.549±0.008	95±3	

[209], [b] [212], [c] [213], [d] [207], [e] [214], [f] [215], [g] [208]

this work. PBEsol results in 2.009 Å for the U-F bond length of UF_6 that is in better agreement with the experiment than the PBE value. The U-F bond length obtained with the *modified* PBE functional is in the worst agreement to the experimental value. On the other hand, this functional predicts much better the enthalpies of reactions than the PBE or PBEsol functionals, including the dissociation enthalpy of UF_6, which will be discussed later. The fact that by switching to a different GGA functional one can improve the prediction of the reaction enthalpies at a cost of worsening the structural parameters and vice versa, is a known shortcoming of current GGA-DFT functionals. The DFT+U approach in general results in larger U-F bond length for UF_6 than the one predicted by the applied GGA functional. However, we will show that, in line with the above conclusions, it also results in much better prediction of the gas-phase reaction enthalpies.

We observe the same trends as for UF_6 in the case of UCl_6 molecule that has the same geometry and the oxidation state of uranium. Also in this case the PBEsol functional results in better match to the measured $U - Cl$ bond length. The experimental U-Cl bond length for uranium trichloride, UCl_3 is 2.549±0.008 Å [216]. All the GGA functionals underestimate this bond length by ~ 0.05 Å. In that case the DFT+U method improves the bond length and the *modified* PBE functional also results in a good match to the experiment. However, all the methods overestimate the Cl-U-Cl bond angle. Interestingly, for that parameter the hybrid functionals, PBE0 and B3LYP, give worse prediction than the PBE and PBEsol methods.

Solids

Uranium-bearing fluorides, chlorides, oxides and α-uranium were studied in this thesis. The initial structures were taken from the available experimental works [184–194]. In Tables 3.10, 3.11 and 3.12 we provide the computed with different methods and measured experimentally lattice parameters of all the considered solids. All the methods usually overestimate the lattice lengths and volumes of the uranium fluorides solids (see the cases of UF_6, α-UF_5 and β-UF_5, Table 3.10). This is consistent with the results obtained for the gas-phase UF_6. Similarly to this case, the PBEsol functional gives the best match to the experiment. The DFT+U method, in general, worsens the agreement, when comparing with the prediction of respective GGA functionals, and *modified* functional gives the worst prediction. Interestingly, all the methods overestimate the lattice parameters of UCl_6 solid (Table 3.11), which is different from the result for the gas-phase UCl_6 (see Table 3.9). However, the PBEsol+U_{LR} method results in good prediction of the lattice parameters of UCl_4 and UCl_3. α-U is the only pure-uranium solid considered here. Both the GGA functionals result in relatively good predictions of its lattice constants. This result is consistent with other computational studies [217]. However, it is not well described by the DFT+U method, including the DFT+U_{LR} cases, which significantly overestimates its volume. Surprisingly, we obtained very good description of the α-U structure with the *modified* PBE

Table 3.10: The lattice parameters of uranium fluoride solids and α-uranium calculated using different methods and measured [17, 18]. All length values are given in Å and volumes are given in Å^3.

	UF_6				α-UF_5			β-UF_5		
	a	b	c	V	a=b	c	V	a=b	c	V
PBE	10.62	9.53	5.58	565	6.93	4.53	217.8	11.56	5.40	721
PBEsol	10.42	9.32	5.46	530	6.75	4.48	204.1	11.41	5.28	687
BPBE	11.50	10.36	6.04	720	7.37	4.54	246.7	11.57	5.49	735
modified PBE	12.16	10.92	6.41	852	8.37	4.67	326.9	18.36	6.70	2260
PBE+U(3 eV)	10.74	9.69	5.67	590	6.95	4.57	220.5	11.64	5.43	736
PBE+U(4.5 eV)	10.82	9.69	5.70	598	6.95	4.59	221.8	11.67	5.45	743
PBE+U(6 eV)	10.82	9.75	5.70	602	6.96	4.61	223.0	11.72	5.45	749
PBE+U_{LR}	10.74	9.68	5.66	588	7.12	4.56	231.6	11.62	5.43	733
PBEsol+U(3 eV)	10.59	9.51	5.57	561	6.85	4.52	212.1	11.51	5.31	703
PBEsol+U(4.5 eV)	10.60	9.52	5.58	563	6.78	4.53	208.6	11.55	5.33	711
PBEsol+U(6 eV)	10.62	9.53	5.58	565	6.79	4.56	210.0	11.61	5.33	718
PBEsol+U_{LR}	10.55	9.45	5.53	551	6.77	4.51	206.5	11.49	5.30	700
exp.	9.90	8.96	5.21	462	6.52	4.47	189.9	11.46	5.20	682
	UF_4				UF_3			α-U		
	a	b	c	V	a=b	c	V	a	b	c	V
PBE	12.88	10.85	8.43	950	7.18	7.42	331	2.73	5.82	4.92	78.1
PBEsol	12.72	10.74	8.32	916	7.05	7.30	314	2.68	5.69	4.86	74.3
BPBE	12.90	10.86	8.43	953	7.20	7.39	332	2.72	5.82	4.93	78.2
modified PBE	14.90	11.53	11.19	1554	7.49	7.58	369	2.76	5.89	4.97	80.8
PBE+U(3 eV)	13.02	10.95	8.51	979	7.27	7.48	343	3.76	6.22	6.05	141.3
PBE+U(4.5 eV)	13.08	11.00	8.54	993	7.33	7.50	349	3.82	6.37	6.18	150.6
PBE+U(6 eV)	13.13	11.06	8.58	1008	7.38	7.55	356	3.86	6.47	6.28	156.9
PBE+U_{LR}	12.96	10.89	8.47	965	7.22	7.41	335	3.61	5.95	5.88	126.4
PBEsol+U(3 eV)	12.87	10.83	8.41	946	7.16	7.37	327	3.65	5.96	5.93	128.8
PBEsol+U(4.5 eV)	12.93	10.89	8.45	960	7.21	7.40	333	3.74	6.19	6.06	140.2
PBEsol+U(6 eV)	12.98	10.95	8.49	974	7.24	7.43	338	3.77	6.34	6.17	147.2
PBEsol+U_{LR}	12.80	10.78	8.38	930	7.09	7.31	318	3.47	5.52	5.77	110.5
exp.	12.73	10.75	8.43	929	7.18	7.35	328	2.84	5.87	4.94	82.1

functional, which badly overestimates the volumes of many other solids (see Tables 3.10-3.11).

3.2.2 Neptunium-, plutonium- and americium-bearing molecules

We studied fluorides, chlorides and oxides of other actinides in different valence state (Np(I-IV), Np(VI), Pu(I-IV), Pu(VI), Am(III) and Am(VI)).

Table 3.11: The lattice parameters of uranium chloride solids calculated using different methods and measured [17, 18]. All length values are given in Å and volumes are given in Å^3.

	UCl_6			UCl_4			UCl_3		
	a=b	c	V	a=b	c	V	a=b	c	V
PBE	11.76	6.46	774	8.36	7.76	543	7.55	4.28	210.6
PBEsol	11.25	6.13	672	8.23	7.47	506	7.37	4.14	194.8
BPBE	13.89	7.81	1305	8.36	7.87	551	7.57	4.27	212.1
modified PBE	15.33	8.50	1729	11.21	15.28	1918	11.76	3.91	445.9
PBE+U(3 eV)	11.76	6.46	775	8.44	7.82	558	7.61	4.39	220.1
PBE+U(4.5 eV)	11.78	6.45	774	8.49	7.90	569	7.66	4.42	224.3
PBE+U(6 eV)	11.78	6.45	775	8.54	7.88	574	7.68	4.44	227.4
PBE+U_{LR}	11.76	6.46	774	8.40	7.87	556	4.56	4.32	213.6
PBEsol+U(3 eV)	11.25	6.15	673	8.33	7.56	524	7.42	4.35	207.0
PBEsol+U(4.5 eV)	11.24	6.15	674	8.37	7.57	531	7.47	4.35	211.1
PBEsol+U(6 eV)	11.24	6.19	677	8.42	7.58	538	7.52	4.37	214.3
PBEsol+U_{LR}	11.28	6.14	676	8.28	7.54	517	7.40	4.23	199.9
exp.	10.95	6.02	625	8.30	7.49	515	7.44	4.32	207.5

Table 3.12: The lattice parameters of uranium oxide solids calculated using different methods and measured [17, 18]. All length values are given in Å and volumes are given in Å^3.

	UO_2		U_3O_8				α-UO_3			
	a=b=c	V	a	b	c	V	a	b	c	V
PBE	5.37	154.8	7.02	11.58	4.16	338	3.74	7.15	4.12	110.2
PBEsol	5.30	149.0	6.77	11.69	4.12	326	3.73	7.00	4.09	106.7
BPBE	5.41	158.6	7.02	11.58	4.16	338	3.74	7.15	4.12	110.2
modified PBE	5.49	165.4	7.28	11.62	4.20	355	3.44	10.77	4.18	174.7
PBE+U(3 eV)	5.54	170.0	7.23	11.53	4.17	347	3.41	9.96	4.17	141.6
PBE+U(4.5 eV)	5.58	173.1	7.28	11.55	4.18	351	3.42	9.97	4.18	142.2
PBE+U(6 eV)	5.62	176.4	7.34	11.57	4.19	355	3.42	10.34	4.19	148.4
PBE+U_{LR}	5.52	167.7	7.20	11.52	4.17	346	3.41	9.96	4.17	141.5
PBEsol+U(3 eV)	5.48	164.3	7.14	11.43	4.14	338	3.71	7.14	4.10	108.7
PBEsol+U(4.5 eV)	5.52	167.5	7.19	11.45	4.15	341	3.70	7.27	4.12	111.0
PBEsol+U(6 eV)	5.55	170.7	7.25	11.48	4.15	345	3.74	7.29	4.14	113.0
PBEsol+U_{LR}	5.45	161.6	7.11	11.43	4.14	336	3.80	6.94	4.11	108.5
exp.	5.47	163.5	6.70	11.95	4.14	332	3.96	6.86	4.17	113.2

Table 3.13: Bond distances in NpF_6 and PuF_6 molecules between actinide and halogen atoms obtained using different computational methods and functionals. Experimental value is also presented for comparison. The bond lengths are given in Å.

Functionals and methods	$Np-F$	$Pu-F$
PBE	2.013	2.012_{av}
PBEsol	1.997	1.994_{av}
PBE+U_{LR}	2.020	2.033_{av}
PBEsol+U_{LR}	2.003	2.011_{av}
B3LYP[a]	1.991	1.977
exp.[b,c]	1.981(9)	1.971(10)

[a] [218], [b] [209], [c] [208]

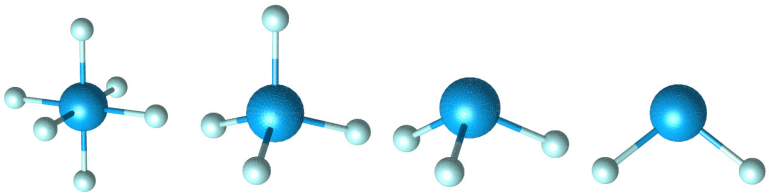

Figure 3.4: Molecules of NpF_6, NpF_4, NpF_3 and NpF_2 in O_h, T_d, C_{3v} and C_{2v} symmetries respectively.

Hexafluorides of all four actinides were optimized in O_h symmetry. Data for pentahalogenides is not available experimentally for most of the actinides and these molecules were not studied in this work. The tetrahalogenides were optimized in T_d symmetry and the trihalogenides of the three actinides were optimized in C_{3v} symmetry. All dioxide molecules have planar geometry with the 180 degree oxygen-actinide-oxygen bond angle. Similar to the UO_3, PuO_3 molecules has T shaped geometry with the dihedral angle equaling 180 degrees. There are only few experimental geometries of the molecules in the gas phase that are available for comparison. Values for PuF_6 and NpF_6 are presented in this paper in Table 3.13. The worst agreement for the actinide-fluoride bond distance is obtained with PBE functional. The overestimation of the bond lengths is a known feature of this functional [210]. The best agreement with the experiment is obtained when using the PBEsol functional [210]. The difference between the experimental value and the value obtained with the latter functional is 0.015 Å for NpF_6 and 0.023 Å for PuF_6. The DFT+U calculations using both the functionals worsen slightly the geometry in comparison to the standard DFT cal-

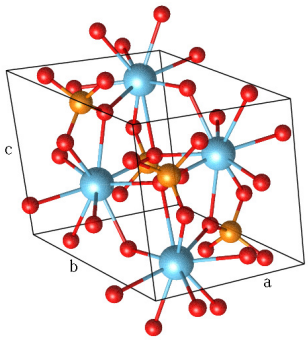

Figure 3.5: Structure of monazite.

culation by ~ 0.3 percent. Overestimation of geometric parameters when using the DFT+U method has already been reported previously by Wen et al. [45]. The case of $Pu-F$ bond length in PuF_6 molecule is different from the discussed cases. Although in the case of NpF_6 all actinide-halogen bonds are equal in length, the calculation of the PuF_6 molecule resulted in four equal $Pu-F$ bonds in equatorial plane, which were shorter than the two bond distances of the axial $Pu-F$ bonds. The average value of these bond lengths is presented in Table 3.13. The DFT+U calculations worsen slightly the bond distance by ~ 1 percent.

3.2.3 Monazite- and xenotime-type ceramics

Within the context of future nuclear waste management strategies monoclinic orthophosphates $Ln PO_4$ (Ln = La to Gd) (Fig. 3.5) are potential candidates for the safe disposal of minor actinides (Np, Am and Cm) and Pu [21]. These monazite-type ceramics appear to be promising for the immobilization of the radionuclides because of exceptional radiation resistance and chemical durability. Such phases are able to take up large amounts of actinides on regular positions in their crystal structures and keep such elements safe permanently. Natural monazites being as old as 3.2 billion years contain up to 52 $wt\%$ ThO_2 and up to 16 $wt\%$ UO_2 without signs of significant radiation damage to their crystalline structure [219]. Because monazite reveals a high

structural flexibility (space group $P\,2_1/n$, $Z = 4$) a simultaneous incorporation of tri- and tetravalent lanthanides and actinides into their structure is possible. Actinides can be integrated in the crystal structure by coupled substitution of the trivalent lanthanides [220]. For a more detailed description of the possible substitutions see Schlenz et al. [21].

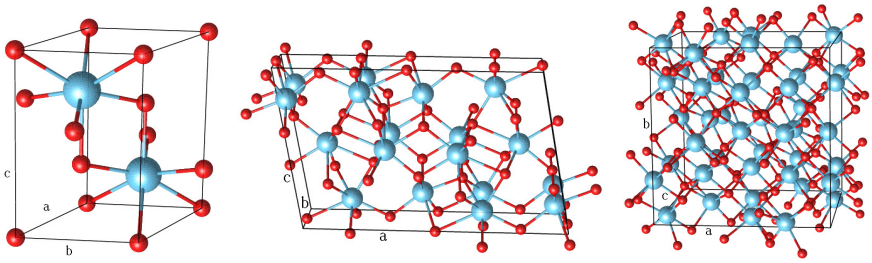

Figure 3.6: Structures of a-, b- and c-type Ln_2O_3 oxides from left to right.

However, our understanding of the behavior of monazite, and in general actinide-bearing materials, upon incorporation of actinides and its subsequent interaction with the environment is still incomplete. This is mainly because the key indicators of the atomic scale characteristics of monazite, such as structure-property relationships are still poorly understood [21], which is one of the main factors that prevents the utilization of this material as safe nuclear waste form.

In this section we present the results of calculations of structural parameters of lanthanide oxides and monazites- and xenotime-type ceramics. The computed values are compared with the following measured structures indicated for each Ln cation: For lanthanide-oxides: A-type: La[221], Ce[222], Pr[223], Nd[224], and Sm[225]; B-type: Sm[226], Eu[227], and Gd[228]; C-type: Sm, Gd, and Dy of Bartos et al. [229], Eu[230] and Tb[231]; For monazite from La to Gd by Ni et al. [232], Tb[233] and Dy[234].

Lattice constants

The structural parameters of lanthanide oxides (Fig. 3.6) obtained by using different computational methods are reported in Figures 3.7 and 3.8 and the respective

Table 3.14: Mean absolute error/mean error of A-type oxides (Ln_2O_3) lattice parameters (Å), volume (Å^3/formula unit), monoclinic angle (deg) and Ln-O bond lengths (Å).

Method	a/b/c	V	Ln-O
PBEsol	0.081/-0.014	4.032/-4.032	0.050/-0.049
PBEsol+U (3.5 eV)	0.062/-0.062	1.661/-1.6601	0.030/-0.023
PBEsol+U (6.0 eV)	0.056/0.021	0.655/0.315	0.020/-0.003
PBEsol+U$_{LR}$	0.048/-0.010	0.693/-0.369	0.021/-0.009
PBE	0.039/0.027	0.943/-0.289	0.028/-0.009
PBE^a	0.106/0.106	2.630/2.630	0.033/-0.009
PBE^b	0.099/0.099	2.555/2.555	0.026/0.026

^{a} $4f$ electrons confined in the core, ^{b} [28]

deviations from experimental values are reported in Table 3.14. In all the cases PBE functional gives larger values than PBEsol for all lattice parameters. PBE gives slightly better results for A-type structures but PBEsol performs better for B-type and C-type oxides. None of the considered standard DFT methods is able to satisfactory reproduce the experimental values with PBE and PBEsol being off by up to 3.5% for lattice constants and by 6% for volume.

The PBEsol+U method with fixed values of the Hubbard U parameter improves the description of lattice parameters with the smallest deviation from the experiment obtained with $U = 6\,\mathrm{eV}$, value which is more consistent with the average of computed U_{LR} values (Table 3.4). We obtained nearly perfect match to the experimental lattice parameters in many cases, namely for La, Nd, Sm (C-type), Eu, Gd, Tb and Dy.

We observed largest disagreement with experiment for lattice constants of A-type Ce_2O_3 and Pr_2O_3. However, even in these cases being only $\sim 1.5\,\%$ off PBEsol+U_{LR} still gives better prediction than PBE or PBEsol functionals. We get similarly good results with PBE+U_{LR} method, which is indicated in Figure 3.7 for few representative oxides.

We obtain a superior match to the experimental values with PBEsol+U_{LR} method in most cases, especially in terms of predicted volumes. This method gives mean deviation from the experiment no larger than 0.3%. Our excellent result for lattice constants of rare-earth oxides using the PBEsol+U_{LR} method indicates, that in order to obtain correct description of the structures using the DFT+U method it is essential

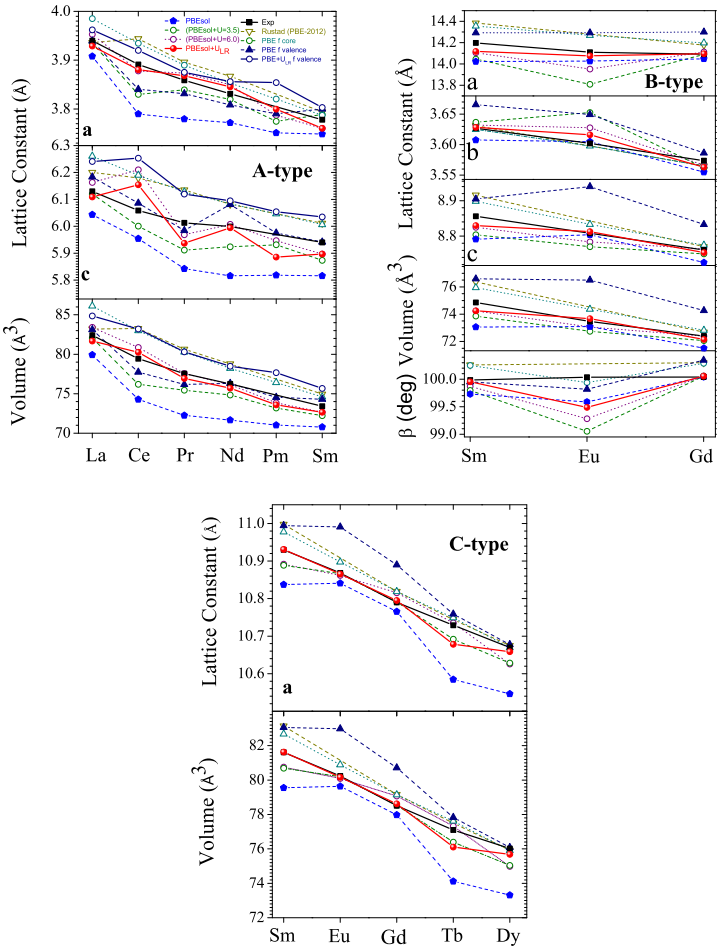

Figure 3.7: Lattice constants of Ln_2O_3 oxides obtained with different methods: PBE with f-electrons in the valence (dark blue up-triangle), PBE with f-electrons in the core (open magenta circle), PBE calculations of Rustad [28] (empty green down-triangle), PBEsol (filled blue pentagon), PBEsol+U with $U = 3.5\,\text{eV}$ (green open circle, dashed line), PBEsol+U with $U = 6\,\text{eV}$ (violet open circle, dashed line), PBEsol+U_{LR} (filled red circle, red solid line) and experimental values (filled black squares, black solid line). The lines are provide to show the trends and enhance the visibility of the data.

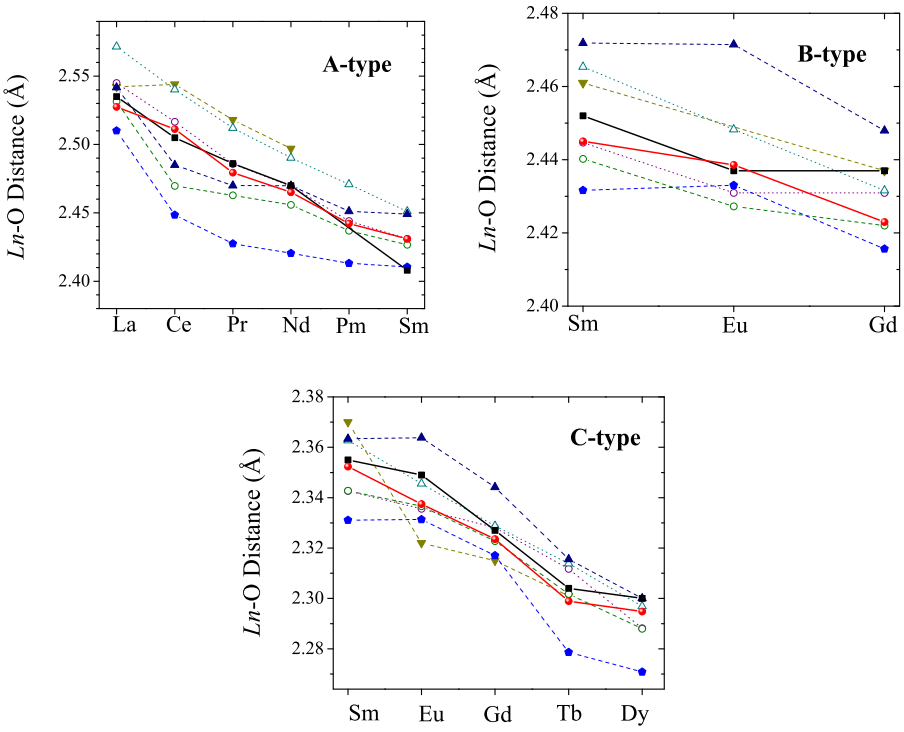

Figure 3.8: *Ln*-O bond lengths in Ln_2O_3. The results of different methods are marked according to convention used in Figure 3.7.

to chose proper DFT functional (PBEsol in this case) and the Hubbard U parameter value, which should be derived not only for each lanthanide-cation but also for each investigated structure.

Looking for the structure-property relationships in materials such as monazite it is important to understand change in the interatomic distances resulting from lanthanide contraction [21]. The results for $Ln-\mathrm{O}$ bond-length in oxides and monazite are given in Figures 3.8 and 3.16. It is evident that PBEsol+U_{LR} results in superior match to the measured values. In case of monazite the agreement with measurement is nearly perfect for most of the *Ln* cations. The goodness of the match is illustrated by mean errors given in Table 3.15, that are a few times smaller for PBEsol+U_{LR} than

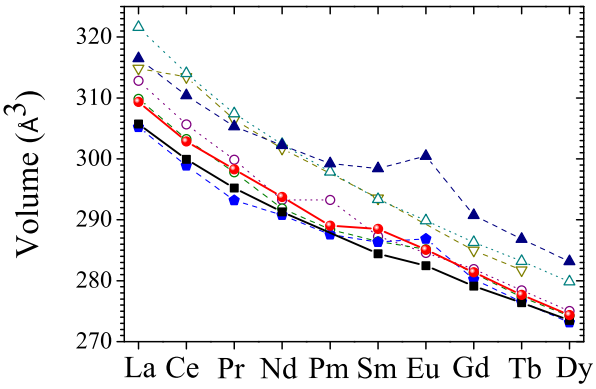

Figure 3.9: The computed and measured volumes of monazites. The results of different methods are marked according to convention used in Figure 3.7.

in the case of PBE or PBEsol methods. This is an astonishing result indicating that PBEsol+U_{LR} method can be successfully used for investigation of structural properties of *Ln*-bearing materials such as monazite-type ceramics, which is important in context of nuclear waste management.

Similarly, nearly perfect agreement with experiment has been reached for $Ln-$P distances in monazites (Fig. 3.16). At the same time P − O bond lengths are overestimated by ~ 0.02 Å, i.e. the same value as the offset of bond-length of PO molecule discussed above, resulting in a systematic offset of the predicted volume shown in figure 3.9. Nevertheless, the experimentally seen monotonic decrease in volume with increasing the atomic number of lanthanides is well reproduced. Good predictions of the $Ln-$O and $Ln-$P bond lengths by PBEsol+U_{LR} suggest that if there were not an offset in P − O bond-lengths this method would result in nearly perfect description of the monazite-type crystal structure. In the discussed figures and tables that describe the structural parameters of the investigated materials we also included results obtained by Rustad [28] who used PBE functional to perform the calculations. Our own PBE results do not match these results in all the considered cases. This is because in his calculations Rustad [28] used pseudopotentials with f-electrons treated

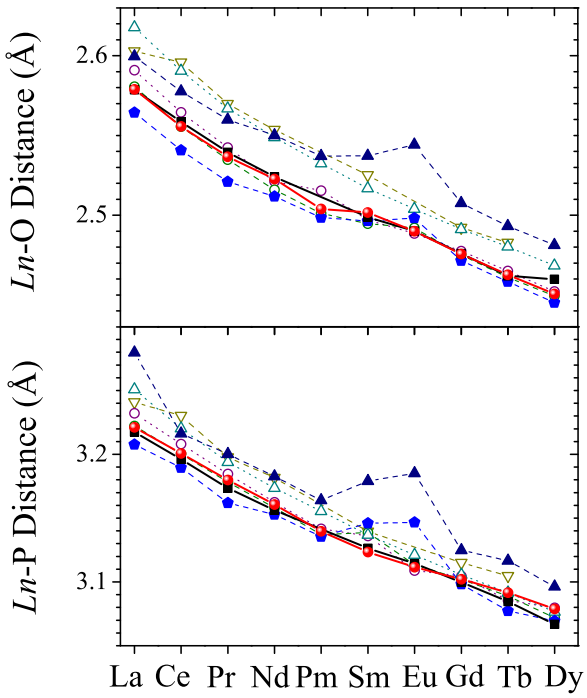

Figure 3.10: $Ln-\mathrm{O}$ and $Ln-\mathrm{P}$ distances in $Ln\mathrm{PO}_4$ obtained with different methods.The results of different methods are marked according to convention used in Figure 3.7.

implicitly, i.e. not treated explicitly as valence electrons but included into the core and modeled by pseudopotential. By using so constructed pseudopotentials we got very similar lattice parameters for all lanthanide-oxides and monazites as Rustad [28], which proofs the origin of discrepancy. Our results clearly show that in order to obtain good structures of lanthanide-bearing materials f-electrons have to be treated explicitly and the strength of the on-site Coulomb repulsion represented by U parameter has to be accurately estimated for each f-element and the investigated structure. We found that the *linear response* approach of Cococcioni and de Gironcoli [72] provides a good estimate of the Hubbard U parameter at least for systems containing lanthanide-oxide components.

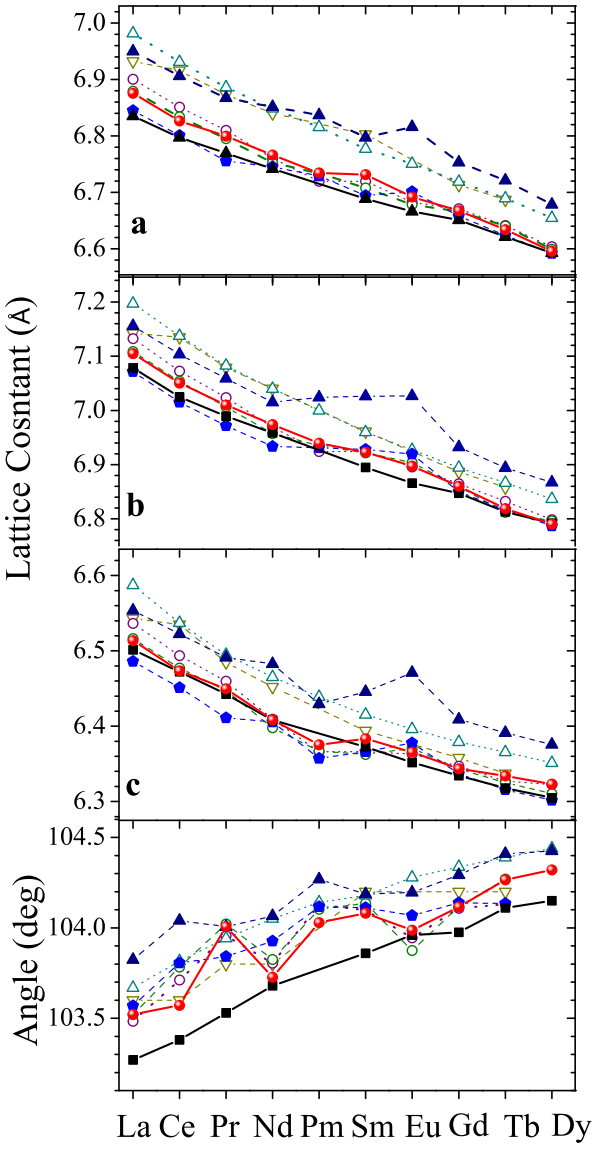

Figure 3.11: Lattice constants of monazite. The results of different methods are marked according to convention used in Figure 3.7.

Table 3.15: Mean absolute error/absolute error of Monazite-type ceramic (LnPO$_4$) lattice parameters, volume (Å^3/formula unit), monoclinic angle (in degrees) and $Ln-$O, P$-$O and $Ln-$P bond lengths. All lengths are in Å).

Method	$a/b/c$	V	β
PBEsol	0.025/0.018	0.732/0.466	0.262/0.262
PBEsol+U=3.5[1]	0.032/0.031	0.910/0.910	0.272/0.253
PBEsol+U=6.0[1]	0.041/0.041	1.233/1.233	0.224/0.220
PBEsol+U_{LR}	0.034/0.034	1.026/1.026	0.224/0.224
PBE	0.107/0.107	3.325/3.325	0.429/0.429
PBE [2]	0.092/0.092	2.880/2.880	0.391/0.391
PBE [3]	0.089/0.089	2.805/2.805	0.275/0.275
	$Ln-$O	$Ln-$P	P$-$O
PBEsol	0.015/-0.004	0.015/0.008	0.020/0.020
PBEsol+U=3.5[1]	0.009/0.002	0.010/0.010	0.021/0.021
PBEsol+U=6.0[1]	0.010/0.006	0.015/0.013	0.021/0.020
PBEsol+U_{LR}	0.002/-0.001	0.005/0.004	0.020/0.020
PBE	0.029/0.029	0.038/0.038	0.021/0.021
PBE [2]	0.022/0.022	0.015/0.015	0.021/0.021
PBE [3]	0.033/0.033	0.030/0.030	0.015/0.015

We have shown that the DFT+U_{LR} method with PBEsol exchange-correlation functional results in very good, even perfect, prediction of the $Ln-$O distances in monazite. We extend these studies to xenotime-type ceramics, which are similar to monazite (LnPO$_4$), but incorporate lanthanides beyond Tb and have a tetragonal symmetry [232]. The computed Hubbard $U = U_{\mathrm{LR}}$ parameter values for xenotime and the respected C-type (hexagonal) oxides are reported in Table 3.5.

In the previous paragraphs we have shown that DFT f-in-core approach results in the reaction enthalpies that are rather consistent with the prediction of DFT+U_{LR} and different from DFT f-in-valence approach. In case of monazite, we were interested in the direct comparison with DFT f-in-core PBE calculations of Rustad [28] and did not performed f-in-core PBEsol calculations. However, having much better performance of PBEsol functional than PBE for monazite it is interesting to compare directly the f-in-valence PBEsol, f-in-core PBEsol and PBEsol+U_{LR} approaches for monazite and xenotime phases. The computed $Ln-$O distances of the two phases is given in Figure 3.12. Similarly to the case of monazite PBEsol+U_{LR} approach results in superior prediction of the $Ln-$O distances for xenotime. Interestingly, DFT f-in-core approach gives good values of the $Ln-$O distances for the first three lanthanides and

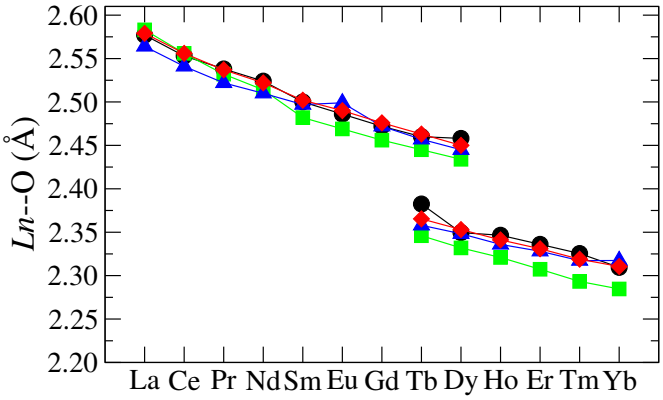

Figure 3.12: The computed and measured $Ln - \mathrm{O}$ bond distances in monazite and xenotime.

then systematically underestimates this parameter by $\sim 0.03\,\text{Å}$.

3.3 Thermochemical parameters of f-materials

In this chapter we discuss the performance of different DFT functionals and the DFT+U method with the fixed and derived Hubbard U parameter values for thermochemical parameters of simple actinide-bearing molecules and solids, lanthanide-bearing oxides and phosphates and pyrochlore-type ceramics.

3.3.1 Uranium-bearing materials

The difference between predicted by DFT and the measured enthalpies of reactions for various uranium-bearing molecular compounds can be as large as 100 kJ/mol [30, 50, 51]. By testing the different computational methods, including various DFT generalized gradient approximations (GGA) and hybrid functionals as well as post Hartree-Fock methods such as MP2 and CCSD(T), Shamov et al. [30] and Schreckenbach and Shamov [31] have shown that in order to reach the experimental accuracy (20 kJ/mol) at least hybrid functionals such as PBE0 have to be used in computation of the enthalpies of reactions involving uranium-bearing molecular compounds. In line with these findings, most of the meaningful DFT studies of actinide-bearing materials utilize the hybrid functionals such as B3LYP, PBE0 or HSE [46, 123–126]. Moreover, studies of Shamov et al. [30], Schreckenbach and Shamov [31] and Odoh and Schreckenbach [136] indicate that the result of such hybrid calculations can also depend on the number of core-electrons modeled by pseudopotentials and that at least 32 electrons of uranium atom ($5s^2 5p^6 5d^{10} 6s^2 6p^6 5f^3 6d^1 7s^2$) should be treated explicitly, which further increases the computational cost. We note however, that this result is still in dispute. For instance, Iche-Tarrat and Marsden [51] have shown that the explicit treatment of 32 electrons of uranium atom only marginally improves the performance of either DFT or hybrid-DFT functionals over the case when only 14 valence electrons of uranium ($6s^2 6p^6 5f^3 6d^1 7s^2$) are treated explicitly. We will show that our results implicitly support the later conclusion.

The usage of hybrid functionals or any post-Hartree-Fock method requires sub-

stantial computational resources. This limits the applicability of these methods to the simplest molecular compounds and solids. Materials that are interesting for nuclear engineering have usually complex chemical compositions and structures with super-cells containing often more than hundred atoms. This is especially true when solid solutions with diluted concentration of elements are of interest [21, 26]. Thus, DFT and its simple modifications, such as DFT+U, remain the only choice if one wants to compute complex materials and simulate their dynamical behavior by methods such as *ab initio* molecular dynamics [54–56] on nowadays supercomputing resources.

Wen et al. [45] have shown that the DFT+U method with a reasonable choice of the Hubbard U parameter can reproduce the band gaps of actinide oxides and correctly predict insulating state for these solids. This method has been successfully used in the description of UO_2 and its metastable states [65, 66], in the calculation of U(VI) aqua complexes on titania particles [50] and for the investigation of incorporation of uranium in the ferric garnet matrices [67]. It also predicts correctly the magnetic state of actinide compounds [68] and the full phonon dispersion of strongly correlated materials [69]. These successes have been achieved sometimes at a cost of worse description of lattice parameters [45] or even anomalous change in volume [235]. In all these studies the same Hubbard U parameter value for uranium of 4.5 eV (or $U_{\text{eff}} = U - J = 4.5\,\text{eV} - 0.5\,\text{eV} = 4\,\text{eV}$) has been used, which has been derived from the spectroscopic measurements of UO_2 [61, 59]. We note however, that there is no guarantee that the value derived for one system should be easily transferable to another, especially that other estimates for neutral uranium atoms provide somehow lower values of $U = 2.3\,\text{eV}$ [62] and $U = 1.9\,\text{eV}$ [64].

In this contribution we systematically test the performance of DFT+U method for the prediction of the thermochemical parameters, namely the reaction enthalpies, of simple uranium-bearing molecular complexes and solids, most of which were considered in previous studies (eg. [30, 51]). We do that in order to compare our results with already published predictions of much more demanding computational methods such as hybrid functionals, MP2 or CCSD(T) [30] and with the available experimental data.

Table 3.16: List of the considered 17 reactions between the gas-phase uranium-containing molecules. The reactions 1-2, 7-12 and 14-16 were computed by Shamov et al. [30].

(1)	$UF_6 \rightarrow UF_5 + F$	(10)	$UO_3 \rightarrow UO_2 + O$
(2)	$UF_5 \rightarrow UF_4 + F$	(11)	$UOF_4 + UO_3 \rightarrow 2UO_2F_2$
(3)	$UF_4 \rightarrow UF_3 + F$	(12)	$2UOF_4 \rightarrow UF_6 + UO_2F_2$
(4)	$UCl_6 \rightarrow UCl_5 + Cl$	(13)	$UO_3 + H_2O \rightarrow UO_2(OH)_2$
(5)	$UCl_5 \rightarrow UCl_4 + Cl$	(14)	$UF_6 + H_2O \rightarrow UOF_4 + 2HF$
(6)	$UCl_4 \rightarrow UCl_3 + Cl$	(15)	$UF_6 + 2H_2O \rightarrow UO_2F_2 + 4HF$
(7)	$UOF_4 \rightarrow UF_4 + O$	(16)	$UF_6 + 3H_2O \rightarrow UO_3 + 6HF$
(8)	$UO_2F_2 \rightarrow UO_2 + 2F$	(17)	$UO_2F_2 + 2H_2O \rightarrow UO_2(OH)_2 + 2HF$
(9)	$UF_6 + 2UO_3 \rightarrow 3UO_2F_2$		

Up to our knowledge there exist no systematic studies of the performance of DFT+U method for prediction of the thermochemical parameters of actinides. The reactions taken into consideration are given in Table 3.16. We considered only the already computed reactions in order to make a broad comparison of the results reported in this work with the results obtained by using different computational methods, including hybrid functionals and higher level post Hartree-Fock methods such as MP2 and CCSD(T) [30]. The thermochemistry data used as a reference were derived from the formation enthalpies taken from Morss et al. [17] and Guillaumont et al. [18]. We computed the reaction enthalpies by taking the differences in the total energies of the reactants. The initial structural parameters of computed solids were taken from different experimental studies and the adequate references are indicated in the relevant text and tables.

Molecular compounds

We selected several reactions involving gas-phase molecules to asses the performance of different methods in the prediction of enthalpies of reactions involving uranium-bearing molecules. As already mentioned, the experimental data exist for all of them and the enthalpies of most of the considered reactions were already computed using different methods of computational quantum chemistry. All the reactions are listed and labeled in Table 3.16. This labeling will be used subsequently in all further discussion in the text. All the reaction enthalpies computed with the standard GGA functionals are

Table 3.17: The reaction enthalpies computed with different DFT methods for the reactions given in Table 3.16 and the respective experimental values [17, 18]. Term PBEmodif indicates the *modified* PBE functional. The enthalpies are given in kJ mol^{-1}.

	PBE	PBEsol	BPBE	PBEmodif	PBE-BPBE corr.	exp.
(1)	422	458	403	324	328	313±17
(2)	514	549	497	413	429	385±22
(3)	619	641	607	541	558	618±27
(4)	278	317	254	176	155	205±20
(5)	312	347	302	217	261	204±20
(6)	414	447	395	339	320	412±25
(7)	554	613	529	441	430	405±20
(8)	1153	1204	1131	964	1045	1033±20
(9)	-207	-206	-208	-214	-213	-311±22
(10)	678	718	658	568	577	576±20
(11)	-113	-114	-105	-114	-72	-170±40
(12)	19	23	1	14	-69	-25±31
(13)	-141	-157	-133	-63	-105	-182±11
(14)	178	190	173	112	152	65±12
(15)	337	356	344	210	373	189±12
(16)	608	638	620	421	666	437±12
(17)	131	125	143	149	189	272±11
mean error	78	101	70	4	35	
M.A.E.	95	119	88	51	74	20

given in Table 3.17. First of all, despite the different pseudopotentials used in our and Shamov et al. [30] studies (large core ultrasoft pseudopotentials were used here, while Shamov et al. [30] used the all electrons or the small core pseudopotential calculations) the PBE results of the two studies are well consistent. The difference, measured by the mean absolute error (M.A.E), between the two calculations is only 3.2 kJ/mol[1]. This result validates our computational setup. The M.A.E. obtained with the PBE functional for all the considered reactions is 95 kJ/mol. Because the mean error (M.E.) is of similar value, this indicates a systematic offset from the measured values. Such a significant systematic error is unacceptably large, having the largest experimental error of 40 kJ/mol. The PBEsol functional results in even larger error, which as already discussed, is a known feature of this functional. In their studies Shamov et al. [30] used the PBE, BPBE and OLYP standard GGA-DFT functionals. These calculations resulted in a systematic offset for all the considered reactions, with BPBE performing slightly better than PBE, and OLYP resulting in reduction of the error by $\sim$ 50%.

[1]Considering only the reactions computed by Shamov et al. [30]

Our calculations show similar trend. The BPBE functional gives slightly better match to the measured values for all the considered reactions. We found that this behavior is not restricted to the reactions between uranium-bearing compounds but has been also observed for the bond energies of metal-ligand complexes [236]. Because the different GGA functionals result in different systematic offsets from the measured values, we decided to test the possibility of using a combination of two functionals in order to get better estimation of the reaction enthalpies. Especially instructive is the mixture of the BPBE and PBE results, because both functionals differ only by the exchange functional (they have the same, PBE correlation energy functional [57]). In Table 3.17 in column labeled by PBE-BPBE corr. the reaction enthalpies obtained by mixing the results of PBE and BPBE functionals as $E_{\mathrm{PBE}} + 5(E_{\mathrm{BPBE}} - E_{\mathrm{PBE}})$ are given, where E indicates enthalpy. As shown in Table 3.17, such a mixing results in significant reduction of the mean error, although M.A.E. is reduced by only 21 kJ/mol. Interestingly, the *modified* PBE functional, with M.E of only 4.1 kJ/mol, significantly improves the prediction of reaction enthalpies. It gives results that are better than predictions of the PBE or PBEsol functionals, not only for the reactions (1) and (2) used in the construction of the functional (see Section 2.2.1), but for most of the considered reactions. This is a promising result. However, we will show that such a simple modification of the PBE functional does not give similarly good results for solids. Shamov et al. [30], Odoh and Schreckenbach [136] and Schreckenbach and Shamov [31] concluded that calculations with the large core pseudopotential (14 valence electrons for uranium, which is also our setup) can result in significant under-performance of the PBE0 functional in prediction of the reaction enthalpies and suggest to use a small core or all-electron calculations in order to get converged energies. Because with the PBE and BPBE functionals we obtained results that are consistent with the all-electron calculations of Shamov et al. [30] and Schreckenbach and Shamov [31], we suspect that the size of the core is not that important, when a GGA functional is used. Interestingly, Iche-Tarrat and Marsden [51] have shown that the 32 electrons core pseudopotential only marginally improves, or even worsens in some cases, the performance over the 14 elec-

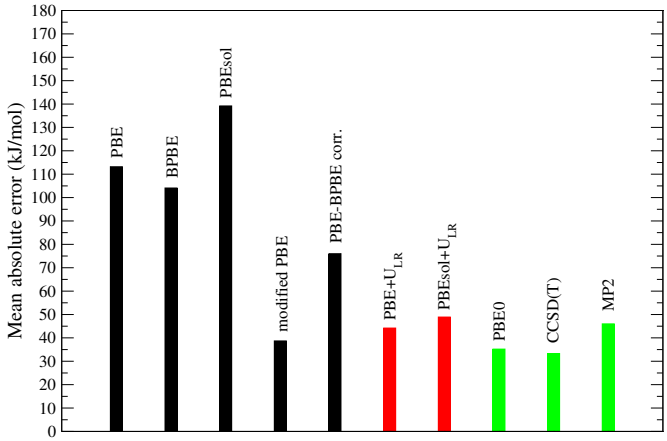

Figure 3.13: The mean absolute error for the eleven reactions considered by Shamov et al. [30] obtained using different methods. The PBE0, CCSD(T) and MP2 results are those of Shamov et al. [30].

trons core pseudopotential in the case of GGA and hybrid functionals. One exception is PBE0, which is also shown in results of Iche-Tarrat and Marsden [51]. Therefore we suspect that the number of valence electrons can impact the result, when that functional is used in calculations. In most of the studies that utilize the DFT+U method the Hubbard U parameter, and sometimes J (representing strength of the on-site electron exchange), is chosen in a way that particular, known properties of the investigated systems, such as the lattice parameters or the band gaps, could be reproduced by calculations. Some studies use *ab initio* based methods for the estimation of the Hubbard U parameter value [56], such as the *linear response* method [72], which we used in our studies, the constrained random phase approximation (cRPA) [164] or simple approaches such as the Slater transition state [71]. The Hubbard U parameter values can be also derived from the spectroscopic measurements [59–64]. We first computed the reaction enthalpies for different Hubbard U parameter values of 0.5 eV, 1.5 eV, 3 eV, 4.5 eV and 6 eV that are kept the same for all the reactants and products. All the results are given in Tables 3.18 and 3.19. It is clearly visible that the DFT+U method improves the prediction of the enthalpies of reactions over the

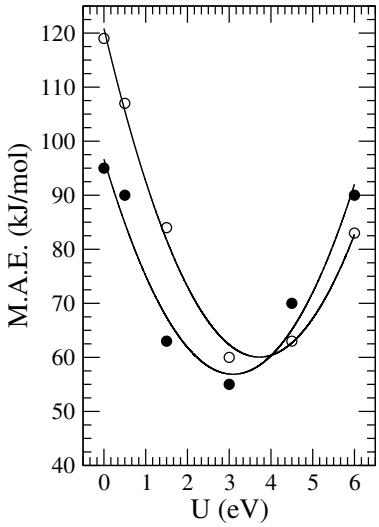

Figure 3.14: The mean absolute error (M.A.E) of the computed enthalpies of reactions given in Table 3.16 as a function of the Hubbard U parameter. Filled and open circles represent the results of PBE+U and PBEsol+U calculations, respectively. The curves represent fits by a parabola that were used to estimate the optimal Hubbard U parameter values (see discussion in the text).

PBE and PBEsol functionals. In the next step, we determined the values of Hubbard U parameter in a way, that it minimizes the deviation from the measured reaction enthalpies (i.e. minimizes the M.A.E.). These values were obtained by fit of the M.A.E. for different values of the U parameter by a parabola. The Hubbard U parameter value is given by the minimum of the fitted curve and the fitting results are illustrated in Figure 3.15. For the PBE+U and PBEsol+U methods we obtained the following values: $U = 3.0 \pm 1.0\,\text{eV}$ and $3.8 \pm 1.0\,\text{eV}$, respectively. We estimated the uncertainties on these values from Figure 2.3 taking into account the mean experimental error of $20\,\text{kJ/mol}/\sqrt{17} \sim 5\,\text{kJ/mol}$.[2] In addition to these studies, we derived the Hubbard U parameters for each considered molecular compound using the *linear response* method proposed by Cococcioni and de Gironcoli [72] (see Section 3.1). The obtained values of U_{LR} are reported in Table 3.1. Interestingly, on average these values are slightly smaller than the ones that minimize the M.A.E. However, as reported in Section 3.1,

[2]Computed as the standard error of the arithmetic mean.

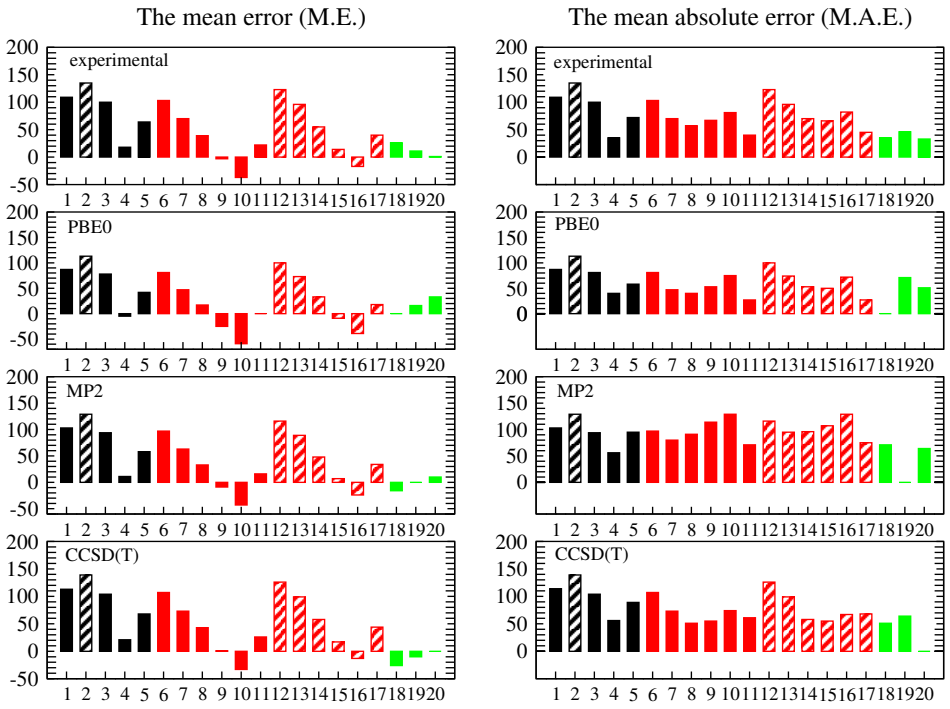

Figure 3.15: The mean absolute error and mean error (in kJ mol^{-1}) of the selected 11 gas-phase reactions considered by Shamov et al. [30] (see Table 3.16) obtained with different methods indicates on the horizontal axes as: (1) PBE, (2) PBEsol, (3) BPBE, (4) modified PBE, (5) PBE-BPBEcorr, (6) PBE+U(U = 0.5 eV), (7) PBE+U(U = 1.5 eV), (8) PBE+U(U = 3 eV), (9) PBE+U(U = 4.5 eV), (10) PBE+U(U = 6 eV), (11) PBE+U_{LR}, (12) PBEsol+U(U = 0.5 eV), (13) PBEsol+U(U = 1.5 eV), (14) PBEsol+U(U = 3 eV), (15) PBEsol+U(U = 4.5 eV), (16) PBEsol+U(U = 6 eV), (17) PBEsol+U_{LR}, (18) PBE0, (19) MP2 and (20) CCSD(T). Here the experimental values [17, 18] and the calculations of Shamov et al. [30] using PBE0, MP2 and CCSD(T) methods were chosen as reference and the references are indicated in the left-upper corners.

it is noticeable that the derived Hubbard U parameters decrease with decreasing the oxidation state of uranium. When only the values computed for U(VI) complexes are considered, the obtained U value of 2.8 eV is in good agreement with the values obtained from minimization of the M.A.E. This is not surprising as most of the considered reactions involve U(VI) complexes. On the other hand, our result indicates that the thermochemistry data can be used to determine the Hubbard U parameter value independently from other experimental methods such as spectroscopy [59–64]. Our

Table 3.18: The reaction enthalpies computed with the PBE+U method for the reactions given in Table 3.16 and the respective experimental values [17, 18]. The $U_{\mathrm{LR,d}}$ column represents the PBE+U_{LR} results corrected with the PBE+U calculations applied to the d-orbitals (see text for details). The enthalpies are given in kJ mol^{-1}.

	0.5 eV	1.5 eV	3 eV	4.5 eV	6 eV	U_{LR}	$U_{\mathrm{LR,d}}$	exp.
(1)	410	386	349	311	271	273	270	313±17
(2)	496	460	405	349	310	402	410	385±22
(3)	609	627	594	559	511	622	621	618±27
(4)	266	241	200	157	100	222	223	205±20
(5)	294	254	193	136	99	198	198	204±20
(6)	399	411	330	300	261	357	361	412±25
(7)	528	474	391	311	248	346	352	405±20
(8)	1176	1107	1120	1079	1048	1048	1015	1033±20
(9)	-232	-283	-363	-443	-497	-260	-225	-311±22
(10)	693	608	598	536	497	579	560	576±20
(11)	-127	-158	-204	-247	-278	-121	-98	-170±40
(12)	23	32	45	52	59	-19	-28	-25±31
(13)	-147	-158	-173	-186	-187	-149	-146	-182±11
(14)	175	170	160	145	130	127	125	65±11
(15)	328	308	275	238	201	272	278	189±12
(16)	607	603	593	579	550	538	530	437±12
(17)	133	138	146	154	162	117	106	272±11
mean error	71	47	14	-23	-55	8	8	
M.A.E.	90	63	55	70	90	45	50	20

studies also show that the *linear response* approach of Cococcioni and de Gironcoli [72] gives U values that minimize the error of DFT+U reaction enthalpies.

Solids

We extended the calculations and analysis performed for the molecular complexes into computation of simple uranium-bearing solids. We wanted to check if by using the mixture of GGA functionals, the *modified* PBE functional and the DFT+U method one can also improve the description of structures and the prediction of reaction enthalpies in the case of periodic systems. As for molecular compounds, in these calculations we derived the Hubbard U parameter value for each solid using the *linear response* approach [72] and the results for the values of U_{LR} are given in Table 3.2. As discussed in Section 3.1, the U_{LR} values derived for the solids are consistent with those derived for the molecular complexes (Table 3.1). Here we also observe that U_{LR} is larger for the U(VI)-bearing solids (UF_6 and UO_3) and is the smallest for the

Table 3.19: The reaction enthalpies computed with the PBEsol+U method for the reactions given in Table 3.16 and the respective experimental values [17, 18]. Columns represent results obtained with the fixed values of U and with $U = U_{\mathrm{LR}}$. The enthalpies are given in kJ mol^{-1}.

reactions	0.5 eV	1.5 eV	3 eV	4.5 eV	6 eV	U_{LR}	exp.
(1)	447	423	387	349	309	322	313±17
(2)	532	496	441	385	328	432	385±22
(3)	634	617	615	584	553	653	618±27
(4)	305	280	240	198	148	261	205±20
(5)	329	289	228	169	123	231	204±20
(6)	429	438	397	332	300	428	412±25
(7)	586	533	452	373	292	410	405±20
(8)	1188	1157	1113	1075	1096	1030	1033±20
(9)	-228	-281	-358	-436	-513	-244	-311±22
(10)	696	648	583	524	526	558	576±20
(11)	-127	-159	-204	-247	-288	-109	-170±40
(12)	27	37	51	57	64	-25	-25±32
(13)	-162	-172	-185	-197	-208	-161	-182±11
(14)	187	182	171	156	140	139	110±11
(15)	348	326	292	255	217	302	189±12
(16)	635	630	618	601	582	574	437±12
(17)	126	132	140	149	157	111	272±11
mean error	90	68	33	-6	-35	28	
M.A.E.	107	84	60	63	83	50	20

Table 3.20: List of the 9 considered reactions between the uranium-bearing solids.

(33)	α-$UF_5 + F \rightarrow UF_6$
(34)	β-$UF_5 + F \rightarrow UF_6$
(35)	$UF_4 + F \rightarrow \alpha$-$UF_5$
(36)	$UF_4 + F \rightarrow \beta$-$UF_5$
(37)	$UF_3 + F \rightarrow UF_4$
(38)	$UO_2 + O \rightarrow \alpha$-$UO_3$
(39)	$3UO_2 + 2O \rightarrow U_3O_8$
(40)	$UCl_4 + 2Cl \rightarrow UCl_6$
(41)	$UCl_3 + Cl \rightarrow UCl_4$

U(III) carrying materials. We computed the enthalpies of nine reactions between the considered solids. All the reactions are provided in Table 3.20. We note that in the calculation of reaction enthalpies for the gas-phase species, F, O and Cl, the energies of atoms are considered, not the relevant molecules (i.e. for instance the energy of F atom is used, not $1/2\,F_2$). The results are provided in Tables 3.21 and 3.22. The PBE and PBEsol functionals result in significant, systematic errors of 168 kJ/mol and 184 kJ/mol respectively. Similarly to the case of the enthalpies of reactions between the molecular compounds, the mixture of PBE and BPBE functionals and the *mod-*

Table 3.21: The reaction enthalpies computed with different DFT methods for the reactions given in Table 3.20 and the respective experimental values [17, 18]. Term PBEmodif indicates the *modified* PBE functional. The enthalpies are given in kJ mol^{-1}.

	PBE	PBEsol	BPBE	PBEmodif	PBE-BPBE corr.	exp.
(33)	-324	-352	-327	-280	-341	-200±8
(34)	-363	-369	-378	-277	-439	-192±6
(35)	-407	-414	-403	-443	-385	-240±10
(36)	-368	-397	-352	-446	-288	-248±8
(37)	-554	-578	-541	-522	-488	-491±9
(38)	-490	-510	-439	-487	-236	-250±3
(39)	-1208	-1191	-1086	-1037	-598	-818±4
(40)	-490	-515	-492	-389	-499	-290±6
(41)	-310	-335	-278	-298	-148	-276±5
mean error	-168	-184	-143	-131	-46	
M.A.E.	168	184	143	131	128	7

ified PBE functional result in improvements over the PBE and PBEsol functionals, although the improvement is not that pronounced as for the molecules. On the other hand the DFT+U method, similarly to the case of reactions between the molecular compounds, significantly improves the reaction enthalpies and the best results are obtained with the DFT+U_{LR} method. The M.A.E. is significantly reduced to 31 kJ/mol and 47 kJ/mol for PBE+U_{LR} and PBEsol+U_{LR} respectively, which is comparable to the error obtained for the enthalpies of reactions between the uranium-bearing molecules. In general, even the DFT+U method with fixed U value ranging from 3 eV to 6 eV substantially improves the prediction of DFT, and such calculations with $U = 4.5$ eV (the value that reproduces the band gap of UO_2) give the best results. The results obtained for solids are thus in line with the conclusions reached from the studies of molecular compounds. The both benchmark calculations indicate that the DFT+U method could allow for meaningful, computer-aided simulations of actinide-bearing materials, including those relevant for nuclear waste management, and that very good results for the thermochemistry can be obtained, when the Hubbard U parameter is derived *ab initio* for each considered molecular or solid structure.

Table 3.22: The reaction enthalpies computed with the DFT+U method for the reactions given in Table 3.20 and the respective experimental values [17, 18]. Columns represent results obtained with the fixed values of U and with $U = U_{\mathrm{LR}}$. The enthalpies are given in kJ mol^{-1}.

	PBE				PBEsol				exp.
reaction	3 eV	4.5 eV	6 eV	U_{LR}	3 eV	4.5 eV	6 eV	U_{LR}	
(33)	-256	-219	-186	-201	-284	-248	-211	-241	-200±8
(34)	-295	-257	-217	-241	-305	-268	-229	-262	-192±6
(35)	-302	-246	-184	-275	-319	-263	-206	-281	-240±10
(36)	-263	-208	-153	-235	-298	-242	-188	-260	-248±8
(37)	-471	-432	-399	-491	-491	-455	-423	-518	-491±9
(38)	-369	-282	-207	-333	-392	-306	-221	-362	-250±3
(39)	-898	-702	-503	-839	-964	-773	-578	-921	-818±4
(40)	-317	-229	-171	-266	-351	-264	-194	-297	-290±6
(41)	-223	-178	-159	-229	-281	-214	-164	-268	-276±5
mean error	-43	28	92	-12	-76	-3	65	-45	
M.A.E.	59	55	97	31	76	41	77	47	7

Table 3.23: List of considered 15 reactions between gas-phase actinide-bearing molecules.

(18)	$NpF_6 \rightarrow NpF_4 + 2F$	(26)	$AmF_6 \rightarrow AmF_3 + 3F$
(19)	$NpF_4 \rightarrow NpF_3 + F$	(27)	$NpCl_4 \rightarrow NpCl_3 + Cl$
(20)	$NpF_3 \rightarrow NpF_2 + F$	(28)	$PuCl_4 \rightarrow PuCl_3 + Cl$
(21)	$NpF_2 \rightarrow NpF + F$	(29)	$NpO_2 \rightarrow NpO + O$
(22)	$PuF_6 \rightarrow PuF_4 + 2F$	(30)	$PuO_3 \rightarrow Pu_2 + O$
(23)	$PuF_4 \rightarrow PuF_3 + F$	(31)	$PuO_2 \rightarrow PuO + O$
(24)	$PuF_3 \rightarrow PuF_2 + F$	(32)	$AmO_2 \rightarrow AmO + O$
(25)	$PuF_2 \rightarrow PuF + F$		

3.3.2 Neptunium-, plutonium- and americium-bearing molecules

following the successful results for uranium-bearing compounds we benchmarked the DFT+U_{LR} methods for other actinides, namely U, Np, Pu and Am. The considered reactions that involve these molecular complexes are presented in Table 3.23.

The Hubbard U parameter values derived for each considered actinide compound is presented in Table 3.3. As discussed in Section 3.1, in general, the Hubbard U parameter values decrease with decreasing the oxidation state of actinide. In this work we made a systematic comparison of the formation enthalpy of 15 reactions involving fluorides, chlorides and oxides of uranium, neptunium, plutonium and americium with experimentally available data [18, 17]. The mean average error (M.A.E.), taking the experimental values as the reference, of the reactions enthalpies obtained with the DFT+U_{LR} method using the PBE and PBEsol functionals was significantly reduced.

Table 3.24: The reaction enthalpies computed with different DFT and DFT+U methods for 15 reactions given in Table 3.23 and respective experimental values [17, 18]. The enthalpies are given in kJ mol^{-1}.

	PBE	PBEsol	PBE+U_{LR}	PBEsol+U_{LR}	exp.
(18)	835	902	575	643	518±42
(19)	528	556	492	515	524±47
(20)	644	668	614	632	573±55
(21)	646	663	645	665	573±55
(22)	345	373	268	294	319±15
(23)	690	759	411	476	422±42
(24)	460	484	389	411	459±28
(25)	584	601	557	575	632±12
(26)	616	637	609	629	805±16
(27)	414	567	357	428	412±25
(28)	950	1034	595	670	685±47
(29)	678	718	579	577	582±22
(30)	707	734	597	626	599±35
(31)	479	521	356	393	407±35
(32)	577	616	460	470	509±65
mean error	89	131	-17	21	
M.A.E.	95	135	41	52	36

The M.A.E. obtained using the PBE functional is 89 kJ/mol. The DFT+U_{LR} method reduces the error to 40 kJ/mol. In the case of the PBEsol functional the difference between the plain DFT and the DFT+U calculations is even larger, 92 kJ/mol (Table 3.24), with the PBEsol+U method better describing the formation enthalpies. Mean error of the 15 reactions is also presented in Table 3.24. The mean error is similar to M.A.E., thus the offset to the experimental values can be considered as systematic. These results are graphically shown in Figure 1.4. Comparison to all electron PBE0 and CCSD(T) calculations is available for reactions 10, 29 and 31 from Tables 3.16 and 3.23 [237, 238, 30]. The M.A.E. for these three reactions is 19 kJ/mol for calculations with DFT+U_{LR} method, 14 kJ/mol for calculations with the PBE0 hybrid functional and 13 kJ/mol for the CCSD(T) calculations.

3.3.3 Monazite- and xenotime-type ceramics

Having good description of structural parameters with PBEsol+U_{LR} performance of the method was tested for the description of energy-related properties of lanthanide

orthophosphates. For that purpose the enthalpies of formation of monazite were computed, assuming the reaction:

$$\frac{1}{2}Ln_2O_3 + \frac{1}{2}P_2O_5 \rightarrow LnPO_4. \tag{3.1}$$

The results are given in Figure 3.16. In our derivation the contribution from zero point energies was neglected, as it was already shown that these are second order effects affecting the derived enthalpies by no more than a few kJ/mol [28], which is substantially less than the error carried by the computational method. Adding 2 kJ/mol error by not accounting for spin-orbit interaction, we can assume, that these calculations carry an error of ~ 10 kJ/mol, but not significantly larger. With both PBE and PBEsol functionals the enthalpies of reactions are overestimated by up to ~ 80 kJ/mol. We got substantially larger offset than that of ~ 40 kJ/mol obtained by Rustad [28]. The only noticeable difference between the two calculations is the treatment of f-electrons. When the f-electrons are treated implicitly by putting them into the core as Rustad [28] did, his reaction enthalpies are reproduced. Comparing to DFT predictions, the DFT+U calculations in this work result in significant change, in both structural parameters and reaction enthalpies, in all considered cases. As is clearly visible in Figure 3.16, with the U parameter derived by the using the *linear response* method one significantly improves the prediction for the reaction enthalpies. Interestingly, PBEsol+U_{LR} results in ~ 40 kJ/mol improvement over DFT and an offset from experimental values [83] of also ~ 40 kJ/mol, which is the value of the offset reported by Rustad [28] in his PBE calculations. If we blindly take the difference between the PBEsol+U_{LR} and the PBEsol calculations and treat it as a correction to DFT, then the results using pseudopotentials with f-electrons included into the core with such a correction would lead to much better agreement with the experimental values. Rustad [28] also performed DFT+U calculations for case of Ce and claims that there is no significant difference in terms of enthalpy of formation (only a few kJ/mol). Our results show that this is rather a coincidence caused by different treatment of f-

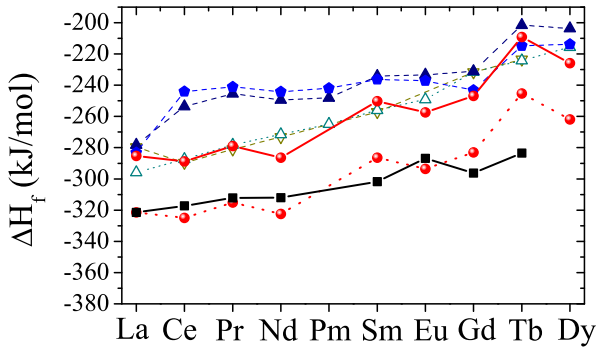

Figure 3.16: Volume of monazite. The results of different methods are marked according to convention used in Figure 3.7.

electrons (to perform the DFT+U calculation these must be included in the valence). For Ce PBE+U calculation with $U = 3\,\mathrm{eV}$ and f electrons treated as valence results in similar structures and reaction enthalpies ($-288.4\,\mathrm{kJ/mol}$) as PBE calculation with f-electrons included into the pseudopotential core ($-285.6\,\mathrm{kJ/mol}$), i.e. effect of U is canceled out by effect of implicit treatment of f electrons. Results for enthalpy of formation of monazite given in Figure 3.16 contain a clue for the origin of the offset between the computed and measured values. First of all, both the DFT and DFT+U methods result in the same reaction enthalpy in case of lanthanum, where there are no f-electrons, which is offset from the measured value by $36.1\,\mathrm{kJ/mol}$. Surprisingly, similar offset is seen in case of other lanthanides, which suggests that it is independent on lanthanide cation. In fact, if one shifts the PBEsol+U_{LR} reaction enthalpies by the offset obtained for lanthanum one ends up at the experimental curve for all the lanthanides, well reproducing experimentally seen increase in the reaction enthalpy with the atomic number of lanthanide (see Figure 3.16). Having a lanthanide-atom independent offset would be rather unexpected, if the offset is related to the treatment of f-electrons. This is because the strength of the on-site Coulomb repulsion represented by U_{LR} parameter varies significantly between lanthanides (see Table 3.4). Therefore, it would be surprising if an error in estimation of energy due to strong correlations

would be independent of the lanthanide-cation. In addition our U_{LR} values result in very good structures of both lanthanide-oxides and monazites, which would not hold if our Hubbard U values were wrong. On the other hand, having the same offset for the lanthanum, where there are no f electrons, as for other lanthanides points into the lanthanide independent (f electrons independent) origin of the discrepancy. The only lanthanide-independent factor in the considered reaction is P_2O_5. Knowing that DFT overestimating $P-O$ bond length is not able to accurately describe the structure of P_2O_5 (see Table 3.15) the constant offset between the computed and measured formation enthalpies can be explained by an error in computations of P_2O_5 and not by Ln-bearing reactants. In order to check this, we computed the PBEsol energy of P_2O_5 by using the experimental structure of Cruickshank [239]. The obtained energy is higher by 29.6 kJ/mol than the one obtained for the fully relaxed structure. When we performed PBEsol+U_{LR} calculations of La_2O_3 and $LaPO_4$ experimental structures, the respected energies that enter Eq. 3.1 are much smaller, 0.1 kJ/mol for the oxide and 4.6 kJ/mol for the monazite. All these results lead to increase in the formation enthalpy of $LaPO_4$ by 24.9 kJ/mol. This number is comparable to the observed energy offset of 36.1 kJ/mol, which supports the conclusion that the inaccurate description of the P_2O_5 structure is the main source of the offset between the computed and the experimental values of the considered formation enthalpies.

The studies performed for monazite-type ceramics were extended on the xenotime-type ceramics ($Ln PO_4$) and prediction of formation enthalpies using the DFT+U_{LR} method and the f-in-core PBESol functional for the $Ln PO_4$ series is shown on the Figure 3.17. The f-in-core PBEsol calculations result in the formation enthalpies that are consistent with the PBEsol+U_{LR} results and both predictions are consistent with the experimental measurements. There is a visible constant-like offset of 30 kJ/mol between the measured and the computed values of the formation enthalpies. In case of monazite we attributed this offset to the overestimation of the $P-O$ bond lengths and consequently overestimation of the volume of P_2O_5. If this is indeed the case we should obtain the same offset for xenotime. Indeed, our calculations of xenotime

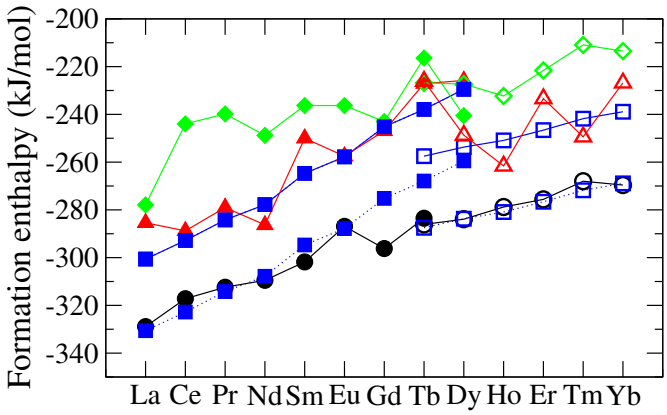

Figure 3.17: The formation enthalpies computed for monazite (filled symbols) and xenotime (open symbols) computed considering the $1/2Ln_2O_3 + 1/2P_2O_5 \rightarrow LnPO_4$ reaction and using the DFT and DFT+U methods.

show constant offset of 30 kJ/mol which support previous explanation. As in the case of monazite, for xenotime DFT f-in-valence approach underestimates the formation enthalpies and the experimentally seen trend along the lanthanide-series is also not well reproduced. On the other hand PBEsol f-in-core approach results in good agreement with the PBEsol+U_{LR} calculations, providing even less noisy and more consistent with the experimental values trend along the lanthanide series. This shows that the DFT f-in-core approach is a good method for computation of the energetics of lanthanide-phosphates and can be considered as a method of choice for further calculations such as the heat capacities of monazites reported in the next section.

3.3.4 Heat capacities of monazite-type ceramics

The characterization of thermodynamic properties of f-materials is of significant importance for in-depth study of potential nuclear waste host materials. Experimental studies of actinide-bearing materials are often problematic due to the activity of the samples. Therefore, many thermodynamically relevant properties of these materials, including the heat capacities, are often estimated with the aid of atomistic modeling (eg. Kaur et al. [240], Li et al. [26]). The heat capacity and entropy are

important thermodynamic parameters useful, for instance, in the assessment of the thermodynamic stability of materials under repository conditions. The pure-phase lanthanide and actinide monazite-type ceramics exist for Ln=La,...,Dy ($Ln$$PO_4$) and An=Pu, Am, Cm ($An$$PO_4$) [241]. The experimental data on the heat capacities and absolute entropies are available for some of these compounds. The low temperature heat capacities and the standard entropies have been measured for $LaPO_4$[242, 174], $CePO_4$[243], $NdPO_4$[244], $EuPO_4$[245] and $GdPO_4$[174]. The high temperature heat capacities have been reported for $LaPO_4$[246], $CePO_4$[246], $NdPO_4$[244], $SmPO_4$[247], $EuPO_4$[247] and $GdPO_4$[246]. For actinides, the analogous data are available only for $PuPO_4$. Thiriet et al. [84] and Benes et al. [248] measured the heat capacity of the pure $PuPO_4$ at low and high temperatures, respectively. Popa et al. [85] measured the low temperature heat capacity of the $La_{0.9}Pu_{0.1}PO_4$ solid solution. Because for many monazites the experimental data on low temperature heat capacities and standard entropies are missing, Thiriet et al. [84] estimated the standard entropies for the whole series of lanthanide monazites assuming that the contribution of vibrational entropy is constant for all these compounds and is equal to the measured standard entropy of $LaPO_4$ [174]. Thiriet et al. [84] further assumed that the vibrational contribution to the standard entropies of $An$$PO_4$ is larger than this of the lanthanides by a factor of 1.10. They computed this factor by comparing the vibrational entropies of various isoelectronic lanthanide and actinide compounds such as sesquioxides, trifluorides and trichlorides. Crystal field theory and the available spectroscopic data were then used for estimation of

the excess entropy arising from the thermal excitation of f electrons. However, these estimates and the underlying assumptions require validation. Here we show that *ab initio* atomistic modeling is an excellent tool for such a purpose. Recently, the heat capacities of the lanthanide monazites were computed *ab initio* by Feng et al. [182]. However, the computed heat capacities are smaller than the measured values. We will show that this deficiency is caused by the neglect of the contribution from the electronic specific heat, which is known to be significant for the considered orthophosphates [84].

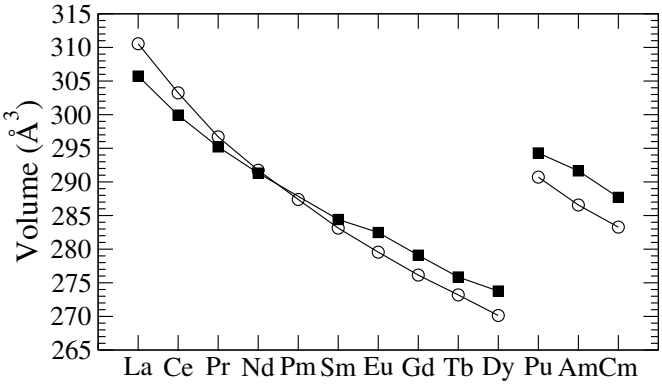

Figure 3.18: The computed (open circles) and measured (filled squares) volumes of $Ln\mathrm{PO}_4$ and $An\mathrm{PO}_4$ monazites.

Feng et al. [182] explain the low heat capacity of GdPO_4, in comparison to the other monazites, by the temperature-induced monazite to zircon phase transition. We will demonstrate that the explicit accounting for the thermal excitation of the f electrons explains this difference without necessity of involvement of another processes. We also note that the local spin density approximation (LSDA), variation of DFT method used by Feng et al. [182], resulted in significantly underestimated (by $\sim 10\%$) volumes of the investigated compounds. Such deficiency must have also affected the computed heat capacities, which indicates that the computational approach has to be carefully chosen in order to get accurate estimation of the thermodynamic properties of monazite-type ceramics. Thermal excitations of f electrons can contribute significantly to the entropy and the heat capacity of monazite-type ceramics [84, 174]. This contribution arises from the electronic thermal excitations inside the partially filled f-shells and is often referred to as the Schottky contribution [175, 174]. The excited electronic levels that contribute to the effect arise from the Stark splitting of the ground state by the crystal electric field. For the elements that show very small excitations of the ground state (eg. Gd^{3+} or Cm^{3+}, Table 3.25) the Schottky contribution to the heat capacity is very small. However, this contribution to the standard entropy can be still significant due to multiplicity of the ground level, g_0. When the energy splitting of the ground state

Table 3.25: The energy levels of Ln^{3+} and An^{3+} in $An : LaCl_3$ and $Ln : LaCl_3$. The results for Ce^{3+} are these estimated for $CePO_4$ monazite by Thiriet et al. [174]. The energy units are cm^{-1}.

Ce^{3+}		Pr^{3+}		Nd^{3+}		Pm^{3+}		Sm^{3+}		Eu^{3+}	
$^2F_{5/2}$	0	$^3H_4$	0	$^4I_{9/2}$	0	$^5I_4$	0	$^6H_{5/2}$	0	$^7F_0$	0
	339		0		113		0		46	$^7F_1$	363
	669		29		128		55		75		363
$^2F_{7/2}$	2217		106		240		55	$^6H_{7/2}$	1009		417
	2669		106		250		78		1060	$^7F_2$	1034
	2903		130	$^4I_{11/2}$	1969		92		1110		1034
	3015		130		2008		92		1186		1041
			156		2020		108	$^6H_{9/2}$	2243		1041
			215		2041		206		2259		1096
		$^3H_5$	2106		2045	$^5I_5$	1548		2331	$^7F_3$	1869
			2138		2053		1563		2357		1885
			2138				1563		2389		1902
			2168				1576				1902
			2168				1576				1925
			2177				1605				1943
			2205				1605				1943
			2205				1608				
			2236				1608				
			2236				1613				
			2269				1623				

Gd^{3+}		Tb^{3+}		Dy^{3+}		Pu^{3+}		Am^{3+}		Cm^{3+}	
$^8S_{7/2}$	0	$^7F_6$	0	$^6H_{15/2}$	0	$^6H_{5/2}$	0	$^7F_0$	0	$^8S_{7/2}$	0
	0.12		0		9		23	$^7F_1$	2718		6
	0.19		55		9		81		2718		6
	0.23		55		20	$^6H_{7/2}$	3097		2779		8
$^6P_{7/2}$	32436		91		51		3213	$^7F_2$	5285	$^6D_{7/2}$	16996
	32458		98		85		3364		5285		17076
	32473		98		126		3450		5289		17223
	32477		98		157	$^6H_{9/2}$	6022		5289		17294
$^6P_{5/2}$	33024		98	$^4H_{13/2}$	3455		6039		5378	$^6P_{5/2}$	20217
	33046		110		3490		6142	$^7F_3$	7436		20280
	33050		118		3493		6153		7449		20363
			118		3523		6287		7492		
			130		3544				7492		
		$^7F_5$	2050		3551				7569		
			2086		3558				7588		
			2086						7588		
			2098								
			2098								
			2120								
			2157								
			2157								
			2173								
			2173								
			2202								

is negligible, the entropy effect can be computed as $Rlng_0$, which gives $S_{exc} \sim Rln8 = 17.3\,JK^{-1}mol^{-1}$ for the cases of Gd^{3+} and Cm^{3+}. The energy levels of Ln^{3+} and An^{3+}, ϵ_i, were estimated with the aid of Crystal Field Theory. For calculating the crystal-field splitting of the energy levels in lanthanide and actinide monazites we used the code

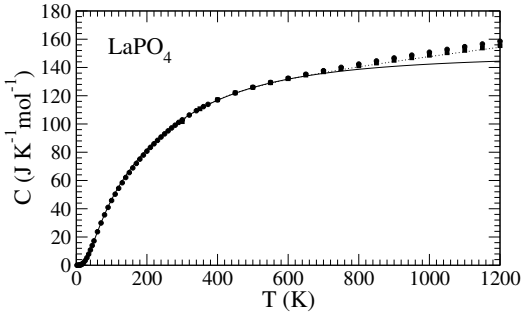

Figure 3.19: The heat capacity of $LaPO_4$. The solid line represents the computed values (at constant volume, C_V) and the dotted line represents the fit with the equation 3.2 discussed in section 3.3.4. The symbols show the experimental results (at constant pressure, C_p) of Gavrichev et al. [242], Thiriet et al. [174] (filled circles) and Popa et al. [246] (filled squares).

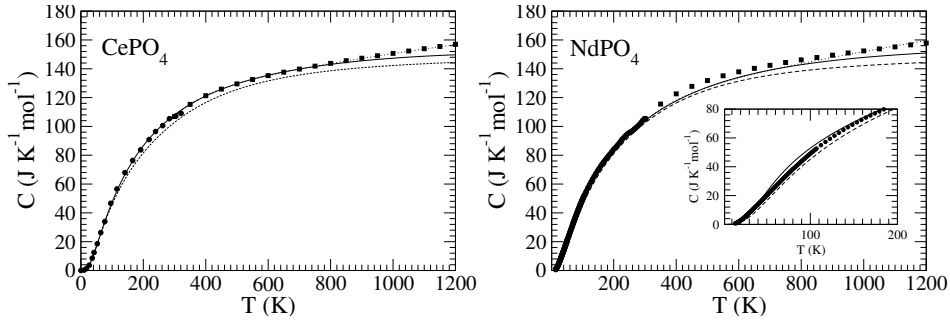

Figure 3.20: The heat capacities of $CePO_4$ and $NdPO_4$. The solid line represents the computed values, the dashed line shows the lattice contribution and the dotted line represents the fit with the equation 3.2 discussed in section 3.3.4. In the left panel the symbols show the experimental results of Thiriet et al. [243] (filled circles) and Popa et al. [246] (filled squares) and in the right panel of Popa et al. [244]. The insert panel shows the low temperature part of the figure.

developed by Edvardsson and Aberg [176]. It performs diagonalization of an effective Hamiltonian which results in prediction of the splitting of the energy levels of a free ion by the electric field of a particular crystalline compound. The parameters of the effective Hamiltonian, namely the electrostatic, the spin-orbit, Judds [178] and Trees [179] parameters, are usually constrained from the spectroscopic data. Unfortunately, the complete set of such data is not yet available for the lanthanide- and actinide-monazites of interest. Partial information is available for Nd-, Eu- and Cu-doped $LaPO_4$ [249, 250]. However, variations in the crystal-field splitting of Ln(III) and

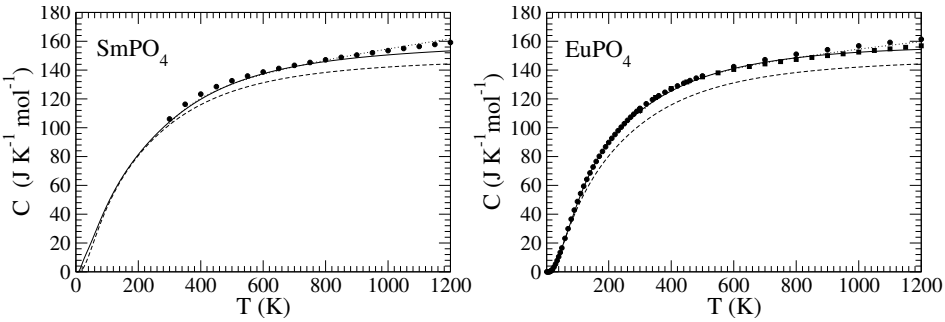

Figure 3.21: The heat capacities of $SmPO_4$ and $EuPO_4$. The solid line represents the computed values, the dashed line shows the lattice contribution and the dotted line represents the fit with Eq. 3.2 discussed in section 3.3.4. In the left panel the symbols show the experimental results of Popa and Konings [247] and of Gavrichev et al. [245] (filled circles) and Popa and Konings [247] (filled squares), in the right panel.

An(III) ions due to different crystal structures of host minerals are usually small. For example, the splitting of the F_0, F_1 and F_2 levels of Eu^{3+} remains approximately the same in $LaCl_3$, LaF_3, $LaPO_4$, and in different polymorphs of $CaCO_3$ [249–251]. These small differences in the energy levels when converted into the Schottky contributions certainly result in small change in the computed heat capacities and the standard entropies. However, these variations are insignificant relative to the experimental uncertainties. For instance, the Schottky contribution of Eu^{3+} varies within the range of $0.5\,\mathrm{J\,mol^{-1}K^{-1}}$ for different crystal structures. Therefore, for practical needs, the Schottky contributions to the heat capacities of monazites can be estimated from the spectroscopic data available for other crystalline phases. An almost complete set of experimental data is available for *Ln* and *An* doped $LaCl_3$ [252, 249, 253], which we decided to use in our calculations. The one

exception is $CePO_4$. Because we were not able to find the relevant data on $CeCl_3$, in the estimations of the Schottky correction for this compound we used the energy levels values estimated for $CePO_4$ by Thiriet et al. [174]. The energy levels used in the calculations of all the considered cations are given in Table 3.25. We will show that they result in the Schottky contributions to the heat capacities and the entropies that are consistent with the previous estimates of Thiriet et al. [84] and Popa and Konings

Table 3.26: The standard heat capacities of $Ln\mathrm{PO_4}$ and $An\mathrm{PO_4}$ monazites at $T = 298.15\,\mathrm{K}$.

Ln/An	$C_{V,\mathrm{lat}}$ ($\mathrm{JK^{-1}mol^{-1}}$)	$C_{V,\mathrm{exc}}$	$C_{V,\mathrm{tot}}$	$C_{P,\mathrm{exp}}$
La	102.8	0.0	102.8	102.6[a]
				101.3[b]
Ce	102.5	5.2	107.7	106.4[c]
Pr	102.2	0.9	103.1	
Nd	102.1	1.7	103.8	104.8[d]
Pm	101.8	0.9	102.7	
Sm	101.7	2.0	103.7	
Eu	101.5	9.7	111.2	112.9[e]
Gd	101.4	0.0	101.4	102.2[f]
Tb	101.2	0.4	101.6	
Dy	101.1	0.5	101.6	
Pu	102.2	0.2	102.4	114.5[g]
Cm	102.0	0.0	102.0	
Am	101.9	0.0	101.9	

[a] [242], [b] [174, 246], [c] [243, 246], [d] [244], [e] [245], [f] [174, 246], [g] [84].

[247].

Heat capacities of $Ln\mathrm{PO_4}$

The measured heat capacities of $Ln\mathrm{PO_4}$ for $Ln = \mathrm{La, Ce, Nd, Sm, Eu}$ and Gd are well reproduced by the calculations (Figures 3.19-3.22). Because La does not have f electrons, the heat capacity of $\mathrm{LaPO_4}$ arises from lattice vibrations only. The calculated heat capacities of $\mathrm{LaPO_4}$ agree well with the measured ones [242, 174, 246] up to $T = 700\,\mathrm{K}$. Within this interval the deviation from the measured values is smaller than $1.5\,\mathrm{JK^{-1}mol^{-1}}$ (Figure 3.19). For temperatures greater than 700 K the calculations underestimate the heat capacity.

This deviation suggests that the quasi-harmonic approximation becomes invalid for $\mathrm{LaPO_4}$ monazite above 700 K. The validity limit of the quasi-harmonic approximation will be further discussed in section 3.3.4. The measured heat capacity of $\mathrm{CePO_4}$ [243, 246] is also well reproduced by our calculations (Figure 3.20). Here the Schottky effect is significant with the contribution to the standard heat capacity of $5.2\,\mathrm{JK^{-1}mol^{-1}}$ (Table 3.26). In the case of $\mathrm{NdPO_4}$ the match to the measured heat capacities is the worst, but still the calculations differ from experiment by not more than $3.5\,\mathrm{JK^{-1}mol^{-1}}$ at $T < 300\,\mathrm{K}$ (Figure 3.20).

Table 3.27: The standard entropies of LnPO$_4$ and AnPO$_4$ monazites at $T = 298.15$ K.

Ln/An	$S_{\rm lat}$ (JK^{-1}mol^{-1})	$S_{\rm exc}$	$S_{\rm tot}$	$S_{\rm exp}$
La	109.8	0.0	109.8	108.7[a]
				108.2[b]
Ce	108.7	10.5	119.2	120.0[c]
Pr	107.9	17.8	125.7	
Nd	107.6	18.3	125.9	122.9[d]
Pm	107.1	18.0	125.1	
Sm	107.1	15.2	122.3	
Eu	106.7	9.2	115.9	116.8[e]
Gd	106.6	17.3	123.9	124.1[f]
Tb	106.3	21.1	127.4	
Dy	106.2	22.8	129.0	
Pu	113.0	14.8	127.8	137.0[g]
Cm	112.5	17.3	129.8	
Am	112.2	0.0	112.2	

[a][242], [b][174, 246], [c][243, 246], [d][244], [e][245], [f][174, 246], [g][84].

The heat capacity of SmPO$_4$ has been measured only at high temperatures ($T >$ 300 K). As shown in Figure 3.21, the high temperature data are well reproduced by the calculations. Interestingly, in this system the Schottky effect becomes significant even at very low temperatures. The reason is that Sm^{3+} has low lying excited states (see Table 3.25) which become populated even at temperatures as low as few K. The measured heat capacities of EuPO$_4$ and GdPO$_4$ are also well reproduced (Figures 3.21 and 3.22). EuPO$_4$ shows the largest Schottky effect with 9.7 JK^{-1}mol^{-1} contribution to the standard heat capacity. Because Gd^{3+} in GdPO$_4$ has half filled f-shells, the splitting of its $^8S_{7/2}$ ground state is insignificant, while its first excited state, $^6P_{7/2}$, has a very high energy of 32436 cm^{-1} (Table 3.25). Therefore, the Schottky contribution to the heat capacity of GdPO$_4$ is negligible (Table 3.25). This explains why the heat capacity of GdPO$_4$ is low and similar to this of LaPO$_4$. In Table 3.26 we give the computed standard heat capacities of all LnPO$_4$ monazites. We note that there is a slight monotonic decrease in the lattice vibrations contribution along the lanthanide series. In DyPO$_4$ the vibrational contribution to the standard heat capacity is 1.7 JK^{-1}mol^{-1} smaller than in LaPO$_4$. This is the effect of the slightly smaller vibrational frequencies of heavier lanthanides. It explains why GdPO$_4$ with its negligible Schottky contribution and a small lattice vibrations contribution has the lowest heat capacity among

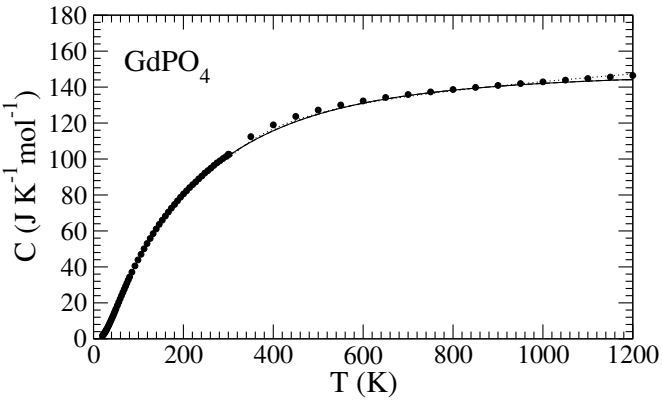

Figure 3.22: The heat capacity of $GdPO_4$. The solid line represents the computed values, the dashed line gives the lattice vibrations contribution and the dotted line represents the fit with the equation 3.2 discussed in section 3.3.4. The symbols show the experimental results of Thiriet et al. [174] and Popa et al. [246].

the lanthanide monazites. Thus the low heat capacity of $GdPO_4$ noted by Feng et al. [182] is a consequence of the electronic structure of Gd^{+3} and its relatively high mass. Therefore, the monazite to zircon phase transition in $GdPO_4$ proposed by Feng et al. [182] to explain the low heat capacity of this compound can be ruled out.

Table 3.27 lists the standard entropies of $Ln PO_4$ monazites. The Schottky contribution to the standard entropy is significant for almost all $Ln PO_4$ monazites. This is because the second term in Eq. 2.40 can be significant even when the crystal-field splitting of the ground state is negligible. In Table 3.27 we compare the predicted values of standard entropies to those derived from the measured heat capacities. The computed values agree well with the measured ones for $LaPO_4$, $CePO_4$, $EuPO_4$ and $GdPO_4$ but the standard entropy of $NdPO_4$ is slightly overestimated. This small excess is caused by the overestimation of the heat capacity of $NdPO_4$ at low temperatures (see the insert panel in Figure 3.20).

Validity of the quasi-harmonic approximation

The heat capacities and the vibrational entropies are computed with the quasi-harmonic approximation [38] in which anharmonic vibrational effects are neglected. This model

Table 3.28: The coefficients of polynomial given by Eq. 3.2 obtained by the least squares fits to the computed values of heat capacities of $Ln\mathrm{PO_4}$ and $An\mathrm{PO_4}$. The units of a, b and c are $\mathrm{JK^{-1}mol^{-1}}$, $10^{-3}\mathrm{JK^{-2}mol^{-1}}$ and $10^{6}\mathrm{JKmol^{-1}}$, respectively

Ln/An	*a*	*b*	*c*
La	120.86	29.31	-2.48
Ce	125.14	27.75	-2.37
Pr	119.40	34.18	-2.46
Nd	119.71	34.63	-2.46
Pm	121.42	34.57	-2.72
Sm	126.91	30.78	-3.02
Eu	135.69	21.76	-2.92
Gd	129.43	16.71	-3.14
Tb	125.15	25.22	-2.96
Dy	127.13	19.93	-2.99
Pu	121.33	28.68	-2.55
Am	117.33	36.70	-2.45
Cm	129.53	16.57	-3.10

usually breaks down above a certain temperature, leading to the underestimation of the heat capacities at high temperatures. The limiting temperature at which the approximation is still valid appear to vary significantly along the *Ln*-series. For $\mathrm{LaPO_4}$ this temperature is about 700 K (Figure 3.19). For $\mathrm{CePO_4}$ and $\mathrm{SmPO_4}$ the validity limit appears to hold up to $T \sim 900\,\mathrm{K}$, while for the heavier lanthanides, i.e. $\mathrm{EuPO_4}$ and $\mathrm{GdPO_4}$, deviations from the harmonic behavior are barely detectable up to $T = 1200\,\mathrm{K}$. This increase in the limiting temperature is apparently related to the decrease in the volume of monazite compounds along the lanthanide series (see Figure 3.18), which reduces the anharmonic effects on lattice vibrations. It is a common practice to approximate the high temperature tail of the heat capacity function by a polynomial in T. For example, Popa and Konings [247] have used the following equation:

$$C = a + bT + cT^{-2}. \tag{3.2}$$

We fitted the parameters of this polynomial to the computed high temperature ($T > 300\,\mathrm{K}$) tails of the heat capacities. The upper temperature of the fitted interval was chosen to be 700 K for $\mathrm{LaPO_4}$, 800 K for $\mathrm{CePO_4}$, $\mathrm{PrPO_4}$, $\mathrm{NdPO_4}$, $\mathrm{PmPO_4}$, $\mathrm{SmPO_4}$ and $\mathrm{PuPO_4}$, 900 K for $\mathrm{EuPO_4}$ and $\mathrm{AmPO_4}$ and 1000 K for $\mathrm{GdPO_4}$, $\mathrm{TbPO_4}$, $\mathrm{DyPO_4}$ and $\mathrm{CmPO_4}$. These temperatures were assumed to match the limit of validity of

the quasi-harmonic approximation discussed in the previous paragraph. The upper temperature limits for the actinide monazites were chosen to be identical to those of their isoelectronic lanthanide compounds. The parameters of the polynomial of Eq. 3.2 obtained for all the considered monazites are given in Table 3.28. The resulting heat capacities are also plotted in Figures 3.19-3.23. With Eq. 3.2 we are able to reproduce the high temperature heat capacities and the procedure emulates the anharmonic effects not accounted for by the quasi-harmonic approximation. Equation 3.2 together with the polynomial parameters given in Table 3.28 can thus be used to estimate the heat capacities of the considered monazites at high temperatures.

Heat capacities of $An\mathrm{PO}_4$

Monazite-type ceramics with trivalent actinide cations exist for An= Pu, Am, Cm [241]. Although the thermal excitations of f electrons contribute significantly to the standard entropy of these compounds (see Table 3.27), the Schottky effect to the standard heat capacity is negligible (Table 3.25). This happens because the excited states of An^{3+} have higher energies than those of Ln^{3+} (see Table 3.25). The only significant contribution to the heat capacity comes from the lattice vibrations. Due to the mass effect, this contribution is slightly larger for the actinide monazites than for their lanthanide analogues (see Table 3.26). The mass effect can be accurately reproduced by substituting the mass of Sm by the mass of Pu in the dynamical matrix computed for SmPO_4. The heat capacity computed from vibrational eigenstates of the modified matrix almost exactly matches this computed directly for PuPO_4. For instance, for $T = 298.15\,\mathrm{K}$ we got $C_v = 102.1\,\mathrm{JK}^{-1}$, which is very close to the value reported in Table 3.25 for PuPO_4. The lattice vibrations contributions to the standard entropies of actinide monazites are also slightly larger than in the lanthanide case (Table 3.27).

Out of the three cases of actinide monazites, the heat capacity has been measured only for PuPO_4 [84, 248]. In Figure 3.23 we compare the results of our calculations to these experimental data. The computed values are substantially smaller than the measured

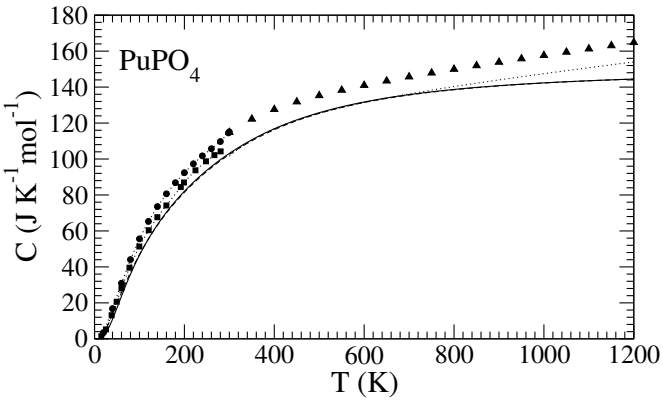

Figure 3.23: The heat capacity of $PuPO_4$. The solid line represents the computed values, the dashed line shows the lattice vibrations contribution and the dotted line represents the fit with the Eq. 3.2 discussed in section 3.3.4. The symbols show the experimental results of Thiriet et al. [84] (filled circles) and Benes et al. [248] (filled triangles). The filled squares represent the heat capacity measured for $La_{0.9}Pu_{0.1}PO_4$ by Popa et al. [85]

ones. We found the difference in the standard heat capacity to be 12.1 $Jmol^{-1}K^{-1}$, which is significant. It is difficult to understand the origin of this discrepancy, especially when the contribution to the heat capacity is expected to arise from the lattice vibrations only, while the effect of mass is adequately taken into account in our simulations. The calculated standard entropy is smaller than the measured value by 9.2 $Jmol^{-1}K^{-1}$. Although the origin of this discrepancy cannot be fully resolved within this study, we note that the calorimetric data on Pu-bearing monazites of Popa et al. [85] and Benes et al. [248] are inconsistent. In Figure 3.23 we plotted the heat capacity of $La_{0.9}Pu_{0.1}PO_4$ solid solution measured by Popa et al. [85] together with the experimental data on pure $PuPO_4$ and $LaPO_4$. The heat capacity data for $La_{0.9}Pu_{0.1}PO_4$ lie between the experimental measurements for $LaPO_4$ and $PuPO_4$, implying that the lattice contributions to the standard heat capacity and the standard entropy of $La_{0.9}Pu_{0.1}PO_4$ are approximately equal to the half sum of the corresponding values for $LaPO_4$ and $PuPO_4$. This result is not expected as, under the assumption of additivity, the data for $La_{0.9}Pu_{0.1}PO_4$ should lie much closer to those of $LaPO_4$. The available data thus suggest that the solid solution of $La_{1-x}Pu_xPO_4$ is characterized by

a very large excess vibrational entropy, which amounts to about $S^E = 27\,\mathrm{Jmol^{-1}K^{-1}}$ at $x = 0.5$. This value is much larger than the effect of ideal configuration entropy of $5.7\,\mathrm{Jmol^{-1}K^{-1}}$, or the excess enthalpy of mixing of $\sim 1\,\mathrm{kJmol^{-1}}$ computed for the $La_{1-x}Pu_xPO_4$ solid solution [26], and thus is unreasonably large. On the other hand, under the assumption of the absence of an excess heat capacity, the data of Popa et al. [85] and the data on $LaPO_4$ [242, 174, 246] could be used to extract the contribution of $PuPO_4$ to the heat capacity of the mixture. The heat capacity of $PuPO_4$ evaluated in this way would amount to about $165\,\mathrm{Jmol^{-1}K^{-1}}$ at 298 K. This value is also unreasonably large. These speculations together with the observed discrepancy between the calculated and measured data for $PuPO_4$ suggest that the data on $PuPO_4$ or $La_{1-x}Pu_xPO_4$, or both, could be subjected to an error. A potential explanation for the mentioned difficulties with the interpretation of the experimental data could be caused by impurity of the samples. For instance, a possible admixture of PuO_2 could lead to a significant Schottky contribution to the heat capacity, similarly to the case of $EuPO_4$. Indeed, Krupa and Carnall [254] have shown that excited states of Pu^{4+} have much lower excitation energies than those of Pu^{3+}. A potential excess contribution to the heat capacity of $PuPO_4$ can also occur due to the activity of the sample. For example, the self-heating of the sample would cause its temperature to be slightly higher than the temperature of the calorimeter. This could make an effect on interpretation of the relaxation calorimetry measurements, as the Physical Property Measurement System (PPMS) software assumes that the temperature relaxes exactly to the temperature of the heat bath. An additional potential difficulty could be related to the use of encapsulation. The heat capacity of the encapsulator, e.g. a two-component epoxy, has to be subtracted from the total heat capacity of the encapsulated sample [255]. A potential uncertainty could come from a difficulty of preparing the epoxy of exact composition, as the two components are involved. The study of Javorsky et al. [255] have shown that inhomogeneities in the epoxy could lead to significant variations in its heat capacity. In view of the outlined problems with the data on Pu-monazites and in view of the absence of experimental data on other actinide monazites, our calculations

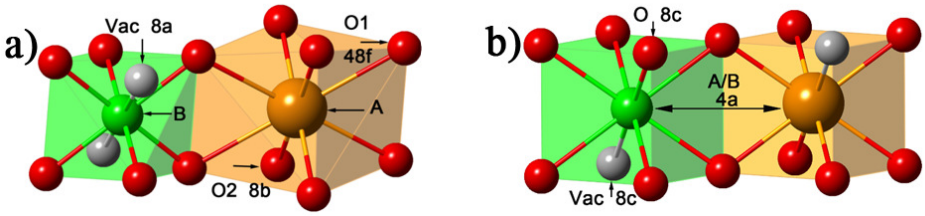

Figure 3.24: Representations of the pyrochlore (a) and the defective fluorite structures (b).

for the actinide compounds cannot be fully validated. However, based on our successful prediction of the heat capacity data on lanthanide monazites, we assume that our calculations should provide realistic estimates of the heat capacities and standard entropies of the actinide analogues. On the other hand, we note that the discrepancies observed for the Pu-monazites points to the need of additional experimental measurements.

3.3.5 Defect formation energies in pyrochlore-type ceramics

Natural pyrochlore oxides ($A_2B_2O_7$) contain up to 30 wt% UO_2 and 9 wt% ThO_2 without damaging their crystalline structure [256]. For this reason, the pyrochlore-type ceramics are considered as a final crystalline form for nuclear waste disposal [86, 15, 87]. The relevant properties of pyrochlores have been systematically investigated by various methods such as the actinide-doping [257–263], the dissolution experiments [35, 19, 264], the ion beam-irradiation [265–275], and by atomistic calculations. The latter includes simulations of the disordering process [276–279] and of the defect formation energetics [271, 280]. The results of these atomistic simulations have been widely used to interpret the experimental findings [22]. Pyrochlore and defective fluorite have cubic symmetry [272]. In figure 3.24 the relationship between their crystalline structures is shown. The local ionic configurations are represented with the cubes that have cations in the center and oxygen or vacancies distributed at the corners. The different cation sites are interconnected via common cube edges. In pyrochlore

cations A and B are eight- and six-fold coordinated, respectively. This leads to an appearance of a superlattice with the ordered arrangement of cations and vacancy sites. In defective fluorite both cations are seven-fold coordinated which makes their positions indistinguishable and results in random distribution of cations and oxygen vacancies [15]. Two main point defects that form in pyrochlore are the cation antisite (CA) and anion Frenkel pair (AFP) defects. The CA defect in pyrochlore is formed by flipping the position of A and B cations and the AFP results from the transfer of a 48f oxygen to the vacant site 8a. The ordered pyrochlore (Fig. 3.24(a)) could be transformed to defective fluorite (Fig. 3.24(b)) by a combination of these defects. It is commonly accepted that the accumulation of these defects leads to the order-disorder (O-D) transition (i.e. transition from the ordered pyrochlore to the disordered defective fluorite) [280, 281]. Although the O-D transition has been extensively studied experimentally [257, 282, 283], the underlying physics of the phase transition remains unclear.

DFT and DFT+U calculations

The relationship between the structural stability of pyrochlore and the defect formation energies (DFE) has been systematically investigated by the force-field (FF) atomistic simulations. These studies have shown that the compounds with smaller cation radius ratio, r_A/r_B, which form defective fluorite have relatively small CA DFE [272, 271, 280, 281]. However, these energies are still at least 2 eV, which is too large for disordering to occur. On the other hand, recent DFT studies of DFEs for selected pyrochlores [284–290] (see Table 3.29) show that these energies are substantially smaller than those predicted with FF methods (e.g. Sickafus et al. [271]). This puts the FF results in doubt and shows the necessity of revision of the previously published DFE contour maps for pyrochlores.

We carried out *ab initio* calculations using two approaches which were successfully applied to study the monazite-type lanthanide-phosphates in previous sections [23, 26]: the DFT+U_{LR} method, with the Hubbard U parameter derived *ab initio* using

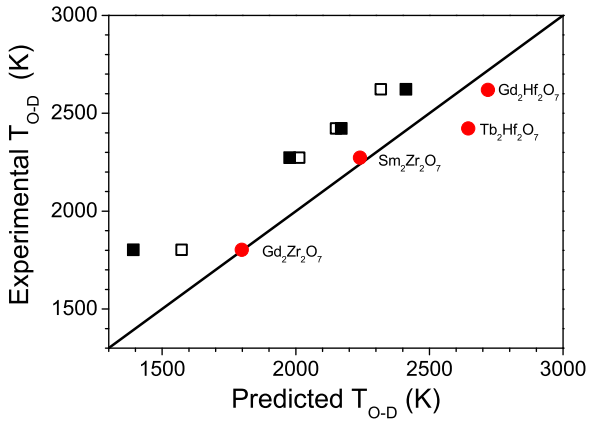

Figure 3.25: Comparison of the calculated O-D transition temperature with the experimental data [291, 292] for selected pyrochlores. The symbols represent DFT results of [183] (black filled squares) and our DFT (black squares) and DFT+U (red filled circles) calculations.

the *linear response* method of Cococcioni and de Gironcoli [72] and the f-in core approach in which f electrons are modeled by the pseudopotential. As we shown in previous sections, the second approach results in energies and structures that are usually better than when f electrons are computed explicitly, and consistent with the DFT+U method [23, 28, 26], being at the same time computationally more stable.

Jiang et al. [183] performed DFT calculations of the O-D transition temperatures for a series of $A_2B_2O_7$ pyrochlores and obtained temperatures that are systematically lower by 250 K than the measured values. In order to test our computational approaches these temperatures were recomputed for $Sm_2Zr_2O_7$, $Gd_2Zr_2O_7$, $Tb_2Hf_2O_7$ and $Gd_2Hf_2O_7$ with the two chosen methods. The Hubbard U parameter values used in the DFT+U calculations are provided in Table 3.6. The results are illustrated in Fig 3.25. The DFT+U_{LR} method significantly improves the DFT prediction of O-D transition temperatures. This clearly indicates that this method improves the description of $4f$ electrons. On the other hand, because of the explicit treatment of f electrons, in many instances the convergence of the DFT+U was very slow, and in some cases

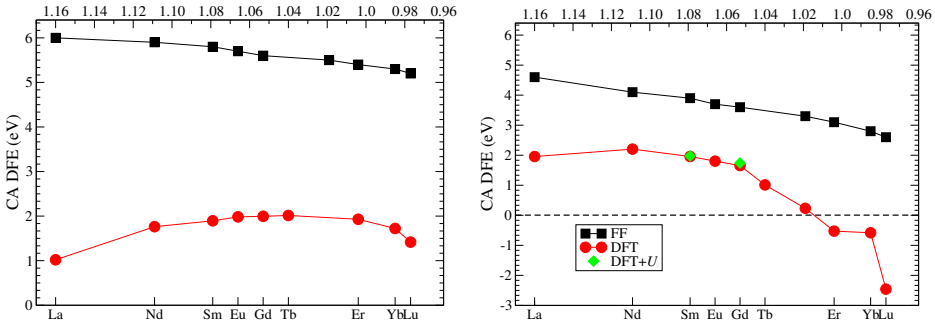

Figure 3.26: The CA DFEs for $A_2Ti_2O_7$ (left) and $A_2Zr_2O_7$ (right) obtained with FF [271] and DFT/DFT+U methods.

Table 3.29: CA DFEs (in eV) obtained in this study (ts), the previous DFT calculations (ps) and with previous FF calculations. The pyrochlore compositions are indicated as (A,B).

Comp.	ts	ps	FF	Comp.	ts	ps	FF
(La,Ti)	1.02	1.93[a]	6.0	(Gd,Sn)	2.93	2.52[d]	4.5
(Sm,Ti)	1.89	2.18[a]	5.8	(Tb,Sn)	2.83	3.58[d]	
(Gd,Ti)	2.00	1.80[b]	5.6	(Y,Sn)	2.48	1.97[c]	4.1
		2.32[a]				3.39[d]	
(Tb,Ti)	2.01	2.31[a]		(Er,Sn)	2.48	3.23[d]	4.0
(Y,Ti)	1.95	1.77[c]	5.5	(Lu,Sn)	2.06	2.16[d]	3.5
		2.29[a]					
(Er,Ti)	1.93	2.24[a]	5.4	(La,Hf)	2.73	2.84[d]	
(Lu,Ti)	1.42	2.06[a]	5.3	(Gd,Hf)	1.60	2.15[d]	
(La,Sn)	3.20	2.83[d]	5.0	(La,Hf)	1.96	1.38[f]	
(Nd,Sn)	3.21	3.42[d]	4.9	(Gd,Zr)	1.66	1.78[b]	3.6
(Sm,Sn)	3.11	3.06[d]	4.6	(Y,Zr)	0.23	0.26[c]	3.3

[a] [285], [b] [282], [c] [284], [d] [287], [e] [289], [f] [290].

it was difficult to reach the ground state. This was never the case with the f-in-core approach. In terms of the energy difference between the two phases, the results of the two computational methods deviate by no more than 0.3 eV. Although it matters for the precise derivation of the O-D transition temperature, such a small difference is negligible comparing to up to ~ 5 eV difference between DFT and FF calculations (Table 3.29) of DFEs. Facing the number of calculations required to recompute the DFE contour maps and the convergence problems with the DFT+U method it was decided to stick to the f-in-core method and use DFT+U_{LR} for a few selected cases to assess the associated uncertainties. In Figure 3.26 we present the results of the calcu-

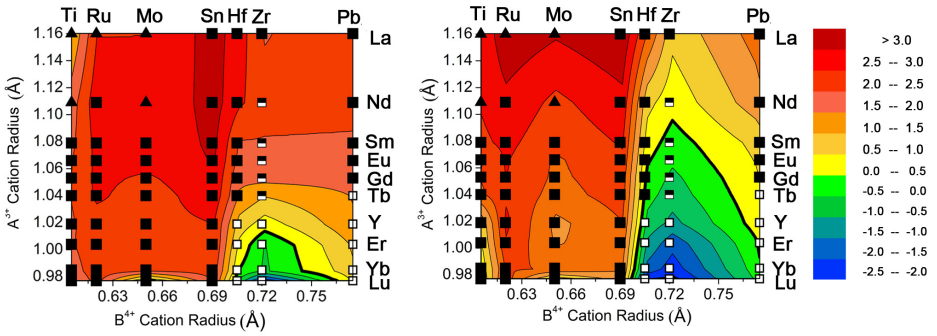

Figure 3.27: The contour maps of CA (left) and AFP (right) DFEs. The experimentally confirmed $A_2B_2O_7$ solid compounds are indicated with different symbols: pyrochlore (black filled squares), defective fluorite (black empty squares) and non-cubic phase (triangles). The thick black line separates the positive and negative DFEs regions. The energy unit is eV.

lations of CA DFEs for titanate and zirconate pyrochlores. Our *ab initio* energies are consistent with previous DFT studies (see Table 3.29) but differ significantly from the FF results of Sickafus et al. [271] and Minervini et al. [280] with *ab initio* DFE being lower by 1 eV to 5 eV. The new energies show also different trends along the lanthanide series. In the case of titanates, the CA DFE increases from La to Gd and decreases for heavier elements, while the FF show a continuous decrease. For zirconates with A = Er to Lu the DFE even becomes negative which indicates instability of pyrochlore and explains why these compositions never form pyrochlore, but the defective fluorite.

In Figure 3.27 we show the contour maps of the DFEs for the broad range of A and B cations. The positions of cations along the axes reflect the A^{3+} and B^{4+} cation ionic radii. The cations A range from La^{3+} to Lu^{3+} and the cations B from Ti^{4+} to Pb^{4+}. On top of the contour maps we plotted symbols indicating the stable phases of the considered $A_2B_2O_7$ oxides. The compositions which form defective fluorite occupy the bottom-right corners of the diagrams with cation A radii smaller than 1.05 Å and cation B radii larger than 0.7 Å. Both contour maps are significantly different from the FF based results of Sickafus et al. [271] and Minervini et al. [280]. The DFT DFEs are substantially lower. In fact the FF DFEs are usually larger by at least a

few eVs, and only the AFP DFEs become small or negative for a few compositions at the lower right corner [280]. There is also substantial difference on the qualitative level. While the FF studies show gradual DFEs decrease across the cation B series (with increasing B cation radius) and an increase across the cation A sequence, our *ab initio* results show a more complex behavior. Both DFE diagrams show an energy maximum along cation B sequences (such as the maximum of CA DFE for Sn). The most striking difference between the present DFT and the previous FF calculations is seen in the lower right corner, exactly for the compositions that form defective fluorite. The CA DFEs are usually smaller than 1 eV in the lower right part of the diagram and some of the compositions that form defective fluorite even show negative values. This is important information, because the easiness of disordering the cation sublattice should be the key factor behind the disordering of the cation sublattice, a structural property of defective fluorite. However, the new CA DFE diagram shows that there are still several compositions which are known to form a defective fluorite and for which the CA DFEs are in the order of 1 eV. This indicates that the disordering of the cation sublattice can not be the sole driver of the O-D transition in pyrochlores. The right panel of Figure 3.27 shows the AFP formation energies. The energy contours of this diagram resemble the contours obtained for the CA defect, but are smaller in value by about 1 eV. As a result, many pyrochlore compositions in the lower right part of the diagram exhibit negative or very small AFP DFEs. Interestingly, these compositions contain all the cases that are known to form defective fluorite instead of pyrochlore. This part of the diagram also overlaps the zirconates that form pyrochlore ($A_2Zr_2O_7$ for $A = \mathrm{Sm}, ..., \mathrm{Tb}$). However, most of these pyrochlores are known to form defective fluorite at high temperatures (see also Fig. 3.25 and the relevant text). The correlation of the smallness and negativeness of the AFP DFEs with the formation of the defective fluorite clearly shows that the easiness of defect formation on the oxygen sublattice is essential to the disordering of the pyrochlores and for subsequent formation of defective fluorites. This is because the still significant energy cost associated with creation of the CA defects can be compensated by the energy gained from accumulation of the

AFP defects. Using the FF approach Minervini et al. [280] have shown that although the energy cost to form single defects is large (a few eV), the energy of formation of a combined defect consisting of an AFP attached to a CA defect can be negative for some of the compositions that form defective fluorite and correlated with the occurrence of the O-D transition. However, the FF energies of this combined defect are still positive and significant (above 2 eV) for many zirconates that are known to form defective fluorite (e.g. $Gd_2Zr_2O_7$). Our *ab initio* calculations show a much better correlation between the negativeness or small value of the AFP formation energy, accompanied by a relative small value of the CA DFEs, with the formation of the defective fluorite. This clearly indicates that the easiness of the defects formation, namely of the AFP, is one of the driving forces behind the O-D transition in pyrochlores.

3.4 Other application studies

The computational methodologies tested in the scope of this dissertation thesis, namely the DFT+U_{LR} method and f-in-core DFT approach, have been used in subsequent, successful calculations of various other properties of nuclear materials performed by the Atomistic Modeling group of Dr. Kowalski at IEK-6. These include calculations of the elastic moduli [293], the excess thermodynamic properties of solid solutions [26], the solid state chemistry of actinides [294, 295] and the composition dependent order-disorder transition in $Nd_{2x}Zr1-xO_{7+x}$ compound [296]. The reported here successful benchmarking and applications indicate that the aforementioned *ab initio* computational approaches can be successfully applied for feasible and reliable calculations of chemically complex f-elements bearing systems. These studies give thus a basis for applied, reliable and computationally feasible computer-aider research of materials related to nuclear waste management.

Chapter 4

Conclusions

4.1 Achievements of this thesis

The main idea of this thesis was to the find, validate and apply feasible *ab initio* computational methods that would allow for reliable simulations of materials considered in the nuclear waste management. We thus extensively tested various DFT-based computational approaches for prediction of the structural and thermodynamic properties of relevant materials, including lanthanide- and actinide-bearing molecular and solids compounds, phosphates, halogenides and zirconates. We were especially interested in the DFT+U approach with the Hubbard U parameter value derived *ab initio*, which makes the method a parameter free approach. In particular, we applied and tested the two recently developed *ab initio* methods, cLDA and cRPA, to derive the values of this parameter (Chapter 2). These tests are first such extensive benchmarking studies performed for lanthanide- and actinide- systems and set a solid ground for future application of the parameter free DFT+U method for f-elements. The obtained results represent thus an important step in a quest to find a feasible an reliable *ab initio* methodology that would allow for the efficient atomistic simulations of nuclear materials.

Initial benchmark calculations were carried out on simple *An*-bearing molecules

and solids (Sections 3.2 and 3.3). The reaction enthalpies calculated using DFT+U_{LR} method for several reactions between *An*-bearing molecules show a significant improvement over DFT results. The accuracy of the results were comparable to higher order, usually more accurate than DFT but computationally very intensive, post Hartree-Fock methods such as MP2 and CCSD(T), and the hybrid-DFT method. This is an important result because the high computational cost of these methods limits their applicability to very simple, usually a few atoms bearing molecules and solids, which, for instance, prevents the full scale *ab initio* atomistic modeling research of chemically complex solids relevant for nuclear waste management. Feasibility of DFT+U_{LR} method we see as the most important achievement because it allows for a successful application of this methods for the simulations of complex, radionuclide-bearing materials. In addition, our results indicate a clear dependence of the Hubbard U parameter value on the oxidation state of the actinide cation, which is an important finding that emphasizes the need for correct accountancy for the strong correlations between f-electrons and to use an *ab initio* derived Hubbard U parameter values to achieve reliable results for f-elements-bearing systems (Section 3.3).

We continued the test studies and investigated the lanthanide-bearing oxides and monazite- and xenotime-type phosphates, the later being materials considered as a matrix for immobilization of radionuclides. We were especially interested in ability of the DFT+U_{LR} method to predict the structural parameters and the formation enthalpies of the investigated materials. It has been previously shown that DFT is not that accurate in these aspects [28]. We found that in order to accurately reproduce the structural parameters of the investigated lanthanide-oxides and phosphates a DFT functional has to be carefully chosen and the on-site Coulomb repulsion between f electrons has to be explicitly taken into account. Our studies show that PBEsol functional outperforms PBE in that aspect and that the DFT+U method describes better than standard DFT the structural parameters and the reaction enthalpies of the investigated materials. We found that the PBEsol+U_{LR} method, where the Hubbard U parameter is derived by *linear response* approach, gives excellent description of the

lattice parameters and the ionic structures of the investigated materials, especially the $Ln-\mathrm{O}$ and $Ln-\mathrm{P}$ distances. This indicates that to obtain the correct description of the structures of lanthanide-bearing materials, f electrons have to be treated explicitly with a correct description of the Coulomb on-site repulsion between f-electrons, strength of which can differ not only between the Ln cations but also can depend on the material (local structural environment of Ln cations). Our studies demonstrate that the method of Cococcioni and de Gironcoli [72] gives reasonable and consistent with the predictions of the cRPA method estimation of the Hubbard U parameter for lanthanides. Although our results show that the DFT+U method allows for meaningful investigation of the Ln-bearing materials with much better accuracy than with standard DFT methods, we found that modeling the f-electrons by pseudopotentials, instead of their explicit treatment, results in very good prediction of the formation enthalpies and a more stable calculation procedure. This method we thus subsequently used in the successful studies of properties of novel ceramic nuclear waste forms.

With the obtained knowledge on the proper methods for computation of monazite-type solids we performed a systematic computational studies of the heat capacities of lanthanide (Ln=Ce, ..., Tb) and actinide (An=Pu, Am and Cm) monazite-type ceramics (Subsection 3.3.4). By considering the lattice vibrations and the thermal excitations of f electrons we obtained an excellent match to all the available and numerous experimental data on the heat capacities and the standard entropies of lanthanide monazites. We found that the contribution from the lattice vibrations to the heat capacity decreases slightly along the lanthanide-series. Further, we have shown that the contribution of electronic excitations to the heat capacities of Pu-, Am- and Cm-monazites is expected to be negligible, while the contribution of the lattice vibrations in these compounds is slightly larger than in lanthanide analogues due to the mass effect. Our results show potential difficulties with the available experimental data, or their correct interpretation, on the heat capacity of $PuPO_4$, which is also indicated by the inconsistency between the different measurements. The excellent agreement between the computed and experimentally measured heat capacities of monazites-type

ceramics is an outcome of the careful atomistic modeling using reliable computational method found and well tested in this dissertation studies. The obtained results allowed us for further characterization and understanding of the thermodynamic properties of these, often experimentally challenging materials.

In addition to computation of the heat capacities, using the derived here computational methodologies, the colleagues from atomistic modeling group at IEK-6 carried out the *ab initio* calculations of $La_{1-x}Ln_xPO_4$ (Ln=Ce, ..., Tb) and $La_{1-x}An_xPO_4$ (An=Pu, Am and Cm) solid solutions in order to derive the excess enthalpies of mixing and the corresponding Margules interaction parameters [26]. The obtained information, which is difficult to obtain by the experimental methods, is important for the assessment of the long-time stability of the monazite-type nuclear waste forms. These studies shows thus that the reliable computer-aided atomistic modeling, such as the one proposed and extensively tested here, is a valuable tool for the derivation of materials properties, measuring which is challenging, or even impossible, to experimental methods.

Another group of materials that is broadly investigated in the literature as a solid matrix for conditioning of radionuclides are pyrochlore-type ceramics ($A_2B_2O_7$). This is because some ordered pyrochlores under irradiation transfer to the disordered, but still crystalline, defect fluorite phase, instead become amorphous [280, 281]. In order to understand the forces driving such a behavior of selected pyrochlores we computed order-disorder transition temperatures and cation antisite and anion Frenkel pair defect formation energies in these materials (Section 3.3.5) - key factors that determine the stability of pyrochlore-type ceramics against irradiation. The obtained excellent match of the computed by DFT+U_{LR} method to measured temperatures of disordering of pyrochlore to defect fluorite, and significant improvement over previously performed DFT studies in this aspect [183], validated the approach for the considered materials and indicate that the conclusions on the performance of the computational method obtained by studying the actinide-compounds and the monazite-type ceramics are generally applicable. The computed defect formation energies contour maps are

substantially, and even dramatically different from the previous force field calculations. They allowed for more detailed understanding of mechanisms driving order-disorder transition from pyrochlore to defective fluorite. Because our studies show a clear correlation between the negativeness of the anion Frenkel pair defect formation energies and the formation of defective fluorite, we conclude that the oxygen diffusion through the formation of these defects is the leading factor driving the order-disorder transition by compensating the large energy required for randomization of the cations sublattice. The applied computational methodology has been subsequently and successfully applied in the combined experimental (XRD and thermochemistry methods) and *ab initio* atomistic modeling studies of the $Nd_xZr_{2-2x}O_{7+x}$ system, where further excellent matches to the experimental data by results of the atomistic simulations were obtained [296].

The performed work in this PhD thesis extensive benchmarking and application studies of the parameter free DFT + U method, and the excellent matches of its prediction to the experimental data in many cases, indicate that the method allows for feasible and reliable *ab initio* simulations of chemically complex f-materials on nowadays supercomputing resources. It thus represents a valuable research tool for investigation of experimentally challenging f-electrons bearing materials and could be of great usage for the fundamental research on the management of nuclear waste.

4.2 Arising problems

In spite of achieved successful results our studies raised another questions and show some remaining difficulties with proposed here *ab initio* approach. For instance, although the Hubbard U parameter values computed with the linear response method resulted in good prediction of the enthalpies and on many time the excellent reproduction of the structural parameters, the band gaps of the investigated lanthanide and actinide solids were underestimated by $\sim 2\,\mathrm{eV}$. For UO_2 the Hubbard U parameter value of 2.1 eV computed with *the linear response* method resulted in the band

gap of 0.7 eV, which is much smaller than the measured value of 2.0 eV. On one hand the experimental band gap of uranium dioxide is reproduced in the literature [46], and in our calculations, with the Hubbard U parameter value of 4.5 eV, which is also the value frequently used in the DFT+U studies. On the other hand, in case of the Mott insulator the value of the Hubbard U parameter should be identical to the value of the band gap, which is the case in our calculations. This intriguing and unresolved problem deserves more in depth investigation. It could be connected to the usage of atomic-type orbitals as projectors in the estimation of the occupations of the f-orbitals, which results in non-negligible occupations of unoccupied orbitals. This problem could be potentially fixed by application of the Wannier functions as projectors, which should be tested in the future.

Obtaining the correct ground magnetic state of the investigated system was often a challenge for several actinide- and lanthanide-bearing materials. On many occasions we had to enforce the occupation number of electrons in the f orbital and control the correctness of the occupation matrix during the calculation. In some cases the converged solution for the ground electronic state could not be even achieved. Although this is a known, already reported in the literature problem [45, 46, 65], it requires an efficient solution in order to realize a full power of the DFT+U method.

In general the accuracy of the derived Hubbard U parameters using the cLDA and cRPA methods must be further tested. Both methods should ideally give the same values of this parameter, which, although the deviations are small, is not always the case. Due to computational limitations, calculating the Hubbard U parameter values using the cRPA method for systems containing more than 40 atoms with the FLEUR/SPEX codes is currently not possible, which should also be improved in the future. Recently, the cRPA method has been implemented in the DFT code ABINIT [297], and is being introduced in other codes, which should give an opportunity for further meaningful tests of this method for derivation of the Hubbard U parameter values.

We obtained many excellent results by modeling the f-electrons by pseudopotential.

While it is also practiced in literature, usually without solid justification, one needs to understand the general applicability of this approach. For instance, although implicit treatment of f-electrons could be a solution for lanthanide elements, which $4f$ orbitals are very localized and rarely participate in the chemistry of the elements, the general applicability of this approach to actinides that have more diffusive $5f$ orbitals is not that certain and has to be tested.

In these studies, although we applied the most powerful computing resources that are currently available, we were still limited to the application of the simple extension of DFT, such as DFT+U method. Having more computing power in the incoming decades it should be possible to compute some of the complex systems with accurate post Hartree-Fock methods or at least with the hybrid- DFT approach. This should allow for more extensive benchmarking and improvements of the feasible computational methods, such as DFT+U, for the prediction of the electronic structures of f elements bearing materials.

4.3 Prospects for the future

The results of our dissertation studies show clear paths for the future developments towards establishments of reliable *ab initio* methodologies that could be successfully applied to the field of nuclear waste management. Regarding the applicability of the parameter free DFT+U method, a one reliable methodology for the computation of the Hubbard U parameters should be established. This will require more test calculations with the cLDA, cRPA and other emerging approaches that should be performed on a large set of $4f$ and $5f$ elements bearing materials and validated on various experimental data sets, including the thermochemical and the optical data. Up to our knowledge there is only one publication available, in which the Hubbard U parameter values are calculated for $5f$-electron-bearing materials using the cRPA approach Amadon et al. [170]. This is because the method has been just recent implemented in the codes and the size of the system that could be computes is very limited by the computing power

demand. Nevertheless, we expect that in the near future the Hubbard U parameters will be much easily computed using the cRPA methodology, allowing for more extensive benchmarking of the method on complex actinide-bearing molecular and solids compounds. This will be an important step allowing for more meaningful comparison of the cRPA approach with other methods, especially with the cLDA approach. Within these studies we already started to work along these lines in collaboration with the colleagues from Quantum Theory of Materials group at Peter Grünberg Institute at Forschungszentrum Jülich. Using recently proposed DFT+U+V [298] approach, in which a novel Hamiltonian is designed to tackle the more delocalized systems, may be a potential option to obtain more reliable values of the Hubbard U parameters for actinides.

Besides here investigated topics and materials, there are other systems and problems for investigation of which the parameter free DFT+U-based atomistic simulation techniques could be useful. Hydration of Ln and An cations, their coordination number in solution and the effects of solvent are important topics when investigating, for instance, the solvent extraction processes in the research on spent nuclear fuel. Performance of the DFT+U method has not been yet studied for Ln or An cation complexes with water molecules or with small organic ligands. Systematic calculations using the DFT+U method with the Hubbard U parameter derived from first principles would be useful for modeling the different thermodynamic parameters of these complexes, such as binding energies and complexation constants involving lanthanide and actinide cations. In that aspect, similar studies as the ones performed in this thesis that require the benchmarking of the DFT+U method against the results obtained by post-Hartree Fock methods could be beneficial. If successfully validated, the parameter free DFT+U method could be used for reliable modeling of large metal-ligand complexes that are of interest for instance in research on partitioning of actinides and lanthanides from spent nuclear fuel. The work on these topics, both experimental and theoretical, is already ongoing at the IEK-6 institute and in collaboration with the partners form other Helmholtz institutions.

Topics such as corrosion of spent nuclear fuel and its dissolution are of significant importance for the safety-case of the nuclear waste in planned deep geological repositories. The expertise on modeling of uranium-bearing molecular and solid complexes gathered in this thesis can be used to investigate the behavior of UO_2 under different redox conditions. The work on this topic is planned to be initiated in the near future and the detailed studies of the available literature are already ongoing in the atomistic modeling group of Dr. Kowalski, where this thesis has been finalized.

Another important topic in the nuclear waste management research is the investigation of radiation damage processes in potential nuclear waste host matrices. Because a radiation damage cascade is a highly energetic phenomenon, to simulate it one has to model systems containing at least several hundreds or even thousands of atoms. Having the world class computational resources, Forschungszentrum Jülich is well equipped to tackle such problems. However, when modeling such large systems, the force field methods have to be used, in which the interatomic interactions are described by an interaction potential (force field). There is a variety of force fields available, although only very limited set for f-elements, and parameters of these force fields are constantly being adjusted for different atoms and molecules. For reliable force field-based simulations of nuclear waste materials, the applied force field must represent an accurate description of the interatomic interactions, especially these involving actinide and lanthanide elements, which can be delivered from the reliable *ab initio* calculations, as for instance the ones performed in these studies. Development of polarizable force fields would allow for simulations of the Raman spectra of complex materials, which, having the popularity of the Raman spectroscopy in the research, would be extremely useful for interpretation of the Raman measurement.

This work shows that it is possible to have a feasible and reliable *ab initio* methodology and that the methods developed and applied here, especially the parameter free DFT+U approach, can be used to successfully complement the experimental research in the field of nuclear waste management and such investigations will be continued in the future. Following the success of this thesis, there are several follow up research ac-

tivities planned in the atomistic modeling group of Dr. Kowalski. These future studies will be performed in collaboration with the experts from both theory and experimental side and will be essential part of the collaborative *"TheoRad"* BMBF project on *"Development and application of quantum chemistry methods for understanding the radionuclides chemistry under the disposal-relevant conditions"* that will be conducted as a joint initiative of various German institutions.

Bibliography

[1] M. Ojovan, W. Lee, An Introduction to Nuclear Waste Immobilisation, Elsevier Science, 2010.

[2] M. Benedict, T. Pigford, H. Levi, Nuclear Chemical Engineering, McGraw-Hill series in nuclear engineering, McGraw-Hill, 1981.

[3] C. Madic, M. Lecomte, P. Baron, B. Boullis, C. R. Phys. 3 (2002) 797 – 811.

[4] Prognose: Anfall endzulagernder waerme entwickelnder radioaktiver abfaelle, `http://www.bfs.de/DE/themen/ne/abfaelle/prognosen/`. Accessed: 2015-12-16.

[5] R. C. Ewing, Proc. Natl. Acad. Sci. 96 (1999) 3432–3439.

[6] Nucleonica gmbh; webkorigen++ (www.nucleonica.com). URL: `www.nucleonica.com`.

[7] Germany - statement to the iaea general conference 2011, `https://www.iaea.org/About/Policy/GC/GC55/Statements/`. Accessed: 2015-09-18.

[8] German atomic energy act, `www.bmub.bund.de/P263-1/`. Accessed: 2015-09-18.

[9] Standortauswahlgesetz - standag, `www.bmub.bund.de/N49950/`. Accessed: 2015-09-18.

[10] Skb selects forsmark for the final repository for spent nuclear fuel, `www.skb.com/future-projects/the-spent-fuel-repository/`. Accessed: 2015-09-18.

[11] Final disposal - onkalo, `www.posiva.fi`. Accessed: 2015-09-18.

[12] Licence granted for finnish used fuel repository, `http://www.world-nuclear-news.org/WR-Licence-granted-for-Finnish-used-fuel-repository-1211155.html`. Accessed: 2016-01-11.

[13] R. C. Ewing, C. R. Geosci. 343 (2011) 219 – 229.

[14] R. Ewing, L. Wang, Rev. Mineral. Geochem. 48 (2002) 673–699.

[15] R. C. Ewing, W. J. Weber, J. Lian, J. Appl. Phys. 95 (2004) 5949.

[16] G. R. Lumpkin, Elements 2 (2006) 365–372.

[17] L. Morss, N. Edelstein, J. Fuger, J. Katz, The Chemistry of the Actinide and Transactinide Elements (Set Vol.1-6), v. 1-6, Springer, 2011.

[18] R. Guillaumont, O. N. E. Agency, F. Mompean, Update on the Chemical Thermodynamics of Uranium, Neptunium, Plutonium, Americium and Technetium, Chemical Thermodynamics Series, Elsevier Science & Technology Books, 2003.

[19] S. Finkeldei, F. Brandt, A. Bukaemskiy, S. Neumeier, G. Modolo, D. Bosbach, Prog. Nucl. Energy 72 (2014) 130–133.

[20] A. Wilden, G. Modolo, S. Lange, F. Sadowski, B. B. Beele, A. Skerencak-Frech, P. J. Panak, M. Iqbal, W. Verboom, A. Geist, D. Bosbach, Solvent Extr. Ion Exc. 32 (2014) 119–137.

[21] H. Schlenz, J. Heuser, A. Neumann, S. Schmitz, D. Bosbach, Z. Kristallogr. 228 (2013) 113.

[22] A. Chroneos, M. Rushton, C. Jiang, L. Tsoukalas, J. Nucl. Mater. 441 (2013) 29–39.

[23] A. Blanca-Romero, P. M. Kowalski, G. Beridze, H. Schlenz, D. Bosbach, J. Comput. Chem. 35 (2014) 1339–1346.

[24] G. Beridze, P. M. Kowalski, J. Phys. Chem. A 118 (2014) 11797–11810.

[25] P. M. Kowalski, G. Beridze, V. L. Vinograd, D. Bosbach, J. Nucl. Mater. 464 (2015) 147 – 154.

[26] Y. Li, P. M. Kowalski, A. Blanca-Romero, V. Vinograd, D. Bosbach, J. Solid State Chem. 220 (2014) 137 – 141.

[27] Y. Li, P. M. Kowalski, G. Beridze, A. R. Birnie, S. Finkeldei, D. Bosbach, Scr. Mater. 107 (2015) 18–21.

[28] J. R. Rustad, Am. Mineral. 97 (2012) 791.

[29] X.-D. Wen, R. L. Martin, T. M. Henderson, G. E. Scuseria, Chem. Rev. 113 (2013) 1063–1096.

[30] G. A. Shamov, G. Schreckenbach, T. N. Vo, Chem. Eur. J. 13 (2007) 4932–4947.

[31] G. Schreckenbach, G. A. Shamov, Acc. Chem. Res. 43 (2010) 19–29.

[32] M. Klinkenberg, A. Neumann, H. Curtius, G. Kaiser, D. Bosbach, Radiochim. Acta 102 (2014) 311–324.

[33] S. Labs, C. Hennig, S. Weiss, H. Curtius, H. Zänker, D. Bosbach, Environ. Sci. Technol. 48 (2014) 854–860.

[34] M. Klinkenberg, S. Neumeier, D. Bosbach, Institute of Energy and Climate Research IEK-6: Nuclear Waste Management Report 2011 / 2012: Material Science for Nuclear Waste Management, Schriften des Forschungszentrums Jülich, Forschungszentrum, Zentralbibliothek, 2013.

[35] S. Finkeldei, F. Brandt, K. Rozov, A. Bukaemskiy, S. Neumeier, D. Bosbach, Appl. Geochem. 49 (2014) 31–41.

[36] B. Xiao, E. Langer, J. Dellen, H. Schlenz, D. Bosbach, E. V. Suleimanov, E. V. Alekseev, Inorg. Chem. 54 (2015) 3022–3030.

[37] N. Yu, V. V. Klepov, P. Kegler, D. Bosbach, T. E. Albrecht-Schmitt, E. V. Alekseev, Inorg. Chem. 53 (2014) 8194–8196.

[38] S. Jahn, P. M. Kowalski, Rev. Mineral. Geochem. 78 (2014) 691–743.

[39] S. Mazevet, M. Challacombe, P. Kowalski, D. Saumon, Astrophys. Space Sci. 307 (2007) 273–277.

[40] K. W. Paul, J. D. Kubicki, D. L. Sparks, Eur. J. Soil Sci. 58 (2007) 978–988.

[41] S. Grimme, J. Antony, T. Schwabe, C. Muck-Lichtenfeld, Org. Biomol. Chem. 5 (2007) 741–758.

[42] M. Putz, D. Mingos, Applications of Density Functional Theory to Biological and Bioinorganic Chemistry, Structure and Bonding, Springer Berlin Heidelberg, 2013.

[43] J. Dash, S. Ray, K. Nallappan, V. Kaware, N. Basutkar, R. G. Gonnade, A. V. Ambade, K. Joshi, B. Pesala, J. Phys. Chem. A 119 (2015) 7991–7999.

[44] E. A. Carter, Science 321 (2008) 800–803.

[45] X.-D. Wen, R. L. Martin, L. E. Roy, G. E. Scuseria, S. P. Rudin, E. R. Batista, T. M. McCleskey, B. L. Scott, E. Bauer, J. J. Joyce, T. Durakiewicz, J. Chem. Phys. 137 (2012) 154707.

[46] X.-D. Wen, R. L. Martin, G. E. Scuseria, S. P. Rudin, E. R. Batista, A. K. Burrell, J. Phys.: Condens. Matter 25 (2013) 025501.

[47] L. Joubert, P. Maldivi, J. Phys. Chem. A 105 (2001) 9068–9076.

[48] F. Schlosser, S. Krüger, N. Rösch, Inorg. Chem. 45 (2006) 1480–1490.

[49] A. Kremleva, B. Martorell, S. Kruger, N. Rosch, Phys. Chem. Chem. Phys. 14 (2012) 5815–5823.

[50] S. O. Odoh, Q.-J. Pan, G. A. Shamov, F. Wang, M. Fayek, G. Schreckenbach, Chem. Eur. J. 18 (2012) 7117–7127.

[51] N. Iche-Tarrat, C. J. Marsden, J. Phys. Chem. A 112 (2008) 7632–7642.

[52] A. D. Becke, J. Chem. Phys. 98 (1993) 1372–1377.

[53] F. Jensen, Introduction to Computational Chemistry, Wiley, 2007.

[54] D. Marx, J. Hutter, Ab initio molecular dynamics: Theory and implementation, in: J. Grotendorst (Ed.), Modern Methods and Algorithms of Quantum Chemistry, Forschungszentrum Jülich, NIC Series, volume 1, 2000, p. 301.

[55] P. M. Kowalski, M. F. Camellone, N. N. Nair, B. Meyer, D. Marx, Phys. Rev. Lett. 105 (2010) 146405.

[56] B. Himmetoglu, A. Floris, S. de Gironcoli, M. Cococcioni, Int. J. Quantum Chem. 114 (2014) 14–49.

[57] J. P. Perdew, K. Burke, M. Ernzerhof, Phys. Rev. Lett. 77 (1996) 3865–3868.

[58] J. Hubbard, P. Roy. Soc. Edinb. A 276 (1963).

[59] Y. Baer, J. Schoenes, Solid State Commun. 33 (1980) 885–888.

[60] T. Yamazaki, A. Kotani, J. Phys. Soc. Jpn. 60 (1991) 49–51.

[61] A. Kotani, T. Yamazaki, Prog. Theor. Phys. Supp. 108 (1992) 117–131.

[62] B. Johansson, Phys. Rev. B 11 (1975) 2740–2743.

[63] S. Hüfner, G. K. Wertheim, Phys. Rev. B 7 (1973) 5086–5090.

[64] J. F. Herbst, R. E. Watson, I. Lindgren, Phys. Rev. B 14 (1976) 3265–3272.

[65] B. Dorado, B. Amadon, M. Freyss, M. Bertolus, Phys. Rev. B 79 (2009) 235125.

[66] S. L. Dudarev, D. N. Manh, A. P. Sutton, Philos. Mag. B 75 (1997) 613.

[67] Z. Rak, R. C. Ewing, U. Becker, Phys. Rev. B 84 (2011) 155128.

[68] S. Elgazzar, J. Rusz, P. M. Oppeneer, E. Colineau, J.-C. Griveau, N. Magnani, J. Rebizant, R. Caciuffo, Phys. Rev. B 81 (2010) 235117.

[69] A. Floris, S. de Gironcoli, E. K. U. Gross, M. Cococcioni, Phys. Rev. B 84 (2011) 161102.

[70] O. Gunnarsson, O. K. Andersen, O. Jepsen, J. Zaanen, Phys. Rev. B 39 (1989) 1708–1722.

[71] V. I. Anisimov, O. Gunnarsson, Phys. Rev. B 43 (1991) 7570–7574.

[72] M. Cococcioni, S. de Gironcoli, Phys. Rev. B 71 (2005) 035105.

[73] M. Springer, F. Aryasetiawan, Phys. Rev. B 57 (1998) 4364–4368.

[74] T. Kotani, J. Phys.: Condens. Matter 12 (2000) 2413.

[75] F. Aryasetiawan, M. Imada, A. Georges, G. Kotliar, S. Biermann, A. I. Lichtenstein, Phys. Rev. B 70 (2004) 195104.

[76] I. V. Solovyev, M. Imada, Phys. Rev. B 71 (2005) 045103.

[77] F. Aryasetiawan, K. Karlsson, O. Jepsen, U. Schönberger, Phys. Rev. B 74 (2006) 125106.

[78] I. V. Solovyev, J. Phys.: Condens. Matter 20 (2008) 293201.

[79] Computational Materials Science and Chemistry: Accelerating Discovery and Innovation through Simulation-Based Engineering and Science, US Department of Energy, 2010.

[80] G. Beridze, A. Birnie, S. Koniski, Y. Ji, P. M. Kowalski (submitted).

[81] P. Giannozzi, S. Baroni, N. Bonini, M. Calandra, R. Car, C. Cavazzoni, D. Ceresoli, G. L. Chiarotti, M. Cococcioni, I. Dabo, A. D. Corso, S. de Gironcoli, S. Fabris, G. Fratesi, R. Gebauer, U. Gerstmann, C. Gougoussis, A. Kokalj, M. Lazzeri, L. Martin-Samos, N. Marzari, F. Mauri, R. Mazzarello, S. Paolini, A. Pasquarello, L. Paulatto, C. Sbraccia, S. Scandolo, G. Sclauzero, A. P. Seitsonen, A. Smogunov, P. Umari, R. M. Wentzcovitch, J. Phys.: Condens. Matter 21 (2009) 395502.

[82] www.flapw.de.

[83] S. Ushakov, K. Helean, A. Navrotsky, J. Mater. Res. 16 (2001) 2623–2633.

[84] C. Thiriet, R. J. M. Konings, F. Wastin, J. Nucl. Mater. 344 (2005) 56–60.

[85] K. Popa, E. Colineau, F. Wastin, R. J. M. Konings, Solid State Commun. 144 (2007) 74 – 77.

[86] A. E. Ringwood, S. Kesson, N. G. Ware, W. Hibberson, A. Major, Nature 278 (1979) 219–223.

[87] S. X. Wang, B. D. Begg, L. M. Wang, R. C. Ewing, W. J. Weber, K. V. Govidan Kutty, J. Mater. Res. 14 (1999) 4470–4473.

[88] Jülich-aachen research alliance, `www.jara.org`. Accessed: 2015-09-18.

[89] C. Gramaccioli, Energy Modelling In Minerals:, EMU Notes in Mineralogy, Eötvös University Press, 2002.

[90] I. Levine, Quantum Chemistry, Pearson Prentice Hall, 2009.

[91] A. Szabo, N. Ostlund, Modern Quantum Chemistry: Introduction to Advanced Electronic Structure Theory, Dover Books on Chemistry Series, Dover Publications, 1996.

[92] W. Koch, M. Holthausen, A chemist's guide to density functional theory, Wiley-VCH, 2000.

[93] C. Møller, M. S. Plesset, Phys. Rev. 46 (1934) 618–622.

[94] J. Čížek, Theor. Chim. Acta 80 (1991) 91–94.

[95] R. A. Kendall, E. Aprà, D. E. Bernholdt, E. J. Bylaska, M. Dupuis, G. I. Fann, R. J. Harrison, J. Ju, J. A. Nichols, J. Nieplocha, T. Straatsma, T. L. Windus, A. T. Wong, Comput. Phys. Commun. 128 (2000) 260 – 283.

[96] M. J. Frisch, G. W. Trucks, H. B. Schlegel, G. E. Scuseria, M. A. Robb, J. R. Cheeseman, G. Scalmani, V. Barone, B. Mennucci, G. A. Petersson, H. Nakatsuji, M. Caricato, X. Li, H. P. Hratchian, A. F. Izmaylov, J. Bloino, G. Zheng, J. L. Sonnenberg, M. Hada, M. Ehara, K. Toyota, R. Fukuda, J. Hasegawa, M. Ishida, T. Nakajima, Y. Honda, O. Kitao, H. Nakai, T. Vreven, J. A. Montgomery, Jr., J. E. Peralta, F. Ogliaro, M. Bearpark, J. J. Heyd, E. Brothers, K. N. Kudin, V. N. Staroverov, R. Kobayashi, J. Normand, K. Raghavachari, A. Rendell, J. C. Burant, S. S. Iyengar, J. Tomasi, M. Cossi, N. Rega, J. M. Millam, M. Klene, J. E. Knox, J. B. Cross, V. Bakken, C. Adamo, J. Jaramillo, R. Gomperts, R. E. Stratmann, O. Yazyev, A. J. Austin, R. Cammi, C. Pomelli, J. W. Ochterski, R. L. Martin, K. Morokuma, V. G. Zakrzewski, G. A. Voth, P. Salvador, J. J. Dannenberg, S. Dapprich, A. D. Daniels, O. Farkas, J. B. Foresman, J. V. Ortiz, J. Cioslowski, D. J. Fox, Gaussian09 Revision D.01. Gaussian Inc. Wallingford CT 2009.

[97] The cp2k developers group, `www.cp2k.org`.

[98] H.-J. Werner, P. J. Knowles, G. Knizia, F. R. Manby, M. Schütz, et al., Molpro, version 2012.1, a package of ab initio programs. URL: `www.molpro.net`.

[99] M. W. Schmidt, K. K. Baldridge, J. A. Boatz, S. T. Elbert, M. S. Gordon, J. H. Jensen, S. Koseki, N. Matsunaga, K. A. Nguyen, S. Su, T. L. Windus, M. Dupuis, J. A. Montgomery, J. Comput. Chem. 14 (1993) 1347–1363.

[100] TURBOMOLE V6.2 2010, a development of University of Karlsruhe and Forschungszentrum Karlsruhe GmbH, 1989-2007, TURBOMOLE GmbH, since 2007; available from
`http://www.turbomole.com`.

[101] I. Chivers, J. Sleightholme, Introduction to Programming with Fortran: With Coverage of Fortran 90, 95, 2003 and 77, Springer, 2006.

[102] L. H. Thomas, Mathematical Proceedings of the Cambridge Philosophical Society 23 (1927) 542–548.

[103] E. Fermi, Rend. Accad. Lincei 6 (1927) 602.

[104] J. C. Slater, Phys. Rev. 81 (1951) 385–390.

[105] P. Hohenberg, W. Kohn, Phys. Rev. 136 (1964) B864–B871.

[106] W. Kohn, L. J. Sham, Phys. Rev. 140 (1965) A1133–A1138.

[107] S. H. Vosko, L. Wilk, M. Nusair, Canad. J. Phys. 58 (1980) 1200–1211.

[108] A. D. Becke, Int. J. Quant. Chem. 23 (1983) 1915–1922.

[109] D. C. Langreth, M. J. Mehl, Phys. Rev. B 28 (1983) 1809–1834.

[110] C. D. Hu, D. C. Langreth, Phys. Scripta 32 (1985) 391.

[111] F. Herman, J. P. Van Dyke, I. B. Ortenburger, Phys. Rev. Lett. 22 (1969) 807–811.

[112] L. Kleinman, S. Lee, Phys. Rev. B 37 (1988) 4634–4636.

[113] L. Kleinman, Phys. Rev. B 30 (1984) 2223–2225.

[114] P. R. Antoniewicz, L. Kleinman, Phys. Rev. B 31 (1985) 6779–6781.

[115] J. P. Perdew, Phys. Rev. Lett. 55 (1985) 1665–1668.

[116] J. P. Perdew, Y. Wang, Phys. Rev. B 33 (1986) 8800–8802.

[117] J. P. Perdew, Y. Wang, Phys. Rev. B 45 (1992) 13244–13249.

[118] J. P. Perdew, A. Ruzsinszky, G. I. Csonka, O. A. Vydrov, G. E. Scuseria, L. A. Constantin, X. Zhou, K. Burke, Phys. Rev. Lett. 100 (2008) 136406.

[119] A. D. Becke, Phys. Rev. A 38 (1988) 3098–3100.

[120] P. J. Stephens, F. J. Devlin, C. F. Chabalowski, M. J. Frisch, J. Phys. Chem. 98 (1994) 11623–11627.

[121] C. Lee, W. Yang, R. G. Parr, Phys. Rev. B 37 (1988) 785–789.

[122] C. Adamo, V. Barone, J. Chem. Phys. 110 (1999) 6158–6170.

[123] A. Bhattacharyya, P. Mohapatra, V. Manchanda, J. Radioanal. Nucl. Chem. 288 (2011) 709–716.

[124] L. Castro, O. P. Lam, S. C. Bart, K. Meyer, L. Maron, Organometallics 29 (2010) 5504–5510.

[125] C. Hennig, A. Ikeda-Ohno, S. Tsushima, A. C. Scheinost, Inorg. Chem. 48 (2009) 5350–5360.

[126] D. Majumdar, K. Balasubramanian, Chem. Phys. Lett. 397 (2004) 26–33.

[127] H. Hellmann, J. Chem. Phys. 3 (1935).

[128] E. Fermi, Nuovo Cimento B 11 (1934) 157–166.

[129] P. Gombas, Zeitschrift für Physik 94 (1935) 473–488.

[130] J. D. Weeks, S. A. Rice, J. Chem. Phys. 49 (1968).

[131] A. Leach, Molecular Modelling: Principles and Applications, Pearson Education, Prentice Hall, 2001.

[132] P. Schwerdtfeger, ChemPhysChem 12 (2011) 3143–3155.

[133] D. R. Hamann, M. Schlüter, C. Chiang, Phys. Rev. Lett. 43 (1979) 1494–1497.

[134] D. Vanderbilt, Phys. Rev. B 41 (1990) 7892–7895.

[135] K. Laasonen, R. Car, C. Lee, D. Vanderbilt, Phys. Rev. B 43 (1991) 6796–6799.

[136] S. O. Odoh, G. Schreckenbach, J. Phys. Chem. A 114 (2010) 1957–1963.

[137] R. Dronskowski, Computational Chemistry of Solid State Materials: A Guide for Materials Scientists, Chemists, Physicists and Others, Wiley, 2005.

[138] G. M. D. K. P. Blaha, K. Schwarz, J. Luitz, WIEN2k, An Augmented Plane Wave + Local Orbitals Program for Calculating Crystal Properties, number v. 2 in Methods of Mathematical Physics, (Karlheinz Schwarz, Techn. Universität Wien, Austria), 2001.

[139] Elk, `elk.sourceforge.net`.

[140] E. Wimmer, H. Krakauer, M. Weinert, A. J. Freeman, Phys. Rev. B 24 (1981) 864–875.

[141] V. I. Anisimov, J. Zaanen, O. K. Andersen, Phys. Rev. B 44 (1991) 943–954.

[142] V. I. Anisimov, I. V. Solovyev, M. A. Korotin, M. T. Czyżyk, G. A. Sawatzky, Phys. Rev. B 48 (1993) 16929–16934.

[143] I. V. Solovyev, P. H. Dederichs, V. I. Anisimov, Phys. Rev. B 50 (1994) 16861–16871.

[144] V. Anisimov, Y. Izyumov, Electronic Structure of Strongly Correlated Materials, Springer Series in Solid-State Sciences, Springer, 2010.

[145] J. Hubbard, P. Roy. Soc. Edinb. A 277 (1964).

[146] J. Hubbard, P. Roy. Soc. Edinb. A 281 (1964).

[147] J. Hubbard, P. Roy. Soc. Edinb. A 285 (1965).

[148] J. Hubbard, P. Roy. Soc. Edinb. A 296 (1967).

[149] J. Hubbard, P. Roy. Soc. Edinb. A 296 (1967).

[150] V. I. Anisimov, F. Aryasetiawan, A. I. Lichtenstein, J. Phys.: Conden. Matter 9 (1997) 767.

[151] M. Cococcioni, Rev. Mineral. Geochem. 71 (2010) 147–167.

[152] A. I. Liechtenstein, V. I. Anisimov, J. Zaanen, Phys. Rev. B 52 (1995) R5467–R5470.

[153] L. Vaugier, H. Jiang, S. Biermann, Phys. Rev. B 86 (2012) 165105.

[154] S. L. Dudarev, G. A. Botton, S. Y. Savrasov, C. J. Humphreys, A. P. Sutton, Phys. Rev. B 57 (1998) 1505–1509.

[155] A. B. Shick, A. I. Liechtenstein, W. E. Pickett, Phys. Rev. B 60 (1999) 10763–10769.

[156] J. P. Perdew, M. Levy, Phys. Rev. Lett. 51 (1983) 1884–1887.

[157] J. P. Perdew, R. G. Parr, M. Levy, J. L. Balduz, Phys. Rev. Lett. 49 (1982) 1691–1694.

[158] R. Courant, D. Hilbert, Methods of Mathematical Physics, number v. 2 in Methods of Mathematical Physics, Interscience Publishers, 1962.

[159] B. Himmetoglu, R. M. Wentzcovitch, M. Cococcioni, Phys. Rev. B 84 (2011) 115108.

[160] E. Şaşıoğlu, I. Galanakis, C. Friedrich, S. Blügel, Phys. Rev. B 88 (2013) 134402.

[161] E. Pavarini, E. Koch, D. Vollhardt, A. E. . Lichtenstein, The LDA+DMFT approach to strongly correlated materials: lecture notes of the autumn school 2011, hands-on LDA+DMFT ; autumn school organized by the DFG research unit 1346 dynamical mean-field approach with predictive power for strongly correlated materials at Forschungszentrum Jülich 4-7 October 2011, volume 1 of *Schriften des Forschungszentrums Jülich. Reihe Modeling and simulation*, Forschungszentrum, Zentralbibliothek, Jülich, 2011. URL: `http://juser.fz-juelich.de/record/136342`, record converted from JUWEL: 18.07.2013.

[162] T. Miyake, F. Aryasetiawan, Phys. Rev. B 77 (2008) 085122.

[163] G. H. Wannier, Phys. Rev. 52 (1937) 191–197.

[164] E. Şaşıoğlu, C. Friedrich, S. Blügel, Phys. Rev. B 83 (2011) 121101.

[165] C. Friedrich, S. Blügel, A. Schindlmayr, Phys. Rev. B 81 (2010) 125102.

[166] N. Marzari, D. Vanderbilt, Phys. Rev. B 56 (1997) 12847–12865.

[167] I. Souza, N. Marzari, D. Vanderbilt, Phys. Rev. B 65 (2001) 035109.

[168] N. Marzari, A. A. Mostofi, J. R. Yates, I. Souza, D. Vanderbilt, Rev. Mod. Phys. 84 (2012) 1419–1475.

[169] E. Wimmer, H. Krakauer, M. Weinert, A. J. Freeman, Phys. Rev. B 24 (1981) 864–875.

[170] B. Amadon, T. Applencourt, F. Bruneval, Phys. Rev. B 89 (2014) 125110.

[171] F. Nilsson, R. Sakuma, F. Aryasetiawan, Phys. Rev. B 88 (2013) 125123.

[172] P. Giannozzi, S. de Gironcoli, P. Pavone, S. Baroni, Phys. Rev. B 43 (1991) 7231–7242.

[173] R. Wang, S. Wang, X. Wu, Physica Scripta 83 (2011) 065707.

[174] C. Thiriet, R. J. M. Konings, P. Javorsky, N. Magnani, F. Wastin, J. Chem. Thermodyn. 37 (2005) 131–139.

[175] E. F. Westrum, Jr, J. Therm. Anal. 30 (1985) 1209–1215.

[176] S. Edvardsson, D. Aberg, Comput. Phys. Commun. 133 (2001) 396 – 406.

[177] G. Burdick, M. Reid, 4fn-4f(n-1) 5d Transitions, volume 37 of *Handbook on the Physics and Chemistry of Rare Earths*, Elsevier, 2007.

[178] B. R. Judd, Phys. Rev. 141 (1966) 4–14.

[179] R. E. Trees, Phys. Rev. 83 (1951) 756–760.

[180] D. Newman, B. Ng, Crystal Field Handbook, Cambridge University Press, 2007.

[181] C. Nielson, G. Koster, Spectroscopic coefficients for the pn, dn, and fn configurations, Cambridge, Mass.: M. I. T. Press., 1963.

[182] J. Feng, B. Xiao, R. Zhou, W. Pan, Acta Mater. 61 (2013) 7364 – 7383.

[183] C. Jiang, C. R. Stanek, K. E. Sickafus, B. P. Uberuaga, Phys. Rev. B 79 (2009) 104203–104207.

[184] G. H. Lander, M. H. Mueller, Acta Crystallogr. Sect. B 26 (1970) 129–136.

[185] J. Taylor, P. Wilson, J. Solid State Chem. 14 (1975) 378–382.

[186] P. G. Eller, A. Larson, J. Peterson, D. Ensor, J. Young, Inorg. Chim. Acta 37 (1979) 129–133.

[187] R. R. Ryan, R. A. Penneman, L. B. Asprey, R. T. Paine, Acta Crystallogr. Sect. B 32 (1976) 3311–3313.

[188] W. H. Zachariasen, Acta Crystallogr. 2 (1949) 388–390.

[189] J. Laveissiere, Bull. Soc. Franc. Mineral. Crist. 90 (1967) 308–310.

[190] J. C. Taylor, P. W. Wilson, Acta Crystallogr. Sect. B 30 (1974) 1481–1484.

[191] T. Schleid, G. Meyer, L. R. Morss, J. Less-Common MET. 132 (1987) 69–77.

[192] S. A. Barrett, A. J. Jacobson, B. C. Tofield, B. E. F. Fender, Acta Crystallogr. Sect. B 38 (1982) 2775–2781.

[193] B. O. Loopstra, E. H. P. Cordfunke, Recl. Trav. Chim. Pays-Bas 85 (1966) 135–142.

[194] B. O. Loopstra, Acta Crystallogr. 17 (1964) 651–654.

[195] J. L. F. Da Silva, Phys. Rev. B 76 (2007) 193108.

[196] S. Fabris, S. de Gironcoli, S. Baroni, G. Vicario, G. Balducci, Phys. Rev. B 71 (2005) 041102.

[197] S. Fabris, S. de Gironcoli, S. Baroni, G. Vicario, G. Balducci, Phys. Rev. B 72 (2005) 237102.

[198] G. Concas, J. K. Dewhurst, A. Sanna, S. Sharma, S. Massidda, Phys. Rev. B 84 (2011) 014427.

[199] J. Kunes, R. Laskowski, Phys. Rev. B 70 (2004) 174415.

[200] J. P. Perdew, Int. J. Quantum Chem. 28 (1985) 497–523.

[201] J. Schoenes, J. Appl. Phys. 49 (1978) 1463–1465.

[202] R. Gillen, S. J. Clark, J. Robertson, Phys. Rev. B 87 (2013) 125116.

[203] H. Jiang, P. Rinke, M. Scheffler, Phys. Rev. B 86 (2012) 125115.

[204] S. Kimura, F. Arai, M. Ikezawa, J. Phys. Soc. Jpn. 69 (2000) 3451.

[205] A. Prokofiev, A. Shelykh, B. Melekh, J. Alloys Compd. 242 (1996) 41.

[206] E. R. Batista, R. L. Martin, P. J. Hay, J. E. Peralta, G. E. Scuseria, J. Chem. Phys. 121 (2004) 2144–2150.

[207] B. Weinstock, R. H. Crist, J. Chem. Phys. 16 (1948) 436–441.

[208] H. Seip, Acta Chem. Scand. 19 (1965) 1955–1968.

[209] P. J. Hay, R. L. Martin, J. Chem. Phys. 109 (1998) 3875–3881.

[210] G. I. Csonka, J. P. Perdew, A. Ruzsinszky, P. H. T. Philipsen, S. Lebègue, J. Paier, O. A. Vydrov, J. G. Ángyán, Phys. Rev. B 79 (2009) 155107.

[211] A. E. Mattsson, R. Armiento, J. Paier, G. Kresse, J. M. Wills, T. R. Mattsson, J. Chem. Phys. 128 (2008) 084714.

[212] T. Privalov, B. Schimmelpfennig, U. Wahlgren, I. Grenthe, J. Phys. Chem. A 106 (2002) 11277–11284.

[213] G. L. Malli, Mol. Phys. 101 (2003) 287–294.

[214] Y. Ezhov, S. Komarov, V. Sevastyanov, V. Bazhanov, J. Struct. Chem. 34 (1993) 473–474.

[215] G. Thornton, N. Edelstein, N. Rösch, R. G. Egdell, D. R. Woodwark, J. Chem. Phys 70 (1979) 5218.

[216] V. Bazhanov, Y. Ezhov, S. Komarov, J. Struct. Chem. 31 (1990) 986–989.

[217] J. Li, Q. Ren, C. Lu, L. Lu, Y. Dai, B. Liu, J. Alloys Compd. 516 (2012) 139–143.

[218] Y.-K. Han, J. Comput. Chem. 22 (2001) 2010–2017.

[219] G. Lumpkin, T. Geisler-Wierwille, Comprehensive Nuclear Materials: Minerals and Natural Analogues, volume 5, Elsevier, Oxford, 2012.

[220] R. J. M. Konings, M. Walter, K. Popa, J. Chem. Thermodyn. 40 (2008) 1305–1308.

[221] W. C. Koehler, E. O. Wollan, Acta Cryst. 6 (1953) 741–742.

[222] H. Baernighausen, G. Schiller, J. Less-Common MET. 110 (1985) 385–390.

[223] O. Greis, R. Ziel, B. Breidenstein, A. Haase, T. Petzel, J. Alloy. Compd. 216 (1994) 255–258.

[224] J. X. Boucherle, J. Schweizer, Acta Cryst. B31 (1975) 2745–2746.

[225] T. Atou, K. Kusaba, Y. Tsuchida, W. Utsumi, T. Yagi, Y. Syono, Mater. Res. Bull. 24 (1989) 1171–1176.

[226] T. Schleid, G. Meyer, J. Less-Common MET. 149 (1989) 73–80.

[227] H. Yakel, Acta Cryst. B: Structural Science 35 (1979) 564–569.

[228] I. Ferguson, Acta Cryst. A 31 (1975) S69.

[229] A. Bartos, K. Lieb, M. Uhrmacher, D. Wiarda, Acta Cryst. B: Structural Science 49 (1993) 165–169.

[230] Z. Heiba, Y. Akin, W. Sigmund, Y. Hascicek, J. Appl. Crystallogr. 36 (2003) 1411–1416.

[231] A. Saiki, N. Ishizawa, N. Mizutani, M. Kato, J. Ceram. Soc. Jpn. 93 (1985) 649–654.

[232] Y. Ni, J. Hughes, A. Mariano, Am. Mineral. 80 (1995) 21–26.

[233] J. López-Solano, P. Rodríguez-Hernández, A. Muñoz, O. Gomis, D. Santamaría-Perez, D. Errandonea, F. J. Manjón, R. S. Kumar, E. Stavrou, C. Raptis, Phys. Rev. B 81 (2010) 144126.

[234] Y. Hikichi, T. Sasaki, S. Suzuki, K. Murayama, M. Miyamoto, J. Am. Ceram. Soc. 71 (1988) 354.

[235] S. Bajaj, C. Sevik, T. Cagin, A. Garay, P. Turchi, R. Arróyave, Comput. Mater. Sci. 59 (2012) 48–56.

[236] N. E. Schultz, Y. Zhao, D. G. Truhlar, J. Phys. Chem. A 109 (2005) 11127–11143.

[237] B. Averkiev, M. Mantina, R. Valero, I. Infante, A. Kovacs, D. Truhlar, L. Gagliardi, Theor. Chem. Acc. 129 (2011) 657–666.

[238] A. Zaitsevskii, N. S. Mosyagin, A. V. Titov, Y. M. Kiselev, J. Chem. Phys. 139 (2013) 034307.

[239] D. W. J. Cruickshank, Acta Crystallogr. 17 (1964) 677.

[240] G. Kaur, P. Panigrahi, M. C. Valsakumar, Model. Simul. Mater. Sci. Eng. 21 (2013) 065014.

[241] N. Clavier, R. Podor, N. Dacheux, J. Eur. Ceram. Soc. 31 (2011) 941–976.

[242] K. S. Gavrichev, M. A. Ryumin, A. V. Tyurin, V. M. Gurevich, L. N. Komissarova, Thermochim. Acta 474 (2008) 47–51.

[243] C. Thiriet, R. J. M. Konings, P. Javorsky, F. Wastin, Phys. Chem. Miner. 31 (2004) 347–352.

[244] K. Popa, F. Jutier, F. Wastin, R. J. M. Konings, J. Chem. Thermodyn. 38 (2006) 1306 – 1311.

[245] K. S. Gavrichev, M. A. Ryumin, A. V. Tyurin, V. M. Gurevich, L. N. Komissarova, Russ. J. Phys. Chem. A 83 (2009) 901–906.

[246] K. Popa, D. Sedmidubsky, O. Benes, C. Thiriet, R. J. M. Konings, J. Chem. Thermodyn. 38 (2006) 825 – 829.

[247] K. Popa, R. J. M. Konings, Thermochim. Acta 445 (2006) 49 – 52.

[248] O. Benes, K. Popa, V. Reuscher, A. Zappia, D. Staicu, R. J. M. Konings, J. Nucl. Mater. 418 (2011) 182–185.

[249] E. Antic-Fidancev, J. Holsa, M. Lemaitre-Blaise, P. Porcher, J. Phys.: Condens. Matter 3 (1991) 6829.

[250] K. S. Holliday, C. Babelot, C. Walther, S. Neumeier, D. Bosbach, T. Stumpf, Radiochim. Acta 100 (2012) 189–195.

[251] M. Schmidt, T. Stumpf, C. Walther, H. Geckeis, T. Fanghaenel, J. Colloid Interface Sci. 351 (2010) 50–56.

[252] D. Newman, B. Ng, Crystal Field Handbook, Cambridge University Press, 2007.

[253] W. T. Carnall, G. L. Goodman, K. Rajnak, R. S. Rana, J. Chem. Phys. 90 (1989) 3443–3457.

[254] J. C. Krupa, W. T. Carnall, J. Chem. Phys. 99 (1993) 8577–8584.

[255] P. Javorsky, F. Wastin, E. Colineau, J. Rebizant, P. Boulet, G. Stewart, J. Nucl. Mater. 344 (2005) 50–55.

[256] G. R. Lumpkin, J. Nucl. Mater. 289 (2001) 136–166.

[257] R. P. Turcotte, J. W. Wald, F. P. Roberts, J. M. Rusin, W. Lutze, J. Am. Ceram. Soc. 65 (1982) 589–593.

[258] W. J. Weber, J. W. Wald, Hj. Matzke, J. Nucl. Mater. 138 (1986) 196–209.

[259] N. P. Laverov, S. V. Yudintsev, V. I. Velichkin, A. N. Lukinykh, S. V. Tomilin, A. A. Lizin, S. V. Stefanovskii, Radiochemistry 51 (2009) 529–536.

[260] N. P. Laverov, S. V. Yudintsev, T. S. Livshits, S. V. Stefanovsky, A. N. Lukinykh, R. C. Ewing, Geochem. Int. 48 (2010) 1–14.

[261] D. M. Strachan, R. D. Scheele, E. C. Buck, J. P. Icenhower, A. E. Kozelisky, R. L. Sell, R. J. Elovich, W. C. Buchmiller, J. Nucl. Mater. 345 (2005) 109 – 135.

[262] R. E. Sykora, P. E. Raison, R. G. Haire, J. Solid State Chem. 178 (2005) 578–583.

[263] K. Holliday, S. Finkeldei, S. Neumeier, C. Walther, D. Bosbach, T. Stumpf, J. Nucl. Mater. 433 (2013) 479–485.

[264] J. P. Icenhower, D. M. Strachan, B. P. McGrail, R. A. Scheele, E. A. Rodriguez, J. L. Steele, V. L. Legore, Am. Mineral. 91 (2006) 39–53.

[265] S. X. Wang, L. M. Wang, R. C. Ewing, K. V. Govidan Kutty, Nucl. Instr. Meth. Phys. Res. B 169 (2000) 135 – 140.

[266] C. Heremans, B. J. Wuensch, J. K. Stalick, E. Prince, J. Solid State Chem. 117 (1995) 108 – 121.

[267] R. C. Ewing, W. J. Weber, F. W. Clinard, Jr, Prog. Nucl. Energy 29 (1995) 63 – 127.

[268] W. J. Weber, R. C. Ewing, C. R. A. Catlow, T. Diaz de la Rubia, L. W. Hobbs, C. Kinoshita, Hj. Matzke, A. T. Motta, M. Nastasi, E. K. H. Salje, E. R. Vance, S. J. Zinkle, J. Mater. Res. 13 (1998) 1434–1484.

[269] B. D. Begg, N. J. Hess, D. E. McCready, S. Thevuthasan, W. J. Weber, J. Nucl. Mater. 289 (2001) 188 – 193.

[270] J. Lian, J. Chen, L. M. Wang, R. C. Ewing, J. M. Farmer, L. A. Boatner, K. B. Helean, Phys. Rev. B 68 (2003) 134107.

[271] K. E. Sickafus, L. Minervini, R. W. Grimes, J. A. Valdez, M. Ishimaru, F. Li, K. J. McClellan, T. Hartmann, Science 289 (2000) 748–751.

[272] K. E. Sickafus, R. W. Grimes, J. A. Valdez, A. Cleave, M. Tang, M. Ishimaru, S. M. Corish, C. R. Stanek, B. P. Uberuaga, Nat. Mater. 6 (2007) 217–223.

[273] J. Lian, X. T. Zu, K. V. G. Kutty, J. Chen, L. M. Wang, R. C. Ewing, Phys. Rev. B 66 (2002) 054108.

[274] G. Sattonnay, N. Sellami, L. Thome, C. Legros, C. Grygiel, I. Monnet, J. Jagielski, I. Jozwik-Biala, P. Simon, Acta Mater. 61 (2013) 6492 – 6505.

[275] J. Lian, W. J. Weber, W. Jiang, L. M. Wang, L. A. Boatner, R. C. Ewing, Nucl. Instr. Meth. Phys. Res. B 250 (2006) 128 – 136.

[276] J. A. Purton, N. L. Allan, J. Mater. Chem. 12 (2002) 2923–2926.

[277] A. Chartier, C. Meis, J.-P. Crocombette, L. R. Corrales, W. J. Weber, Phys. Rev. B 67 (2003) 174102.

[278] A. Chartier, C. Meis, J.-P. Crocombette, W. J. Weber, L. R. Corrales, Phys. Rev. Lett. 94 (2005) 025505.

[279] A. Chartier, G. Catillon, J.-P. Crocombette, Phys. Rev. Lett. 102 (2009) 155503.

[280] L. Minervini, R. W. Grimes, K. E. Sickafus, J. Am. Ceram. Soc. 83 (2000) 1873–1878.

[281] P. J. Wilde, C. R. A. Catlow, Solid State Ion. 112 (1998) 173–183.

[282] F. X. Zhang, J. W. Wang, J. Lian, M. K. Lang, U. Becker, R. C. Ewing, Phys. Rev. Lett. 100 (2008) 045503.

[283] M. Lang, F. Zhang, J. Zhang, J. Wang, B. Schuster, C. Trautmann, R. Neumann, U. Becker, R. C. Ewing, Nat. Mater. 8 (2009) 793–797.

[284] W. Panero, L. Stixrude, R. Ewing, Phys. Rev. B 70 (2004) 054110.

[285] L. Chen, X. Su, Y. Li, OALib Journal 1 (2014) 1–8.

[286] J. Wang, R. C. Ewing, U. Becker, Mater. Res. Express 1 (2014) 035501.

[287] Z. J. Chen, H. Y. Xiao, X. T. Zu, F. Gao, J. Appl. Phys. 104 (2008) 093702.

[288] H. Y. Xiao, F. Gao, W. J. Weber, J. Phys.: Condes. Matter 22 (2010) 415801.

[289] N. Li, H. Y. Xiao, X. T. Zu, L. M. Wang, R. C. Ewing, J. Lian, F. Gao, J. Appl. Phys. 102 (2007) 063704.

[290] A. Chartier, C. Meis, W. J. Weber, L. R. Corrales, Phys. Rev. B 65 (2002) 134116.

[291] C. R. Stanek, R. W. Grimes, J. Am. Ceram. Soc 85 (2002) 2139.

[292] M. J. D. Rushton, R. W. Grimes, C. R. Stanek, S. Owens, J. Mater. Res. 19 (2004) 1603–1604.

[293] P. M. Kowalski, Y. Li (2015) submitted.

[294] S. Wu, P. M. Kowalski, N. Yu, T. Malcherek, W. Depmeier, D. Bosbach, S. Wang, E. V. Suleimanov, T. E. Albrecht-Schmitt, E. V. Alekseev, Inorg. Chem. 53 (2014) 7650–7660.

[295] B. Xiao, P. Kegler, T. M. Gesing, L. Robben, A. Blanca-Romero, P. M. Kowalski, Y. Li, V. Klepov, D. Bosbach, E. V. Alekseev, Chem. Eur. J. 22 (2015) 946–958.

[296] S. Finkeldei, P. Kegler, P. M. Kowalski, C. Schreinemachers, F. Brandt, A. A. Bukaemskiy, V. L. Vinograd, G. Beridze, A. Shelyug, A. Navrotsky, B. D. (2016) In preparation.

[297] X. Gonze, B. Amadon, P.-M. Anglade, J.-M. Beuken, F. Bottin, P. Boulanger, F. Bruneval, D. Caliste, R. Caracas, M. Côté, T. Deutsch, L. Genovese, P. Ghosez, M. Giantomassi, S. Goedecker, D. Hamann, P. Hermet, F. Jollet, G. Jomard, S. Leroux, M. Mancini, S. Mazevet, M. Oliveira, G. Onida, Y. Pouillon, T. Rangel, G.-M. Rignanese, D. Sangalli, R. Shaltaf, M. Torrent, M. Verstraete, G. Zerah, J. Zwanziger, Comput. Phys. Commun. 180 (2009) 2582 – 2615.

[298] V. Leiria Campo, Jr., M. Cococcioni, J. Phys.: Condens. Matter 22 (2010) 055602.

List of publications

Journal contributions

1. S. Finkeldei, Ph. Kegler, P. M. Kowalski, C. Schreinemachers, F. Brandt, A. A. Bukaemskiy, V. L. Vinograd, **G. Beridze**, A. Shelyug, A. Navrotsky, D. Bosbach, Composition depending order/disorder transition in $Nd_{2x}Zr_{1-x}O_{2+x}$ pyrochlores. A combined structural, thermochemical and ab initio modelling study, *In preparation* (2016)

2. **G. Beridze**, A. Birnie, S. Koniski, Y. Ji and P. M. Kowalski, Feasible and reliable ab initio calculation of nuclear f-materials, *Submitted* (2015)

3. Y. Li, P. M. Kowalski, **G. Beridze**, A. Blanca-Romero, Y. Ji, V. L. Vinograd, J. Gale and D. Bosbach, Atomistic simulations of ceramic materials relevant for nuclear waste management: cases of monazite and pyrochlore, *accepted* in Ceramic Transactions (2015).

4. P. M. Kowalski, **G. Beridze**, Y. Li, Y. Ji, C. Friedrich, E. Şaşıoğlu and S. Blügel, Feasible and reliable *ab initio* approach to computation of materials relevant for nuclear waste management, *accepted* in Ceramic Transactions (2015).

5. Y. Li, P. M. Kowalski, **G. Beridze**, A. Birnie, S. Finkeldei and D. Bosbach, Defect formation energies in $A_2B_2O_7$ pyrochlores, Scr. Mater., 107, 18 (2015).

6. P. M. Kowalski, **G. Beridze**, V. Vinograd and D. Bosbach, Heat capacities of lanthanide and actinide monazite-type ceramics, J. Nucl. Mater., 464, 147 (2015).

7. **G. Beridze** and P. M. Kowalski, Benchmarking the DFT+U Method for Thermochemical Calculations of Uranium Molecular Compounds and Solids, J. Phys. Chem. A, 118, 11797 (2014).

8. A. Blanca-Romero, P. M. Kowalski, **G. Beridze**, H. Schlenz and D. Bosbach, Performance of DFT+U method for prediction of structural and thermodynamic parameters of monazite-type ceramics, J. Comput. Chem., 35, 1339 (2014). **(Acknowledged by a cover page)**

Reports

1. P. M. Kowalski, **G. Beridze**, Y. Li and Y. Ji, Predicting properties of ceramic waste forms from first principles, Institute of energy and Climate Research IEK-6: Nuclear Waste Management, Report 2013/2014 "Material Science for Nuclear Waste Management" edited by Klinkenberg, M., Neumeier, S. and Bosbach, D. (2015)

2. P. M. Kowalski, **G. Beridze** and A. Blanca-Romero, Efficient methods for computation of actinides: uranium compounds and monazite orthophosphates from first principles, Institute of energy and Climate Research IEK-6: Nuclear Waste Management, Report 2011/2012 "Material Science for Nuclear Waste Management" edited by Klinkenberg, M., Neumeier, S. and Bosbach, D. (2013)

Attended schools and conferences

Conferences

Talks

1. Cracow Colloquium on f-electron systems, June 2015, Cracow, Poland
   Efficient calculations of f-materials relevant for nuclear waste management using DFT+U method

2. Second Joint Student Workshop on f-Element Chemistry, June 2015, Karlsruhe, Germany
   Feasible and reliable modeling of f-element-bearing materials with DFT+U method

3. E-MRS Spring Meeting, May 2015, Lille, France
   Feasible and reliable computation of novel ceramic waste forms

Posters

1. Psi-k conference, September 2015, San Sebastian, Spain
   Calculation of f-electron-bearing materials using DFT+U method

2. 9th international conference on f-elements, September 2015, Oxford, UK
   Computing lanthanide- and actinide-bearing materials with DFT+U method

3. Goldschmidt conference, August 2015, Prague, Czech Republic
   Ab initio modeling of computationally challenging Earth (f-) materials. **(Poster prize of the European Mineralogical Union)**

4. E-MRS Fall Meeting, September 2014, Warsaw, Poland
   Efficient ab-initio methods for computation of materials relevant for nuclear waste management

5. Advancing the Chemistry of the f-elements, July 2014, Edinburgh, UK
   DFT+U calculations of actinide- and lanthanide-bearing materials relevant for nuclear waste management

6. What about U? – Strong correlations from first principles, June 2014, Lausanne, Switzerland
   Performance of DFT+U method for actinide- and lanthanide-bearing materials relevant for nuclear waste management

7. 78th Annual Meeting of the DPG, March 2014, Berlin, Germany
   Ab initio calculations of f-element compounds and solids with DFT+U method

Schools

1. juDFT: Hands-on DFT codes from Jülich, September 2014, Jülich, Germany

2. EMTCCM School on Theoretical Solid State Chemistry, May 2014, Zaragoza, Spain

3. Yambo hands-on tutorial on electronic and optical excitations, April 2013, Lausanne, Switzerland

4. ACTINET ThUL Spring School in Actinide Chemistry, January 2013, Karlsruhe, Germany

Band / Volume 312
Development of Embedded Thermocouple Sensors for Thermal Barrier Coatings (TBCs) by a Laser Cladding Process
Y. Zhang (2016), II, 108 pp
ISBN: 978-3-95806-129-3

Band / Volume 313
Streamwater transit time distributions at the catchment scale: constraining uncertainties through identification of spatio-temporal controls
M. Stockinger (2016), XIX, 161 pp
ISBN: 978-3-95806-131-6

Band / Volume 314
Entwicklung eines metallbasierten Substratkonzepts für energieeffiziente Gastrennmembranen
J. A. Kot (2016), xi, 201 pp
ISBN: 978-3-95806-134-7

Band / Volume 315
Langzeitbeobachtung der Dosisbelastung der Bevölkerung in radioaktiv kontaminierten Gebieten Weißrusslands - Korma-Studie II (1998 – 2015) -
P. Zoriy, H. Dederichs, J. Pillath, B. Heuel-Fabianek, P. Hill, R. Lennartz (2016), ca 104 pp
ISBN: 978-3-95806-137-8

Band / Volume 316
Oxidation Mechanisms of Metallic Carrier Materials for Gas Separation Membranes
M. Schiek (2016), 148 pp
ISBN: 978-3-95806-138-5

Band / Volume 317
Thermoschockverhalten und temperaturabhängige Eigenschaften kohlenstoffarmer und –freier Feuerfestwerkstoffe
A. Böhm (2016), VI, 153 pp
ISBN: 978-3-95806-139-2

Band / Volume 318
Theoretical and experimental studies of runaway electrons in the TEXTOR tokamak
S.S. Abdullaev, K.H. Finken, K. Wongrach, O. Willi (2016), X, 109 pp
ISBN: 978-3-95806-140-8

Band / Volume 319
Modelling Thermodynamic Properties of Intercalation Compounds for Lithium Ion Batteries
S. O. Dang (2016), x, 133 pp
ISBN: 978-3-95806-141-5

Band / Volume 320
Atmospheric Mixing in a Lagrangian Framework
M. Tao (2016), 146 pp
ISBN: 978-3-95806-142-2

Band / Volume 321
Statistical analysis and combination of active and passive microwave remote sensing methods for soil moisture retrieval
K. Rötzer (2016), XIV, 112 pp
ISBN: 978-3-95806-143-9

Band / Volume 322
Langzeitstabilität der Polymerelektrolyt-Wasserelektrolyse bei reduziertem Iridiumgehalt
C. G. Rakousky (2016), VII, 199 pp
ISBN: 978-3-95806-147-7

Band / Volume 323
Light induced water splitting using multijunction thin film silicon solar cells
F. Urbain (2016), xi, 173, XLVI pp
ISBN: 978-3-95806-148-4

Band / Volume 324
Properties of convective gravity waves derived by combining global modeling and satellite observations
Q. T. Trinh (2016), 140 pp
ISBN: 978-3-95806-150-7

Band / Volume 325
Feasible and Reliable Ab initio Atomistic Modeling for Nuclear Waste Management
G. Beridze (2016), xix, 128 pp
ISBN: 978-3-95806-151-4

Weitere ***Schriften des Verlags im Forschungszentrum Jülich*** unter
http://wwwzb1.fz-juelich.de/verlagextern1/index.asp

Energie & Umwelt /
Energy & Environment
Band / Volume 325
ISBN 978-3-95806-151-4